Sample Preconcentration and *In-situ* Digestion of Solids Using a Graphite Furnace as Sample Introduction System for Inductively Coupled Plasma-Atomic Emission Spectrometry and Mass Spectrometry

by

Jean-François Alary

Department of Chemistry

McGill University, Montreal

February 1998

A Thesis submitted to the Faculty of Graduate Studies and Research in partial fulfillment of the requirements of the degree of Doctor of Philosophy

0-612-44344-2

Guidelines

The following text has been reproduced, and included as instructed, from the *"Guidelines Concerning Thesis Preparation"*, Faculty of Graduate Studies and Research, McGill University, in order to inform the external reader of Faculty Regulations:

> ***2) Manuscripts and Authorship:***
>
> *Candidates have the option, subject to the approval of their department, of including, as part of their thesis, copies of the text of a paper(s) submitted for publication, or the clearly-duplicated text of a published paper(s), provided that these copies are bound as an integral part of the thesis.*
>
> *If this option if chosen, connecting texts, providing logical bridges between the different papers, are mandatory.*
>
> *The thesis must still conform to all other requirements of the "Guidelines Concerning Thesis Preparation" and should be in a literary form that is more than a mere collection of manuscripts published or to be published. The thesis must include. as separate chapters or sections: (1) a Table of Contents, (2) a general abstract in English and French, (3) an introduction which clearly states the rationale and objectives of the study, (4) a comprehensive general review of the background literature to the subject of the thesis, when this review is appropriate, and (5) a final overall conclusion and/or summary.*

Additional material (procedural and design data, as well as descriptions of equipment used) must be provided where appropriate and in sufficient detail (e.g. in appendices) to allow a clear and precise judgment to be made of the importance and originality of the research reported in the thesis.

In the case of manuscripts co-authored by the candidate and others, the candidate is required to make an explicit statement in the thesis of who contributed to such work and to what extent; supervisors must attest to the accuracy of such claims at the Ph.D. Oral Defense. Since the task of the examiners is made more difficult in these cases, it is in the canditate's interest to make perfectly clear the responsibilities of the different authors of co-authored papers.

Abstract

The coupling of an electrothermal vaporization unit (ETV) with inductively coupled plasma (ICP) instruments has been used to perform preconcentration of liquid samples and direct analysis of trace metals in difficult mineral matrices. A determination of refractory elements in a zeolite matrix was performed using a modified ETV furnace with an argon/Freon gas mixture. The zeolite sample was deposited in the furnace tube as a slurry and a complete destruction of the hard matrix was obtained through halogenation. The operating conditions were optimized for a viewing height of 15 mm and for a 1 kW plasma. Detection limits of 1.4 μg/g for Cr, 7.4 μg/g for Mn and 0.3 μg/g for V were obtained for this difficult matrix and the levels found agreed well with those measured from a routine X-ray fluorescence analysis. For liquid standards, improvement factors of 5 to 25 were obtained for several elements with Freon ETV when compared with conventional nebulization. In a different set of experiments, a preconcentration of liquid samples was achieved by spraying the sample against the inner wall of the graphite tube of an ETV unit using a conventional concentric nebulizer. The tube was maintained at 160°C at spraying to evaporate the sample water to the atmosphere. Modifications to the commercial ETV unit used included the addition of a spraying stage in the analytical sequence, provisions for controlling the swinging arm holding the spray nebulizer and alteration to the temperature programming and gas flow pathways to inhibit the recondensation of water within the furnace. The detection limits obtained in atomic emission spectrometry (AES) for a sample volume of 1 ml were 0.06 ng/ml for Cd, 0.3 ng/ml for Pb, 0.02 ng/ml for Zn and 0.04 ng/ml for Cu and the improvement factors were in direct proportion with the volume of deposited sample. In ICP for mass spectrometry

(MS), the shape of ETV transients were distorted by a surge of water vapor originating from the furnace. Argides (Ar^+, Ar_2^+) and molecular species derived from the dissociation of water in the plasma (ArH^+, O_2^+) were used to diagnose the plasma during the sample pulse. A direct relationship between ArH^+ abundance and the water loading of the plasma was established and was used to optimize the furnace temperature programming. The spray sample deposition provided variable gain in detection limits although in lesser proportion than expected from the preconcentration factor. High blanks and signal suppression at concentrations above 100 ng/ml restricted the dynamic range spanned to three orders of magnitude at best. Nevertheless, transient signals ratioed with Ar_2^+ and ArH^+ signals resulted in significant improvements of the analytical figures of merit.

Résumé

La préconcentration d'échantillons liquides et l'analyse de métaux au niveau de traces dans une matrice minérale très stable a été réalisée en utilisant des fours à graphite (FG) accouplés à un plasma à couplage inductif. Plusieurs éléments réfractaires ont été évalués directement dans une matrice de zéolite en utilisant un four au graphite modifié de façon à permettre l'emploi d'un mélange gazeux argon/fréon. L'échantillon de zéolite a été déposé dans le tube de graphite sous forme de suspension et une digestion complète de la matrice minérale a été obtenue par formation d'halogénures. Des limites de détection de 1.4 µg/g pour le chrome, de 7.4 µg/g pour le manganèse et de 0.3 µg/g pour le vanadium ont été obtenues dans cette matrice particulièrement stable, et les niveaux mesurés s'accordent avec ceux déterminées par une analyse de routine avec fluorescence aux rayons X. D'autre part, les standards liquides montrent des performances en limite de détection de 5 à 25 fois meilleures en FG avec mélange gazeux au fréon qu'en nébulisation conventionnelle. Dans une autre série d'expériences, une préconcentration d'échantillons aqueux a été réalisée par nébulisation directe contre les parois internes d'un tube FG. Le tube est maintenu à une température de 160°C et l'eau évaporée est évacuée vers l'atmosphère. Les modifications apportées au four comprennent l'addition d'une étape de nébulisation, l'ajout d'un contrôle du positionnement du bras porteur du nébulizeur concentrique, et des changements à la programmation en température et aux débits de gaz afin d'empêcher la condensation de l'eau dans le four. Les limites de détection obtenues en émission atomique pour un volume d'échantillon de 1 ml sont de 0.06 ng/ml pour le cadmium, 0.3 ng/ml pour le plomb, 0.02 ng/ml pour le zinc et 0.04 ng/ml pour le cuivre. Le facteur d'amélioration observé est généralement en relation

directe avec le volume d'échantillon déposé. Avec un plasma couplé à un spectromètre de masse, la forme du signal transient est modifiée par l'arrivée de vapeur d'eau provenant du four. Certains argénures (Ar^+, Ar_2^+) et autres espèces moléculaires dérivées de la fragmentation de l'eau dans le plasma (ArH^+, O_2^+) ont été utilisés afin de diagnostiquer le plasma en cours d'opération. Une relation directe entre la charge instantanée du plasma en eau et le niveau d'ArH^+ observé a été établie et utilisée par la suite afin d'optimiser la programmation en température de la fournaise. Des blancs élevés et une suppression du signal au dessus de 100 ng/ml ont restreints le domaine dynamique à trois ordres de grandeur au mieux et les facteurs d'amélioration en limite de détection sont moindres que ceux observés en émission atomique. Cependant, les performances analytiques ont été améliorées en effectuant une normalisation des signaux transients avec les signaux d'Ar_2^+ ou ArH^+ mesurés en simultané avec les analytes.

Acknowledgments

I wish first to express my deepest acknowledgements to Professor Eric D. Salin who, as thesis director, welcomed me into his research team and never stopped providing me with inspiration and encouragement. His invaluable contribution to the accomplishment of this work has made it happened, finally.

Also, I warmly thank all my fellow students and friends in the laboratory. They are just too many to be named individually. Some were finishing their work when I came in and others started their curriculum before I left. I just wish I was helpful to the latter the same as the former were to me. Support from other members of the analytical chemistry group - the professors and graduate students - and of the Chemistry Department in general were also greatly appreciated. I especially thank Fred Kluck and Bill Bastian for the patience they have always shown in deciphering my often confused drawings and accompanying explanations.

Finally, my wife Mariléa deserves special acknowledgment for constantly standing by me over those years. Without her, this achievement would not have been possible. My daughter Julia, who entered our lives at this time, had a tough examination in her first days of life. The energy and determination she exhibited at this occasion were, and still is, greatly inspirational to me. Special thanks also to my family, father, mother and sisters and brother, for their constant support throughout and especially during difficult passages.

Contribution to Original Knowledge

The use of argon/freon gas mixture in ETV-ICP-AES has proved to efficiently disrupt hard sample matrices such as zeolites and to allow the analysis of refractory elements usually exhibiting poor detection limits with this technique.

A commercial ETV instrument has been modified for spray deposition of liquid sample in graphite furnaces and a significant concentration factor has been achieved for several analytes by spraying sample volumes of a milliliter size. The concentration factors were reflected in the detection limits measured in ETV-ICP-AES.

The same preconcentration of sample by spray deposition was less beneficial to the detection limits measured in ETV-ICP-MS, and degraded dynamic ranges and high blanks were observed. However, a better deposition of sample over the graphite surface was obtained, leading to sharper transient signals.

In Spray ETV-ICP-MS, the water vapor originating from the furnace at sample vaporization affected the shape of transient signals in a different manner for several elements. Selected argide species formed in the argon plasma provided instant insights in the energetic state of the plasma and were useful for the partial correction of transient shapes by signal ratioing. The argon dimer (Ar_2), argon hydride (ArH) and argon ion (Ar^+) proved to be especially useful in providing an evaluation of the survivability conditions for molecular species, of the amount of water present, and of the energy transfer efficiency respectively, in the plasma.

List of Tables

List of Figures

Table of Contents

Chapter 1

Chapter 2

Chapter 3

Chapter 4

Chapter 1

INTRODUCTION

The determination of the elemental composition of a sample is one of the essential missions of modern analytical chemistry. One part of the demand originates from industries dealing with high performance materials which exhibit characteristics often dependent on the level of trace elements. The microelectronics and ceramics industries, as well as all industrial sectors using high performance alloys, among others, are prime candidates to benefit from improved elemental analytical techniques. Also, the various environmental issues triggered by an increasing awareness of the public and by more stringent governmental regulations have also furnished strong incentives to develop better ways of determining toxic metals in natural and artificial matrices. All of this often leaves the analytical chemist faced with the following challenges that seem at first glance contradictory: lowering detection limits, obtaining accurate results, dealing with more difficult and complex matrices, eliminating the effects of interferences and optimizing the cost/benefit ratio of analysis. With these objectives in mind, analytical chemists are constantly improving their techniques by either revising older methods or by borrowing from related fields. This is the case for the methods using radio-frequency based (RF) plasmas which are better known as Inductively Coupled Plasmas (ICP's) [1,2]. The high temperature developed in these plasmas are used to break down sample matrices, dissociate molecular species and provide enough energy to atoms to provoke the emission of characteristic atomic bands, as in ICP for Atomic Emission

Spectrometry (ICP-AES), or to form a cloud of ionized atoms which is sampled and analyzed by mass spectrometry, as in ICP for Mass Spectrometry (ICP-MS). Although current analytical plasma instrumentation still involves significant investment, the benefits are so valuable that they largely warrant the effort made to develop and improve these techniques. In the future, it is expected that analytical plasmas based on mass spectrometry will grow in popularity given their vastly superior sensitivity and their applicability to most elements of the periodic table [3,4]. The ICP-AES, however, will probably remain the "Work Horse" of elemental determination in the years to come as it is a robust and fully developed technique that meets the demand in numerous applications [5]. More importantly, the people involved in elemental analysis have used this technique for a long period of time [6], and have therefore become very familiar with its advantages as well as its drawbacks. The ICP-MS still has a long way to go before reaching the same degree of familiarity from the user community although it is a rapidly maturing technique [3], seventeen years after its introduction [7].

1.1 Plasmas

The plasma is at the very heart of ICP based instrumentations. Although the concept of the plasma is modern, the Ancients had already recognized fire as one of the four basic elements making the world, in addition to air, water and earth. The first man-made plasmas appeared with the progressive mastering of electrical discharges but tremendous advances occurred in the 1950s as a byproduct of the effort to produce controlled thermonuclear fusion [8].

The radio-frequency (RF) plasmas used in elemental analysis are qualified as "condensed-state" plasmas as the participating atoms maintain an electronic structure around the core [8]. In fact, they are mainly composed of singly ionized atoms and free electrons which themselves do not amount to more than one tenth of a percent of the total mass of the plasma gas [4,9-11]. They are most often operated at atmospheric pressure, except for special applications [12]. Another important characteristic, probably one of most important from the analyst's point of view, is the temperature of the various species making up the plasma [13-17]. Since the RF energy is deposited exclusively in charged species, it has to be redistributed to neutral particles through complex collisional and radiative processes [18-20]. These processes usually generate different temperature scales as we separately address the electrons, the ionized atoms or the neutral atoms kinetic temperatures. Other processes such as ionization of atomic species, excitation of atomic and ionic species, and rotational temperature of surviving diatomic species also exhibit specific temperature values. In general, a temperature in the 2500-8000 K range is commonly accepted depending on the measuring species [13,21-24]. Also, the plasma is constantly out of equilibrium as it involves dynamic fluxes of gas entering and leaving the plasma space. Most often, however, the plasma meets the requirement of Local Thermal Equilibrium (LTE) which is sufficient for analytical uses. LTE is achieved within a plasma when Planck's radiation law only is violated, which implies that radiation is emitted without being reabsorbed by the plasma material [20].

Analytical ICP plasmas are usually operated at 27.12 Mhz, one of the reserved frequencies for Industrial, Medical and Scientific (IMS) applications, although signal-to-background ratios in atomic emission and plasma robustness can both be improved with higher frequencies [25-27]. Most plasmas are formed and maintained in a stream of argon. The use of other plasma gases and gas mixtures was proposed but none was ever widely adopted [28-32].

1.2 Spectrometry

1.2.1 Atomic Emission Spectrometry

In ICP-AES, the emission from atoms and ions are collected and separated by a spectrometer in the visible and UV wavelengths. The ICP has been described as being an almost ideal excitation source for elemental analysis by atomic emission spectrometry [6]. Detection limits in the ng/ml range for many elements and an enhanced robustness regarding chemical and ionization interferences are among the major advantages exhibited by this technique. A linear dynamic range of more than three orders of magnitude is also one of the performance characteristics for ICP-AES instruments. These advantages are related mainly to the fact that analytes transit through the hot plasma with an appreciable residence time of several milliseconds. Argon plasmas are also chemically inert and exhibit low background emission in the wavelength region of interest for the determination of most elements (200-400 nm).

Recent developments in detector and spectrometer technologies [1,5] have resulted in modern instruments combining an Echelle spectrometer with a CCD camera type detector, an axially viewed plasma and ultrasonic nebulization. This type of instrumentation provides detection limits ranging from 0.5 ng/ml for Mn, to 36 ng/ml for Se [33].

1.2.2 Mass Spectrometry

In mass spectrometry, a sample of the ionic population of the plasma is extracted and transmitted to a quadrupole mass spectrometer/detector arrangement. This technique exhibits considerably lower detection limit when compared with atomic emission as there is no fundamental source of background signal [11]. Moreover, the ability to discriminate isotopic concentrations makes this technique especially appealing to earth sciences studies [34-38] and allows the average analyst to perform isotopic dilutions, one of the most robust calibration strategies currently known [35,39-41].

The ICP can be considered a very efficient but not extremely energetic source of ionization [11]. As mentioned earlier, it is the spectrochemical discharge technique having the greatest degree of immunity to chemical interferences. The ion extraction process is, however, extremely critical as it is actually an attempt to extract charged species that have a tendency to rapidly recombine when removed from the energetic environment of the plasma.

The extraction is achieved in several steps by aiming the plasma at the orifice of the sampler cone (1 mm i.d.) [42] in the zone of the plasma of maximal concentration of analyte ions [4,43]. A supersonic jet is created from the extracted plasma material into an intermediate vacuum (~1 torr) on the downstream side of the orifice [44]. The skimmer cone, a second metal cone placed behind the sampler cone and having a similar central opening, admits the central part of the jet into the high vacuum spectrometer chamber. An electrostatic lens set then focuses the ion beam onto the quadrupole entry.

Most of the matrix effects and interfering ions appear in the sampler-skimmer and lens set portions of the path [44]. Several matrix effects ascribed to ICP-MS take place within the ionic beam from the electrostatic repulsion that the cations exert on each other [30,45-50]. Diatomic species also form in the plasma and can severely interfere with the analytes, especially at trace levels. Diatomic species are usually a combination of argon with oxygen and hydrogen from the sample water, and argide and oxide derivatives of the sample matrix elements [50-56]. Double ionization is also observed for metals with low second ionization potential such as Ba and the rare earth elements [57,58].

1.3 Sample Introduction

1.3.1 Liquid Samples

Most certainly, the sample introduction in ICP spectrometry is the "Achilles Heels" of the technique as was pointed out by Browner [59]. The sample introduction techniques for liquids were initially directly translated from the flame spectrometry instrumentation. Liquid samples represent an attractive form to the analyst even if their use often involves a time consuming digestion step in the analytical sequence. This form is homogeneous and allows quantitative dilutions and additions, and a direct comparison with liquid standards.

1.3.1.1 Pneumatic Nebulization

While pneumatic nebulization is an attractive way of liquid sample introduction in ICP spectrometry because of its simplicity and reliability, it is a technique that suffers from an inherently low transfer efficiency. The situation is worst for ICPs as the efficiency of the classical tandem nebulizer/spray chamber is rarely above 1% in plasmas, as opposed to 10% in flame atomic absorption [59]. The two main classes of pneumatic nebulizers used with ICPs are the cross-flow and concentric nebulizers. Both types generate mists from the action of a high velocity gas stream onto a liquid film. In all cases, a spray chamber is placed between the nebulizer and the plasma to reject the large droplets from the fine mist. They comes in a variety of shapes but the most widely used is the Scott double pass type.

The all-glass concentric nebulizers [60-63] are the pneumatic nebulizer most commonly used in ICP spectrometry. They are inexpensive and can generate aerosols with sufficient uniformity to yield results with good precision (1% RSD). They are relatively intolerant, however, to high levels of dissolved solids and susceptible to blockage by particles because of the very small annular gap (10-35 μm) [64].

The cross-flow nebulizers include the ones adapted for ICP spectrometry and use the classical design of a gas stream intercepting the liquid at a right angle [65]. The V-groove, Légère, Babington and Hildebrand (or grid) nebulizers [66-69] can also be considered as derivatives of the original cross-flow design. These nebulizers are noisier but can accommodate much higher dissolved content and most can directly nebulize slurries. However, these characteristics are not attractive for ICP-MS, notably since the sampler and skimmer cones are particularly sensitive to blockage for any concentration over 0.25% in dissolved solid.

In a separate class are the High-Pressure Nebulizers (HNP) in which high velocity is imparted to a liquid stream into still gas [70], the mist forms from the interaction of the fast moving liquid with the surrounding atmosphere. A variation of this technique consists in impacting the high velocity stream with a surface to generate the mist. Other less used nebulizers include the glass frit nebulizer [71] and the thermospray nebulizer [72].

1.3.1.2 Ultrasonic Nebulization

Ultrasonic nebulization (USN) exhibits a higher transport efficiency (30%) but requires a desolvation stage to minimize the solvent load on the plasma [73]. On average, ten times more analytes is transferred to the plasma and the theoretical improvement in detection limits is expected to be of the same magnitude, however, adverse effects from sample build up at injector tips or at the sampler and skimmer cones in ICP-MS should be taken into consideration. The interferences are also exacerbated. It is not surprising that these drawbacks as well as the high cost of the instrumentation have limited the popularity of USN. However, simple and yet efficient USN's can be built at low cost from commercial ultrasonic humidifiers They exhibit long term stabilities of 1-2% [74,75].

1.3.1.3 Sample Preconcentration Using FIA

Sample preconcentration is achieved by evaporation, solvent extraction, co-precipitation, ion-exchange, size exclusion gel and usually is applied to liquid samples. This topic is therefore placed in the section on Liquid Introduction.

Flow Injection Analysis (FIA) techniques appeared during the 1970's and were first intended for performing analytical reactions on a continuous basis [76,77]. High sample throughput, simplicity of equipment and excellent precision, due to reproducible sample pulses and in some cases matrix removal, are among the advantages exhibited by these techniques. Among the most popular uses of FI manifolds for ICP atomic analysis are sample preconcentration by coprecipitation, liquid-liquid extraction and solid phase extraction. The last class of application is the most widely used and generally involves the use of an ion exchange resin such as Chelex-100 to either remove concentrated ionic matrices or to concentrate analytes. Other material used for preconcentration include activated alumina and activated carbon. On-line column-based operation can be automated easily and offers better protection against contamination from the laboratory environment than sample preparation in open vessels. In addition, a variety of sample preparation strategies including dilution, standard addition and internal and external calibration can be easily implemented using an FI manifold.

Electrochemical preconcentration on graphite or mercury electrodes were envisioned once to be capable of bringing appreciable improvements in detection limits [78,79]. Several minutes of electrodeposition, however, were not sufficient to determine most elements in natural waters.

1.3.2 Solid Samples

Solid samples submitted to fusion or acid digestion are exposed to contamination, incomplete dissolution and evaporative losses of the most volatile elements. Moreover, these steps add complexity to the analytical sequence, are usually time consuming and involve manipulation of hazardous acids. In regards to these inconveniences, it was initially proposed that one introduces solid and slurry samples directly into the plasma as it is a higher temperature source than flames. Complex solid matrices such as geological samples, ceramics and refractory compounds were expected to be efficiently torn apart to their atomic constituents and the atoms would then be ionized or excited for analysis.

1.3.2.1 Solids

Sample introduction techniques for solid materials involve either the direct introduction of powdered samples, or the use of energetic radiation or an electrical plasma to generate a cloud of microparticles.

In the first group of techniques, we find the "swirl cup" is a well established techniques in which argon gas is injected in an agitated cup containing the sample [80]. Alternatively, a narrow tube containing the sample powder is translated smoothly toward the opening of a capillary tube into which argon gas is flowing [80a]. In both cases, the powder is entrained directly to the plasma by the flowing gas. A "fluidized bed chamber" can also be employed for forming a homogeneous cloud of sample by mechanical agitation of the container [81,81a,82]. The argon gas is introduced through a glass frit and a cyclone situated between the fluidized bed and the plasma eliminates the large particles and agglomerates. In all techniques involving powders, however, the possibility of particle segregation due to density differences is always present.

The second group includes the use of spark discharges to produce an elutriation of the sample [83-85]. The fine aerosol generated is nebulized along with water and introduced in the plasma as a conventional mist. An argon flow can also be passed over "microarcs" electrodes and be later introduced to the ICP. With microarcs, the matrix and ionization effects are minimals although the precision can be affected by the shape and nature of the sample electrodes.

Laser Ablation (LA) is the technique showing the most rapidly growing popularity among solid sampling techniques for ICP spectrometry [86-88]. It is now proposed as an optional attachment by most ICP-MS manufacturers. In LA, a laser is focused on a small area of the surface of the solid and the high energy released locally generates a cloud of small particles from the sample. This technique is extremely desirable when the sample is to be preserved or when sampling with high spatial or in depth resolution are required. Moreover, this technique can address a wide variety of sample irrespective of electrical conductivity, physical form, or organic or inorganic nature involved. Nevertheless, some concerns about the regularity and reflectivity of the surface must be kept in mind.

The instrumentation includes a high power laser and focusing optics, an ablation chamber and a proper aerosol transfer interface to the ICP torch [88]. Nd:YAG, CO_2, nitrogen and excimer lasers are commonly used to produce high power beams. As the laser is focused within spots of 10 to 20 μm of diameter, energy densities of the order of 10^7 W/cm^2 are developed at the sample surface. The ablation chamber has to be designed to accommodate sample translation and rotation, to minimize memory effects, to transfer efficiently the particle cloud to the plasma and to provide a good view of the sample - often through a microscope with a video arrangement - to the user. Various designs have been proposed ranging from the simple chamber mounted at the base of the ICP torch proposed by Carr and Horlick [89] to the more complex arrangement of Arrowsmith and Hughes [90]. Typically, the LA can be operated in single shot laser firings giving off transient signal responses [91], or in continuous laser operation with steady-state response over a limited time frame [92].

Reported detection limits for LA differ as the technique depends greatly on parameters of operation and quality of the samples, but range from 200 μg/g for Cu and Ni with ICP-AES [92] to 0.2 μg/g for Nb using ICP-MS [93] (all in steel samples). However, the precision compares unfavorably with nebulization and is commonly in the 5-10% range for geological and metallurgical samples. Also, truly quantitative determinations are achieved only with similar solid standards.

1.3.2.2 Slurries

The introduction of solids as slurries is an intermediate strategy that, although requiring the sample to be in the form of finely divided particles, allows the use of the more conventional and less expensive nebulization systems presented earlier [94]. It can address a variety of sample type ranging from milk powders [95], animal tissues [96] and botanical samples [97], to coals [98,99], ceramics [21], soils [100] and sediments [99,101]. Nevertheless, the introduction of a sample having a solid and a liquid phase adds to the level of complexity of the system. The size of particles is of prime importance for the stability of the suspension as well as for the ability of the plasma to atomize the solid efficiently. It has been demonstrated, for example, that refractory materials such as alumina are atomized almost quantitatively only for particle diameters of 2.5 μm or less [102]. It has also be shown that particles diameters larger than a certain threshold value (<5 μm) do not reach the plasma, which can lead to analyte segregation losses [94]. The grinding technique which is required to reduce the sampler to powder has also to be considered carefully. As most grinders involve high and prolonged impacting between the sample and a grinding material, it is common to find a significant level of contamination after a long period [94]. Agate and zirconia are widely used as grinding material. The use of dispersants (surfactants) is also mandatory in most cases to stabilize the suspension [103]. Of particular interest to the slurry stability is the Zeta Potential (ZP) exhibited by the particles in the suspension. A ZP value approaching zero should be avoided as it indicates that no electrostatic stabilizing mechanisms is in action and that particle agglomeration may occur. Cross-flow type nebulizers and more often the V-groove Babington type nebulizers are used for slurry nebulization [104]. Calibration strategies using internal standards [105] or standard additions [106] are usually well adapted to slurry nebulization, although external calibration can be used if the liquid standards are matrix matched with the liquid phase of the suspension [107]. As a last resort, standard slurries can be used [108].

1.3.3 Thermal Methods

The thermal methods of sample introduction are universal as they apply to either liquid, slurries or solid samples. In these methods, the sample is deposited onto a material resistant to high temperatures and heated to vaporization point. The sample forms a dry aerosol that is atomized and analyzed by the ICP instrument. The source of thermal energy can be electrical as in Electrothermal Vaporization Units (ETV) or the energy can be drawn from the plasma itself as in Direct Sample Insertion (DSI). The material used is usually graphite (or one of its modified forms) or metal of high boiling point such as tungsten or tantalum. Although LA does use thermal vaporization, it does not apply to liquids and is therefore not considered in this section.

For these methods, the detection system should be able to handle the fast transient signals generated by the sample pulse (<10 sec.) [88,109]. Although this characteristic usually poses no problem with direct reading spectrometers for atomic emission, it prohibits multielemental determination with scanning spectrometers. These techniques also require the use of background correction in ICP-AES, as the plasma basic emissions are shifted under the influence of insertion of the DSI probe or sample pulse in ETV. The background correction strategy most commonly used for direct reading spectrometers involves the use of an oscillating quartz refractor plate [110]. However, more recent spectrometers equipped with diode arrays or CID detectors perform very efficient background correction. In ICP-MS, quadrupole mass spectrometers used in commercial instruments are operating in quasi-simultaneous mode - they are in fact fast scanning systems - and consequently suffer from sensitivity losses when the time frame of the transient has to be segmented between several *m/z* locations. In practice, no more than 6 to 10 elements can be simultaneously measured during a single ETV firing or DSI probe insertion. However, the background signal remain insensitive to the perturbations induced in the plasma and no correction has therefore to be introduced.

1.3.3.1 Direct Sample Insertion

Insertion of sample carrying probes directly in the plasma center were first attempted by Salin and Horlick [111] and Sommer and Ohls [112]. The fundamental principle involves the deposition of a small quantity of sample material onto a probe that is later inserted into the plasma. The graphite electrodes traditionally used for DC arc emission spectrometry are ideal starting materials for the machining of DSI probes [88]. Spectroscopically pure electrodes are readily available commercially. Graphite is easily machined but can interact with some analytes that form carbides and for this reason, often requires the use of chemical modifiers [113,114]. Other materials and geometries were used as well that include metal cups and wire loops [115,116]. As the energy for sample vaporization is extracted from the plasma, the geometry of the probe is very important in obtaining a sharp and intense transient signal. Wire loops are superior in that respect since they heat rapidly and yield good detection limits. However, the metal of the wire can evaporate along with the sample and generate spectral interferences. Tungsten evaporated from tungsten wires, for example, causes a high background signal that degrades detection limits for several metals in ICP-AES . In addition, the wire erodes faster with sample in nitric and perchloric acid.

The probe propulsion system should position the probe swiftly and reproducibly, a result best attained with pneumatic and stepper-motor driven designs [117,118]. Modified Fassel torchs having a wide central opening with no injector bore, and a mechanism preventing the introduction of atmospheric gases during the probe insertion should be used [119]. The use of a modified 24-positions autosampler carrousel with proper insulation from atmosphere has also been reported [120]. The most severe limitation to routine use of DSI arises from the difficulty of rapid change over between DSI and nebulization, which is a consequence of the complexity of the instrumentation. However, production of a convenient DSI attachment is certainly possible with an appropriate engineering effort. The best performances are achieved with probes with thin stems and walls that provide a low thermal mass [121]. However, these probes are difficult to produce and fragile to handle although each survives several hundred insertions in routine use [122].

Direct sample introduction has the great advantage of being inherently 100% efficient and usually exhibits detection limits an order of magnitude lower than nebulization [88]. It consumes a minute amount of sample and, as mentioned above, accepts samples in either liquid or solid form. In standard practice, liquid samples are dried before insertion. As a consequence, DSI operates in a dry plasma, an appealing feature especially for ICP-MS in which the majority of molecular interferences are caused by oxides and hydroxides derivatives of the matrix when water is the solvent. In ICP-AES, a high plasma power is desirable for best analytical performances.

In DSI, the volatility of the analyte is mostly responsible for the shape and duration in time of the transient signal. Cadmium deposited onto a tungsten wire of low thermal mass exhibits a sharp (100 ms) and intense peak [88]. In contrast, carbide forming elements vaporized from a graphite probe and refractory samples in general show peak tailings, suffer from memory effect and exhibit poor sensitivity. The precision of these measurements oscillates between 3% and 10% which is more than with nebulization and may depend on variable sample volume, inhomogeneities in sample matrix and differences in probe insertion velocity and end positioning. Application of DSI include analysis of botanical [118], geological [123], metallurgical [124] and refractory materials [125].

Recently, a variation of DSI has been reported by this laboratory which involves spraying a liquid sample directly into the probe and evaporating the solvent using either a block heater or inductive heating [122]. The preconcentration of the sample thus achieved allows an average 500-fold reduction in detection limits in ICP-AES and ICP-MS for an extended set of elements. In ICP-MS, sample preconcentration resulted in impressively low detection limits of, for example,. 0.55 pg/ml for Cu, 0.25 pg/ml for Zn and 0.1 pg/ml for Pb. Good agreements with certified trace metals values were obtained for a natural water reference sample.

1.3.3.2 Electrothermal Vaporization

The fundamental difference between DSI and ETV is the way the analyte is transported to the plasma core. In DSI, the supporting material is pushed in and the sample vaporizes directly within the plasma. In ETV, the sample vaporization occurs far from the plasma and the aerosol has to be carried to the plasma torch by a gas stream. The energy source for sample vaporization is the Joule effect produced by an electrical current in the supporting material. The ETV instruments used for sample introduction into ICP instrumentation were either adapted from Graphite Furnace for Atomic Absorption Spectrometry (GFAAS) instrumentation [126-133] or specifically designed for ICP spectrometry [113,134-137]. These units generally provide the user with a fine and reproducible control over the temperature programming of the furnace, which is a great advantage if an analytical strategy requires the sample to be dried or ashed. A separation of the matrix can usually be achieved with a careful selection of the heating sequence. ETV instruments are able to reach 2800°C, which is similar to the 2500-3000°C temperature range exhibited by DSI probes when immersed in a plasma.

The ETVs can accommodate slurry, liquid and solid samples and are free from matrix interferences caused by viscous samples. Sample concentration and speciation are also possible and a lot of work on chemical modifiers for GFAAS in the literature can be applied to ETV-ICP. Detection limits are usually one to two orders of magnitude better than those of nebulization and are obtained from a small mass of sample (5-100 mg).

1.3.3.2.1 Instrumentation

The ETV instrumentation is centered around the vaporizer unit, usually enclosed within an argon-filled container. The various geometries adopted for the vaporizer include tubes, ribbons, boats, filaments, foils and rods.

The most widely used material is graphite although it is rarely used without surface treatment either by formation of a pyrolytic coating or by modification with metal carbide [138]. The modification of the graphite by formation of a metal carbide can be achieved from treatment with solutions of compounds of elements such as Zr, W, and especially Ta [136,139,140]. A carbon cup was employed by Ng and Caruso [136,141] while a carbon rod was preferred by Kirkbright [113,134,142-144]. Tubes are also widely used as they are available commercially for GFAAS instruments and exhibit a dead volume of less than 1 ml [130,131].

Metallic platforms include tungsten and tantalum foils 1 mm thick or molybdenum and rhenium strips 0.1 mm thick [145], platinum and tungsten filaments [146]. Tungsten ribbons with a 50 µl depression as sample reservoir are also used with a hydrogen/argon gas mixture to prevent oxidation of the metallic support [137]. A tantalum filament was utilized in the first adaptation of an electrothermal device for ICP-AES by Nixon *et al.* [147]. Volatilization of osmium from a glass (Pyrex) cup was attempted with mitigated success [148]. The sample was vaporized at a moderate temperature and merged with a mist of water for analysis by ICP-MS.

The ETV chamber is usually connected with the torch by a Tygon tubing. The bulkier design of commercial units usually requires a connection length of 50 to 80 cm, which can cause transport losses. More compact designs allow the unit to be mounted directly below the ICP torch box so that only few centimeters of tubing are required to connect them [149]. Direct mating of the ETV with the ICP torch has also been described [150-153]. This configuration eliminates the connecting tube and greatly reduces diffusion and sample losses on the inner walls of the conduits.

1.3.3.2.2 Mechanism of Vaporization

Even with some pretreatment, the graphite still forms a reactive surface and is a relatively porous material. The migration of Cd, Cu and Ag from deposited solution was investigated [154-156]. These studies revealed that the transient signal obtained in GFAAS is greatly influenced by the nature of the interaction of each metal with active sites in the graphite, as well as by the mechanism involved in the diffusion of the metal back to the surface. Copper, for example, is vaporized from small droplets of metals while cadmium evaporates as separated atoms.

Styris has provided a thorough review of the various chemical mechanisms involved in sample vaporization [157]. The basic mechanisms involve solid-state and gas-phase reactions occurring in a inherently dynamic environment. The complex nature of the vaporization is related also to the dependencies of these processes on temperature, lattice strain and lattice defects in the graphite. In general, the vaporization of metals can be grouped in four classes [157,158]:

1. Reduction of solid oxides on the graphite surface (M = Co, Cr, Cu, Fe, Mo, Ni, Pb, Sn and V),

$$MO(s) + C(s) \rightarrow M(l) \leftrightarrow \tfrac{1}{2}M_2(g) \rightarrow M(g) \qquad (1\text{-}1)$$

2. Thermal decomposition of solid oxides (M = Al, Cd an Zn),

$$MO(s) \rightarrow M(g) + \tfrac{1}{2}O_2(g) \qquad (1\text{-}2)$$

3. Dissociation of gaseous oxides (M = Cd, Mg, Mn, and Zn),

$$MO(s) \leftrightarrow MO(g) \rightarrow M(g) + \tfrac{1}{2}O_2(g) \qquad (1\text{-}3)$$

4. Dissociation of halide molecules in the vapour phase (M = Cd, Fe and Zn; X = Cl),

$$MX_2(s) \rightarrow MX_2(l) \rightarrow MX(g) + X(g) \rightarrow M(g) \qquad (1\text{-}4)$$

Styris [157] concluded this review with the general observation that the Langmuir gas film formed at the surface of the graphite, and the atomizer surface, are the principal controlling factors in atomization/vaporization processes. The gas film favors gas-phase reactions and reactions with adsorbed species. Oxygen also plays a central role as it may lock active sites on the graphite surface.

1.3.3.2.3 Transport Efficiency

As mentioned earlier, the mechanisms of atomization elucidated in GFAAS studies can sometimes be transposed to ETV. A fundamental distinction between the two techniques however, is that in ETV-ICP, the formation of an atomic cloud of elements is not required and is, in fact, not desirable. When ETVs are used as sample introduction system, we use the term *vaporization* instead of *atomization*. The concept of sample vaporization includes the formation of a large variety of particles size ranging from single atoms to micron size aggregates. This process has been described as *thermal dispersion* and most of the description that follows is taken from the cornerstone paper of Kàntor [159] on that subject. Large aggregates are formed in a step following the initial evaporation of the metal from the surface. At this point, the metal vapor generally undergoes a physical condensation process as the atomic cloud is carried away from the hot surface and mixed with colder gas layers. Particles evolve from the nuclei and eventually form a dry aerosol that can be efficiently transported to the plasma torch. The formation of the final dispersion occurs in several steps and can involve either self-nucleating species as in *homogeneous nucleation* or physical condensation of the vapor on already existing particles as in *heterogeneous nucleation*.

In homogeneous nucleation, the formation of stable nuclei takes place when the clusters occurring naturally in the saturated vapor phase from collisions of species grow beyond a critical size. The critical diameter d_p^* depends on the surface tension of the liquid droplets (σ), the molecular volume of the vapor (V_m) and the saturation ratio S, according to eqn 1-5:

$$d_p^* = 4\sigma V_m / kT \ln S \qquad (1\text{-}5)$$

Where k is the Boltzmann's constant and T is the temperature. The saturation ratio S is a measure of the supersaturation magnitude and is defined as the ratio of partial vapor pressure p_{vap}, over the equilibrium vapor pressure at the temperature of nucleation, $p_e(T)$:

$$S = p_{vap} / p_e(T) \qquad (1\text{-}6)$$

Supersaturation is required to form stable nuclei as the vapor tension exhibited by the liquid over small nuclei is higher than normal due to the degree of curvature of the surface (Kelvin effect). At a given saturation S, nuclei having a diameter greater than d_p^* grow while those having a smaller diameter evaporate. In the particular conditions found in ETVs at sample vaporization, the partial vapor pressure attained for a given element can be estimated using eqn 7:

$$p_{vap} = N_s T_g R / V_g t_v \qquad (1\text{-}7)$$

Where p_{vap} is expressed in atm, N_s is the amount of vapor of evaporated sample (in mol), T_g the temperature and V_g the flow rate of the carrier gas (without heating), R the gas constant and t_v the mean evaporation time of the major fraction of the sample. The different volatilities of the substances involved come into play at this point. For a given partial pressure p_{vap}, a higher degree of supersaturation is attained for substances with low volatility (the equilibrium vapor pressure $p_e(T)$ for these substances are low, see eqn 6). Stable nuclei are therefore formed more readily. Heterogeneous condensation takes place when the concentration of particles evolved from nuclei reaches a critical level. The vapor then condenses directly on already formed particles. *Brownian coagulation* occurs at a higher concentration of particles by adherence of two particles following a collision. However, *coalescence* and *sintering* of particles become appreciable when the initial concentration in vapor is over 1-10 μg/cm^3 and can cause analyte losses by gravitational separation.

Taking into consideration the condensation mechanisms from nuclei growth to brownian coagulation, it was demonstrated that the mean particles diameter is proportional to the initial vapor concentration raised to the power of 0.4, which indicates that a *"large change of vapour concentration is required to produce a significant change in the aerosol characteristics*" [160]. This is a prerequisite for obtaining a high dynamic range from ETV used as a sample introduction system.

Volatile elements, however, can be transported efficiently in the presence of particles formed from less volatile compounds. In this case, the volatile vapor condenses on the surface of already formed particles. With the fast heating rates used with ETV instrumentation, substances with different volatilities will coexist in the carrier gas stream and this process is likely to occur especially with highly concentrated matrices. The condensation of analyte vapor on particles of foreign origin is expected to enhance the transport efficiency and therefore generate a *carrier effect*, especially for the more volatile elements. However, if coalescence and sintering of particles formed from the major sample component occur, it will also carry along a significant part of the volatile analytes and cause losses.

Cadmium evaporated as a monocomponent is a limit case as it is one of the most volatile elements. The evaporation of cadmium has been studied in several reports [142,143,161,162] and the general observations were that the atomic vapor persisted a long distance away from the evaporating surface (up to 3 meters). Moreover, the transport efficiencies were generally low - usually less than 50% without the use of modifiers - and varied greatly according to the initial amount of cadmium evaporated, being as low as 9% when just 1 ng of metal was deposited [143]. Losses of cadmium vapor occurred from deposition onto the inner walls of the tubing. In comparison, atomic Ag and Cu persisted less than 2 cm away from the graphite rod and exhibited more important dynamic ranges than cadmium in similar conditions [161]. Other volatile metals likely to show losses from vapor deposition are Zn [163] and As [143].

It appears that the design of the ETV is a critical parameter for the aerosol formation. The proper mixing of the hot analyte vapor with colder gas streams generates the saturation of vapor required for the formation of growing nuclei. Another contribution to the transport of analytes is the nature of the evaporating surface. A direct measurement of particles size at the exit of a graphite furnace revealed that as much as 1.2 µg of carbon particles is emitted during an ETV empty firing [164]. The majority of particles have a diameter in the 0.1-0.2 µm range. When 0.1 µg of NaCl is added to the furnace, the number of particles and the total area on particle surface available for condensation both showed a marginal increase. Deposition of bigger particles of 5 µm of diameter appeared to be more severe in bended tubes than in longer straight tubes. These carbon particles may act as physical carriers for volatile analytes in ETV instruments using graphite as a support material.

1.3.3.2.4 Chemical Modifiers

The use of chemical modifiers in furnaces has been proposed to stabilize analytes and control atomization in GFAAS applications. Styris provided a good review of the numerous chemical additives in use in GFAAS and of the chemical mechanisms involved [157]. However, in ETV coupled to ICP instruments the purpose of using chemical modifiers is to enhance the volatility of the analyte and prevent losses by condensation in the connection tubing. Some modifiers are used as stabilizers to avoid losses in early stages of the temperature program.

The modifiers act primarily as physical carriers of analyte elements. The general trend for any given modifier is that the enhancement observed is similar for elements of different volatilities and chemical properties. The results obtained by Ediger and Beres [165] brought the authors to state as general rules that the matrix nature is of little importance and that the effect is more dependent on the initial amount of analyte. Signal suppression, however, is observed for very high matrix loading due to particles coalescence or, for ICP-MS, space charge effects. The use of palladium nitrate, sodium chloride and magnesium nitrate as transport enhancers were investigated and in most cases resulted in enhanced signal and a better linearity in the low end of the calibration curves for 20 elements. Organic modifiers provided the formation of carbon particles that generated the same benefits as the inorganic modifiers due to the carrier effect. The author suggested that a specific chemical interaction occurs for palladium added over mercury and tellurium added over cadmium, because of the unexpected signal enhancement observed in both cases. Grégoire and Sturgeon [133] advocated the use of diluted seawater as a universal modifier for ETV-ICP-MS, because it consists of light elements that do not generate serious space-charge effects and also because of the minimal interferences caused by the molecular ions formed. The monitoring of the argon dimer species (Ar_2^+) is also proposed for detecting any signal suppression from high matrix loads. Several studies investigated specific analyte/modifier pairs such as cadmium enhanced by selenium [143] or uranium [166], thallium enhanced by lead and copper matrices [167], or osmium enhanced in the presence of tellurium [168].

Another class of chemical modifiers releases the analytes from the interaction with the atomizer surface by chemical reaction. It is well known that some classes of elements form refractory carbides with the graphite surface. This is the case for the elements of group IV, V and VIA of the periodic table and also of the rare earth elements. For example, tungsten carbide have a boiling point of 6000°C. The formation of chloride or fluoride derivatives of these metals form compounds exhibiting boiling points below 2500°C [169]. The ETV provides a controllable temperature and the long reaction time required to easily accomplish the halogenation reaction.

The halogenating agent can be introduced into the furnace as a solid additive as proposed by Nickel and Zadgorska [170]. Several fluoride and chloride compounds - inorganics or organics - were tried. However, a combination of BaO plus CoF_2 was found to be the most effective for analyzing a ceramic powder by ETV-ICP-AES. With this combination of modifiers, a total disruption of the investigated silicon carbide ceramic was observed. Polytetrafluoroethylene in a slurry form was also introduced as halogenating agent for the determination of Mo in food samples [171] and chromium in biological samples [172]. A detection limit of 0.7 ng/ml for Mo in foods was obtained with total elimination of memory effects. Ammonium chloride proved to be effective by reacting with V, U and Cr and dynamic ranges spanning three orders of magnitude with sub-nanogram detection limits were obtained in ETV-ICP-AES using this modifier [136].

Modifiers in gaseous form exhibit several practical advantages over solid modifiers. They are easily available at a high degree of purity, they are present throughout the high temperature cycle and they allow an easy automation of the analytical process. The first attempt at using gaseous halogenating agent was reported by Kirkbright [144] for the determination of B, Mo, Zr, Cr and W over a graphite rod ETV-ICP-AES. Carbon tetrachloride and trifluoromethane (Freon-23) where introduced into the argon stream to prevent the formation of carbides. Loss of boron presumably as BCl_3 was observed at the drying stage with the argon/CCl_4 mixture, a problem solved by the replacement of CCl_4 with the thermally more stable Freon-23. All memory effects observed in pure argon atmosphere disappeared with the use of both gas mixtures and detection limits were enhanced. The use of Cl_2/argon mixture was also attempted by Matousek *et al.* [173] in ETV-ICP-AES for Cr, V, Ti, W and Zr. Formation of chlorides of these metals was invoked to explain analytical performances identical to the one observed in halocarbon atmosphere. One may question, however, the appropriateness of using gaseous chlorine, a highly corrosive gas, for routine work. Ren and Salin [132,169,174] modified a commercial ETV unit for use with corrosive carrier gas flow and used a Freon-12/argon mixture. Freon-12 (dichlorodifluoromethane) has the advantage of releasing chlorine and fluorine species that both react with the sample. Very good detection limits and linear response were obtained from liquid standards. However, acceptable to good results were observed for coal fly ash and marine sediments reference materials. Barnes and Fodor have also proposed the use of a freon containing chlorine and fluorine (chlorodifluoromethane) for the determination of 13 elements in urine samples with a graphite rod ETV-ICP-AES [128]. The determination of W and Mo at low levels in geological samples by isotope dilution was attempted in ETV-ICP-MS with introduction of Freon-23 [38]. The samples were submitted to alkaline fusion with sodium carbonate and nitrate salts, and the determination done directly on the melt. Although the detection limits attained for both metals were excellent, the memory effect for tungsten could not be entirely removed with the use of a halogenating agent. Recently, Goltz *et al.* [175] suggested the use of Freon-23 for enhancing the transient signals from rare earth elements in ETV-ICP-MS. Transients were improved and peak tailing eliminated for Lu, Tb and Gd. Lutecium actually vaporized at a lower temperature when Freon-23 was added suggesting that halide species may have been formed.

1.3.3.2.5 Sample Preconcentration in ETV

A preliminary concentration of the analytes in an electrothermal vaporizer was attempted by several workers. Using an aerosol deposition technique already proposed for GFAAS [131], a preconcentration of liquid sample was obtained by Matusiewicz and Barnes [131] by depositing a sample aerosol on the surface of a graphite platform in controlled conditions. The surface was kept typically at 110°C, allowing the water to be evaporated and evacuated during the deposition. However, the commercial FASTAC nebulizer used exhibited a transfer efficiency of 10%, and the detection limits for Cr, Cu, Mn and Ni obtained with aerosol deposition of 50 μl of sample were similar to the ones obtained from direct deposition of a 5 μl aliquot. A separation from electrolytes and organics and a selective preconcentration of As, Cr, Cu, Ni, and Se from an urine standard reference material was achieved on a poly(dithiocarbamate) resin [128]. The resin was subsequently dissolved in a small volume of concentrated HCl and evaluated using a graphite rod ETV-ICP-AES instrument. This technique offered a standardization of the matrix in addition to providing some level of preconcentration. A good agreement with certified values was observed.

1.3.3.2.6 Applications of ETV for ICP Atomic Analysis.

Numerous applications of the ETV for ICP instruments were reported and several good reviews on that subject can be consulted by the reader [61,88,135,176,177]. Recent applications not mentioned earlier in this chapter include the determination of trace metals in botanical samples [97], in powdered coal, total diet, lobster hepatopancreas samples [178,179] and oyster tissue samples [178], in total diet and milk powder samples [180], in vehicle exhaust particles and pond sediment [181], and in mussel tissue, olive leaves, rye grass, sea lettuce, tomato leaves and light sandy soil and sediments samples [53]. The elements investigated usually exhibit some toxicity or biological activity. Lead was evaluated in fly ash samples [182], arsenic hydride generated from drinking water and urine samples was trapped on Pd strips and subsequently determined by ETV-ICP-MS [145], and phosphorus in metal silicon samples was measured by ETV-ICP-AES after acid digestion and extraction with 4-methyl-2-pentanone (MIBK) [183]. Trace and major elements were determined in marine sediment and coal fly ash samples by ETV-ICP-AES using an argon/freon gas mixture [174]. The same workers have also analyzed several refractory oxides and carbides as pure compounds using the same instruments and gas mixture [169].

The microsampling capability, the good detection limits, and the relative robustness toward matrices of the ETV-ICP techniques are advantageous for the determination of trace metals in botanical, biological, geological and environmental samples. The major drawbacks are that sample homogeneity is mandatory especially for solid samples because of the small sample sizes, and the use of chemical modifiers is often required for the analysis of real samples. Also, operating parameters have to be adapted to each type of sample and there is still no universal strategy applicable to the routine analysis of various matrices. The potential of this technique is however recognized by major ICP-MS manufacturers and most of them offer an ETV attachment for sample introduction with their instruments.

1.4 Summary of Thesis Content

This study began with an attempt at preconcentrating samples in graphite furnaces from nebulization of sample and with the use of an halogenating gas mixture to break down and analyze mineral matrices. The experimental results contained in this thesis are as follows:

- ***Chapter 2*** describes the use of an argon/freon gas mixture to analyze refractory elements in a stable mineral matrix (zeolite), using a graphite furnace ETV unit modified for this purpose.
- ***Chapter 3*** presents the result obtained when liquid samples are preconcentrated in a graphite furnace by spraying, and analyzed later by ICP-AES.
- ***Chapter 4*** proposes the use of plasma argides species in ETV-ICP-MS studies to provide an instant diagnosis of the plasma state, especially with regard to the water load, and to correct transient shapes by signal convolution.
- ***Chapter 5*** presents the results of sample spray preconcentration in graphite furnace coupled with ICP-MS instrumentation.

1.5 References

[1] *Inductively Coupled Plasmas in Analytical Atomic Spectrometry*, Eds. A. Montaser and D. W. Golightly, VCH Publishers, New York, 2nd Edition (1992).

[2] *Inductively Coupled Plasma Emission Spectrometry Part I. Methodology, Instrumentation and Performance*, Ed. P.W.J.M. Boumans, John Wiley & Sons, New York, 1st Edition (1987).

[3] G. Horlick, *J. Anal. At. Spectrom.* **9,** 593 (1994).

[4] G. Horlick and Y. Shao, *Inductively Coupled Plasma -Mass Spectrometry for Elemental Analysis*, in *Inductively Coupled Plasmas in Analytical Atomic Spectrometry*, Eds. A. Montaser and D. W. Golightly, pp. 551-612, VCH Publishers, New York (1992).

[5] G. M. Hieftje, *Spectrochim. Acta* **44B,** 113 (1989).

[6] G. A. Meyer, *Anal. Chem.* **59,** 1345a (1987).

[7] R. S. Houk, *Anal. Chem.* **52,** 297a (1980).

[8] C. Moore, *Mass Spectrometry*, in *Kirk-Othmer Encyclopedia of Chemical Technology*. pp. 1071-1094, vol. 15 (1993).

[9] H. Niu and R. S. Houk, *Spectrochim. Acta* **51B,** 779 (1996).

[10] D. J. Douglas, *Fundamental Aspects of Inductively Coupled Plasma-Mass Spectrometry*, in *Inductively Coupled Plasmas in Analytical Atomic Spectrometry,* Eds. A. Montaser and D. W. Golightly, pp. 613-650, VCH Publishers, Inc, New York (1992).

[11] R. S. Houk, *Anal. Chem.* **58,** 97A (1986).

[12] X. Yan, T. Tanaka and H. Kawaguchi, *Appl. Spectrosc.* **50,** 182 (1995).

[13] T. J. Cleland and F. R. Meeks, *Spectrochim. Acta* **51B,** 1487 (1996).

[14] J. S. Crain, F. G. Smith and R. S. Houk, *Spectrochim. Acta* **45B,** 249 (1990).

[15] A. F. Parisi, G. D. Rayson, G. M. Hieftje and J. W. Olesik, *Spectrochim. Acta* **42B,** 361 (1987).

[16] Y. Q. Tang and C. Trassy, *Spectrochim. Acta* **41B,** 143 (1986).

[17] N. Furuta, *Spectrochim. Acta* **40B,** 1013 (1985).

[18] J. A. M. van der Mullen, *Spectrochim. Acta* **45B,** 1 (1990).

[19] J. A. M. van der Mullen, *Spectrochim. Acta* **45B,** 233 (1990).

[20] J. A. M. van der Mullen, *Spectrochim. Acta* **44B,** 1067 (1989).

[21] M. Huang and G. M. Hieftje, *Spectrochim. Acta* **44B,** 793 (1989).

[22] J. A. M. van der Mullen, S. Nowak, A. C. A. P. van Lammeren, D. C. Schrain and B. van der Syde, *Spectrochim. Acta* **43B,** 317 (1988).

[23] J.-M. Mermet, *Spectrochim. Acta* **30B,** 383 (1975).

[24] I. Marawi, B. Bielski, J. A. Caruso and F. R. Meeks, *J. Anal. At. Spectrom.* **7,** 899 (1992).

[25] E. Michaud-Poussel and J.-M. Mermet, *Spectrochim. Acta* **42B,** 1163 (1987).

[26] A. Batal, J. Jarosz and J.-M. Mermet, *Spectrochim. Acta* **36B,** 983 (1981).

[27] P. W. J. M. Boumans and J. J. A. M. Vrakking, *Spectrochim. Acta* **42B,** 553 (1987).

[28] M. Cai, I. Ishii, R. H. Clifford, A. Montaser, B. A. Palmer and L. R. Layman, *Spectrochim. Acta* **49B,** 1081 (1994).

[29] N. N. Sesi, A. Mackenzie, K. E. Shanks, P. Yang and G. M. Hieftje, *Spectrochim. Acta* **49B,** 1259 (1994).

[30] J. W. H. Lam and G. Horlick, *Spectrochim. Acta* **45B,** 1327 (1990).

[31] J. W. H. Lam and G. Horlick, *Spectrochim. Acta* **45B,** 1313 (1990).

[32] M. Murillo and J.-M. Mermet, *Spectrochim. Acta* **44B,** 359 (1989).

[33] J. C. Ivaldi and J. F. Tyson, *Spectrochim. Acta* **50B,** 1207 (1995).

[34] D. C. Grégoire, *Anal. Proc.* **29,** 276 (1992).

[35] D. C. Grégoire, *Prog. Analyt. Spectrosc.* **12,** 433 (1989).

[36] J. W. McLaren, D. Beauchemin and S. S. Berman, *Spectrochim. Acta* **43B,** 413 (1988).

[37] D. Beauchemin, J. W. McLaren, A. P. Mykytiuk and S. S. Berman, *Anal. Chem.* **59,** 778 (1987).

[38] C. J. Park and E. M. Hall, *J. Anal. At. Spectrom.* **2,** 473 (1987).

[39] H. Klinkenberg, W. Van Borm and F. Souren, *Spectrochim. Acta* **51B,** 139 (1996).

[40] D. Beauchemin, J. W. McLaren and S. S. Berman, *Spectrochim. Acta* **42B,** 467 (1987).

[41] Q. Xie and R. Kerrich, *J. Anal. At. Spectrom.* **10,** 99 (1995).

[42] A. Gray and A. R. Date, *Analyst* **108,** 1033 (1983).

[43] S. R. Koirtyohann, S. J. Jones and D. A. Yates, *Anal. Chem.* **52,** 1965 (1980).

[44] R. S. Houk, *ICP-MS III Instrument Selection and Applications*. (1996).

[45] S. D. Tanner, L. M. Cousins and D. J. Douglas, *Appl. Spectrosc.* **48,** 1367 (1994).

[46] D. M. Chambers, B. M. Ross and G. M. Hieftje, *Spectrochim. Acta* **46B,** 785 (1991).

[47] D. M. Chambers and G. M. Hieftje, *Spectrochim. Acta* **46B,** 761 (1991).

[48] M. A. Vaughan and G. Horlick, *Spectrochim. Acta* **45B,** 1301 (1990).

[49] J. S. Crain, R. S. Houk and F. G. Smith, *Spectrochim. Acta* **43B,** 1355 (1988).

[50] A. Gray, *Spectrochim. Acta* **41B,** (1986).

[51] S. J. Georgitis, M. Plantz and S. Anderson, *A Comparison of Techniques for the Reduction of ArO Interference in ICP-MS*, Varian Corp. (1996).

[52] S. D. Tanner, *J. Anal. At. Spectrom.* **10,** 905 (1995).

[53] F. Vanhaecke, L. Galbács, S. Boonen, L. Moens and R. Dams, *J. Anal. At. Spectrom.* **10,** 1047 (1995).

[54] E. Poussel, J.-M. Mermet and D. Deruaz, *J. Anal. At. Spectrom.* **9,** 61 (1994).

[55] Y. Shao and G. Horlick, *Appl. Spectrosc.* **45,** 143 (1991).

[56] M. A. Vaughan and G. Horlick, *Spectrochim. Acta* **45B,** 1289 (1990).

[57] D. J. Douglas, *Spectrochim. Acta* **41B,** 197 (1986).

[58] A. Gray, *ICP Inf. News.* **10,** 196 (1984).

[59] R. F. Browner and A. W. Boorn, *Anal. Chem.* **58,** 786A (1984).

[60] J. E. Meinhard, *ICP Inf. News.* **2,** 163 (1976).

[61] A. G. T. Gustavsson, *Liquid Sample Introduction into Plasmas,* in *Inductively Coupled Plasmas in Analytical Atomic Spectrometry,* Eds. A. Montaser and D. W. Golightly, pp. 679-720, VCH Publishers, New York (1992).

[62] A. G. T. Gustavsson, *Anal. Chem.* **56,** 815 (1984).

[63] A. G. T. Gustavsson, *Anal. Chem.* **55,** 94 (1983).

[64] S. Greenfield and A. Montaser, *Common RF Generators, Torches, and Sample Introduction Systems*, in *Inductively Coupled Plasmas in Analytical Atomic Spectrometry,* Eds. A. Montaser and D. W. Golightly, pp. 187-246, VCH Publishers, New York (1992).

[65] R. N. Kniseley, H. Amenson, C. C. Butler and V. A. Fassel, *Appl. Spectrosc.* **28,** 285 (1974).

[66] G. Légère and P. Burgener, *ICP Inf. News.* **13,** 521 (1982).

[67] R. S. Babington, *Popular Sci.* 102 (1973).

[68] S. Walter and A. Hatterer, *J. Anal. At. Spectrom.* **9,** 525 (1994).

[69] T. R. Smith and M. B. Denton, *Appl. Spectrosc.* **44,** 21 (1990).

[70] V. Hernandis, J. L. Todoli, A. Canals and J. V. Sala, *Spectrochim. Acta* **50B,** 985 (1995).

[71] F. E. Lichte, *Anal. Chem.* **54,** 638 (1982).

[72] G. A. Meyer, J. S. Roeck and M. L. Vestal, *ICP Inf. News.* **10,** 955 (1985).

[73] V. A. Fassel and B. R. Bear, *Spectrochim. Acta* **41B,** 1089 (1997).

[74] R. H. Clifford, A. Montaser, S. P. Dolan and S. G. Capar, *Anal. Chem.* **62,** 2745 (1990).

[75] Q. Jin, C. Zhu, K. Brushwyler and G. M. Hieftje, *Appl. Spectrosc.* **44,** 183 (1990).

[76] K. K. Stewart, G. R. Beecher and P. E. Hare, *Anal. Biochem.* (1997).

[77] J. Ruzicka and E. H. Hansen, *Anal. Chim. Acta* **78,** 145 (1975).

[78] M. Abdullah, K. Fuwa and H. Haraguchi, *Appl. Spectrosc.* **41,** 715 (1987).

[79] M. M. Habib and E. D. Salin, *Anal. Chem.* **57,** 2055 (1985).

[80] H. C. Hoare and R. A. Mostyn, *Anal. Chem.* **39,** 1153 (1967).

[80a] R. Guevremont and K. N. De Silva, *Spectrochim. Acta* **47B,** 371 (1992).

[81] K. N. De Silva and R. Guevremont, *Spectrochim. Acta* **45B,** 997 (1990).

[81a] R. Guevremont and K. N. De Silva, *Spectrochim. Acta* **46B,** 67 (1991).

[82] R. M. Dagnall, D. J. Smith and T. S. West, *Anal. Chim. Acta* **54,** 397 (1971).

[83] A. Aziz, J. A. C. Broekaert, K. Laqua and F. Leis, *Spectrochim. Acta* **39B,** 1091 (1984).

[84] J. P. Keilson, R. D. Deutsch and G. M. Hieftje, *Appl. Spectrosc.* **37,** 451 (1983).

[85] R. H. Scott, *Spectrochim. Acta* **33B,** 123 (1978).

[86] E. R. Denoyer, K. J. Fredeen and J. W. Hager, *Anal. Chem.* **63,** 445A (1991).

[87] M. Thompson, J. E. Goulter and F. Sieper, *Analyst* **106,** 82 (1981).

[88] C. W. McLeod, M. W. Routh and M. W. Tikkanen, *Introduction of Solids into Plasmas*, in *Inductively Coupled Plasmas in Analytical Atomic Spectrometry,* Eds. A. Montaser and D. W. Golightly, pp. 721-780, VCH Publishers, New York (1992).

[89] J. W. Carr and G. Horlick, *Spectrochim. Acta* **37B,** 1 (1982).

[90] P. Arrowsmith and S. K. Hughes, *Appl. Spectrosc.* **42,** 1231 (1988).

[91] T. Mochizuki, A. Sakashita, H. Iwata, T. Kagaya, T. Shimamura and P. Blair, *Anal. Sci.* **4,** 403 (1988).

[92] D. A. Cremers, F. L. Archuleta and H. C. Dilworth, *SPIE* **540,** 542 (1985).

[93] P. Arrowsmith, *Anal. Chem.* **59,** 1437 (1987).

[94] L. Ebdon, M. Foulkes and K. Sutton, *J. Anal. At. Spectrom.* **12,** 213 (1997).

[95] J. R. Dean, L. Ebdon and R. Massey, *J. Anal. At. Spectrom.* **2,** 369 (1987).

[96] N. Mohamed, R. M. Brown and R. C. Fry, *Appl. Spectrosc.* **35,** 153 (1981).

[97] Y. Qin, Z. Jiang, Y. Zeng and B. Hu, *J. Anal. At. Spectrom.* **10,** 455 (1995).

[98] L. Ebdon, M. Foulkes, H. G. Parry and C. T. Tye, *J. Anal. At. Spectrom.* **3,** 753 (1988).

[99] H. G. Parry and L. Ebdon, *Anal. Proc.* **25,** 69 (1988).

[100] J. G. Williams, A. L. Gray, P. Norman and L. Ebdon, *J. Anal. At. Spectrom.* **2,** 469 (1987).

[101] V. Karanassios, L. Usypchuck, P. Moss and E. D. Salin, *J. Anal. At. Spectrom.* **7,** 1243 (1992).

[102] L. Ebdon, M. Foulkes and S. J. Hill, *J. Anal. At. Spectrom.* **5,** 67 (1990).

[103] J. C. Fariñas, R. Moreno and J.-M. Mermet, *J. Anal. At. Spectrom.* **9,** 841 (1994).

[104] L. S. Gervais and E. D. Salin, *J. Anal. At. Spectrom.* **6,** 41 (1991).

[105] G. Záray, I. Varga and T. Kántor, *J. Anal. At. Spectrom.* **9,** 707 (1994).

[106] L. Halicz and I. B. Brenner, *Spectrochim. Acta* **42B,** 207 (1987).

[107] L. Ebdon, M. Foulkes and K. O'Hanlon, *Anal. Chim. Acta* **311,** 123 (1995).

[108] P. Goodall, M. E. Foulkes and L. Ebdon, *Spectrochim. Acta* **48B,** 1563 (1993).

[109] W. T. Chan and G. Horlick, *Appl. Spectrosc.* **44,** 380 (1990).

[110] M. Umemoto and M. Kubota, *Spectrochim. Acta* **42B,** 491 (1987).

[111] E. D. Salin and G. Horlick, *Anal. Chem.* **51,** 2284 (1979).

[112] D. Sommers and K. Ohls, *Fresenius' Z. Anal. Chem.* **304,** 97 (1980).

[113] G. F. Kirkbright and Z. Li-Xing, *Analyst* **107,** 617 (1982).

[114] V. Karanassios, V. Abdullah and G. Horlick, *Spectrochim. Acta* **45B,** 119 (1990).

[115] E. D. Salin and R. L. A. Sing, *Anal. Chem.* **56,** 2596 (1984).

[116] G. E. M. Hall, J.-C. Pelchat, D. W. Boomer and M. J. Powell, *J. Anal. At. Spectrom.* **3,** 791 (1988).

[117] R. L. A. Sing and E. D. Salin, *Anal. Chem.* **61,** 163 (1989).

[118] M. Abdullah and H. Haraguchi, *Anal. Chem.* **57,** 2059 (1985).

[119] Y. Shao and G. Horlick, *Appl. Spectrosc.* **40,** 368 (1986).

[120] V. Karanassios, V. Abdullah and G. Horlick, *Spectrochim. Acta* **45B,** 105 (1990).

[121] V. Karanassios and G. Horlick, *Spectrochim. Acta* **45B,** 85 (1990).

[122] R. Rattray and E. D. Salin, *J. Anal. At. Spectrom.* **10,** (1995).

[123] L. Blain and E. D. Salin, *Spectrochim. Acta* **47B,** 399 (1992).

[124] C. W. McLeod, P. A. Clarke and D. J. Mowthorpe, *Spectrochim. Acta* **41B,** 63 (1986).

[125] G. Zaray, J. A. C. Broekaert and F. Leis, *Spectrochim. Acta* **43B,** 241 (1988).

[126] J. M. Carey, E. Hywel Evans, J. A. Caruso and W.-L. Shen, *Spectrochim. Acta* **46B,** 1711 (1991).

[127] W.-L. Shen, J. A. Caruso, F. L. Fricke and R. D. Satzger, *J. Anal. At. Spectrom.* **5,** 451 (1990).

[128] R. M. Barnes and P. Fodor, *Spectrochim. Acta* **38B,** 1191 (1983).

[129] A. Aziz, J. A. C. Broekaert and F. Leis, *Spectrochim. Acta* **37B,** 369 (1982).

[130] H. Matusiewicz and R. M. Barnes, *Spectrochim. Acta* **40B,** 29 (1985).

[131] H. Matusiewicz and R. M. Barnes, *Spectrochim. Acta* **40B,** 41 (1985).

[132] J. M. Ren and E. D. Salin, *J. Anal. At. Spectrom.* **8,** 59 (1993).

[133] D. C. Grégoire and R. E. Sturgeon, *Spectrochim. Acta* **48B,** 1347 (1993).

[134] A. M. Gunn, D. L. Millard and G. F. Kirkbright, *Analyst* **103,** 1066 (1978).

[135] K. C. Ng and J. A. Caruso, *Appl. Spectrosc.* **39,** 719 (1985).

[136] K. C. Ng and J. A. Caruso, *Analyst* **108,** 476 (1983).

[137] R. Tsukahara and M. Kubota, *Spectrochim. Acta* **45B,** 779 (1990).

[138] A. B. Volynsky, *Spectrochim. Acta* **50B,** 1417 (1995).

[139] A. B. Volynsky, *J. Anal. Chem. USSR* **42,** 1223 (1987).

[140] V. J. Zatka, *Anal. Chem.* **50,** 538 (1978).

[141] K. C. Ng and J. A. Caruso, *Anal. Chem.* **9,** 1513 (1983).

[142] G. F. Kirkbright, D. L. Millard and R. D. Snook, *Anal. Proc. (Chem. Soc. London)* **17,** 16 (1980).

[143] D. L. Millard, H. C. Shan and G. F. Kirkbright, *Analyst* **105,** 502 (1980).

[144] G. F. Kirkbright and R. D. Snook, *Anal. Chem.* **51,** 1938 (1979).

[145] I. Marawi, L. K. Olson, J. Wang and J. A. Caruso, *J. Anal. At. Spectrom.* **10,** 7 (1995).

[146] E. Kitazume, *Anal. Chem.* **55,** 802 (1983).

[147] D. E. Nixon, A. F. Fassel and R. N. Kniseley, *Anal. Chem.* **46,** 210 (1974).

[148] T. Hirata, T. Akagi, H. Shimizu and A. Masuda, *Anal. Chem.* **61,** 2263 (1989).

[149] W. M. Blakemore, P. H. Casey and W. R. Collie, *Anal. Chem.* **56,** 1376 (1984).

[150] M. W. Tikkanen and T. M. Niemczyk, *Anal. Chem.* (1997).

[151] K. Ohls, *Mikrochim. Acta* **III,** 337 (1989).

[152] K. Ohls, J. Dewies and H. Loepp, *ICP Inf. News.* 177 (1986).

[153] K. Ohls and B. Hutsch, *ICP Inf. News.* **12,** 170 (1986).

[154] J. G. Jackson, R. W. Fonseca and J. A. Holcombe, *Spectrochim. Acta* **50B,** 1837 (1995).

[155] C. Eloi, J. Robertson and V. Majidi, *Anal. Atom. Spectrom.* **8,** 217 (1993).

[156] R. W. Fonseca, J. McNally and J. A. Holcombe, *Spectrochim. Acta* **48B,** 79 (1993).

[157] D. L. Styris and D. A. Redfield, *Spectrochimica Acta Rev.* **15,** 71 (1993).

[158] R. E. Sturgeon and C. L. Chakrabarti, *Prog. Analyt. Spectrosc.* **1,** 5 (1978).

[159] T. Kántor, *Spectrochim. Acta* **43B,** 1299 (1988).

[160] R. C. Flagan and S. Friedlander, *Particle formation in pulverised coal combustion-a review*. In *Recent Developments in Aerosol Science*, Ed. D. T. Shaw, John Wiley & Sons, New-York (1978).

[161] J. R. Dean and R. D. Snook, *J. Anal. At. Spectrom.* **1,** 461 (1986).

[162] P. Crabi, Cavalli, N. Achilli, G. Rossi and N. Omenetto, *At. Spectrosc.* **3,** 81 (1982).

[163] T. Kántor, E. Pungor, J. Szatisz and L. Bezúr, *Talanta* **26,** 357 (1979).

[164] C. M. Sparks, J. A. Holcombe and T. L. Pinkston, *Spectrochim. Acta* **48B,** 1607 (1993).

[165] R. D. Ediger and S. A. Beres, *Spectrochim. Acta* **47B,** 907 (1992).

[166] G. F. Kirkbright and R. D. Snook, *Appl. Spectrosc.* **37,** 11 (1983).

[167] C. J. Park and G. E. M. Hall, *Curr. Res., Geol. Survey Can.* **86-1B,** 767 (1986).

[168] D. C. Grégoire, *Anal. Chem.* **62,** 141 (1990).

[169] J. M. Ren and E. D. Salin, *Spectrochim. Acta* **49B,** 555 (1994).

[170] H. Nickel and Z. Zadgorska, *Spectrochim. Acta* **48B,** 25 (1993).

[171] B. Hu, Z. Jiang and Y. Zeng, *J. Anal. At. Spectrom.* **6,** 623 (1991).

[172] B. Hu, Z. Jiang, Y. Zeng and H. Zhu, *Anal. Sci.* **7,** 433 (1991).

[173] J. P. Matousek, R. T. Satumba and R. A. Bootes, *Spectrochim. Acta* **44B,** 1009 (1989).

[174] J. M. Ren and E. D. Salin, *Spectrochim. Acta* **49B,** 567 (1994).

[175] D. M. Goltz, D. C. Grégoire and C. L. Chakrabarti, *Spectrochim. Acta* **50B,** 1365 (1995).

[176] P. G. Mitchell and J. Sneddon, *Talanta* **34,** 849 (1987).

[177] H. Matusiewicz, *J. Anal. At. Spectrom.* **1,** 171 (1986).

[178] R. W. Fonseca and N. J. Miller-Ihli, *Appl. Spectrosc.* **49,** 1403 (1995).

[179] D. C. Grégoire, N. J. Miller-Ihli and R. E. Sturgeon, *J. Anal. At. Spectrom.* **9,** 605 (1994).

[180] R. W. Fonseca and N. J. Miller-Ihli, *Spectrochim. Acta* **51B,** 1591 (1996).

[181] I. Atsuya, T. Itoh and T. Kurotaki, *Spectrochim. Acta* **46B,** 103 (1991).

[182] S. A. Darke, C. J. Pickford and J. F. Tyson, *Anal. Proc.* **26,** 379 (1989).

[183] I. Ida, H. Yoshikawa, Y. Ishibashi and N. Gunji, *Anal. Sci.* **5,** 615 (1989).

Chapter 2

ZEOLITE SLURRY ANALYSIS USING FREON ASSISTED GRAPHITE FURNACE VAPORIZATION FOR INDUCTIVELY COUPLED PLASMA ATOMIC EMISSION SPECTROMETRY

In the course of experiments with ETV-ICP-AES, a peculiar analytical problem was submitted to professor Salin by visiting scientists from the University of Habana, in Cuba. A variety of zeolites was being used as experimental medication for treating a disease that had affected a significant part of the island's population in the preceding months. Zeolites form a class of minerals that exhibit catalytic activities and ion exchange capability. Obviously, the scientists were greatly interested in knowing the trace metal composition of this material of natural origin. It therefore represented a very interesting challenge from a scientific point of view as well as from a human perspective.

At that time, Jan-Min Ren had just terminated his thesis work on the use of gaseous chemical modifier for enhancing the volatilization of metals having high boiling points. The rational of this research work was to expose the analytes to a small amount of dichlorodifluoromethane, a gaseous halocarbon of small molecular weight also known by the trademark name Freon-12™, during sample vaporization at high temperature in order to improve the transport efficiency of the metals [1-3]. The use of Freon-12 was especially aimed at metals from groups IVA, VA and VIA of the periodic table, known to form carbides in the presence of graphite. One of these metals, tungsten, forms a carbide that exhibits the highest known boiling point. The transport enhancement was expected to proceed through formation of volatile chlorides and fluorides formed from reactive radicals, originating from the breaking of the Freon-12 molecule at high temperatures. Promising results were reported from the work of Ren and Salin using liquid standards and solid reference materials [1,2].

It was therefore decided to apply this technique to zeolite analysis to enhance analyte transport and to disrupt and digest the mineral in order to improve analyte recovery from the matrix. We used an ETV unit with in-house modifications introduced by Ren and Salin [3], and ran the experiments with a special interest in signal optimization. Professor Genaro Hernandez, a visiting scientist and one of the co-authors, and Jean-François Alary, were responsible for the experimental setup and ran the experiments under the supervision of professor Salin. The experimental results were treated by J.-F.A. and reported in a paper written by Alary, Hernandez and Salin, entitled *"Zeolite Slurry Analysis Using Freon Assisted Graphite Furnace Vaporization for Inductively Coupled Plasma Atomic Emission Spectrometry"* by Jean-François Alary, Genaro Hernandez and Eric D. Salin, Department of Chemistry, McGill University, Montreal, Quebec, Canada H3A 2K6 (J.-F.A and E.D.S.) and Institute of Materials and Reagents for Electronics (IMRE), University of Havana, Habana, Cuba (G.H.). The paper appeared in *Applied Spectroscopy*, volume 49, number 12, page 1796 (1995).

2.1 Abstract

Halogen assisted electrothermal vaporization (ETV) was used as a sample introduction mechanism for inductively coupled plasma atomic emission spectrometry. Freon-12™ was used as a gas phase halogenation reagent in the ETV graphite furnace to enhance vaporization of carbide forming elements by converting them into metal halides.

With Freon ETV, detection levels for Zn, Pb, Cd, Mn, V, Cu, Ti and Ca were lower than those obtained with conventional nebulization of liquid standards. A zeolite sample was analyzed for the refractory elements chromium and vanadium. Without freon, the signals for these elements were very low, however, with freon, the signals were dramatically improved. Detection limits of 1.4 μg/g and 0.3 μg/g respectively were obtained for these elements. A Sheathing and Cooling gas flow was introduced to reduce analyte vapor condensation on tubing walls and to promote aggregate formation. This additional flow enhanced the quality of signal with the zeolite but proved to be detrimental for the determination of refractory elements in liquid standards with or without halogenation. The precision of determination for the zeolite sample varied from 3% for cadmium, to 6% for lead.

2.2 Introduction

Conventional nebulization is widely used for inductively coupled plasma atomic spectrometry (ICP-AES) due to its simplicity and low cost [4]. Among the disadvantages of nebulization, however, are the poor handling of slurries [5] and other solid forms, and the requirement for a sample volume of at least 1 ml. Electrothermal Vaporization (ETV) for ICP-AES [6] has shown several advantages over conventional pneumatic nebulization. With the use of graphite furnace [3,7-10] or metal filament [11], electrothermal vaporization can offer a solid sample capability as well as better detection for microliters amount of sample. Moreover, since full control over the drying and vaporization stages is available, a carefully selected temperature program may vaporize the liquid or solid matrix separately from the elements of interest. For these reasons, ETV-ICP-AES has been proposed for the analysis of trace multielements in solid matrices such as ceramics [12].

Electrothermal vaporization, however, is still not a panacea for elemental analysis with the ICP. Kantor [13] has summarized the various effects that cause the transport efficiency of the aerosol to be dependent on sample and matrix loading. A stable aerosol will form through condensation, aggregation and coalescence in temperature conditions specific for each element. Efforts to improve ETV sample introduction devices have been directed toward increasing the efficiency of sample transport into the plasma, which results in lowered detection limits and improved linearity of calibration curves. Although significant improvements were obtained in that respect through various configurations for the furnace and its connection to the torch [3,6], a parallel approach consists for using chemical modifiers to form volatile halides. Some modifiers that have been tested include ammonium chloride [10], polytetrafluoroethylene [14,15], barium oxide and cobalt fluoride mixtures [12], copper and manganese chlorides [16], and gaseous chlorine/argon [17-19] and halocarbons/argon mixtures [1,2,20-22]. In general, they resulted in an enhancement of the transient signal, notably for carbide forming elements of group IVA, VA and VIA, and a reduction of carry-over effects for these metals.

This study is the continuation of previous work [1,2] done using Freon-12™ (CF2Cl2) as a chemical modifier added in small proportions to the carrier gas [22]. Although no direct observation of halides species were reported in literature [1,2,20-22], thermochemical equilibrium data [23] indicate that chlorides are formed from most carbide forming elements at the temperature levels achieved in a graphite furnace. In the same conditions, fluorine reacts preferentially with just a few elements such as titanium, aluminum and silicon [23], although Freon-23 (CHF3) was proved to enhance the determination of tungsten, titanium, zirconium and uranium [21,22]. Since aluminum and silicon are often the main constituents of numerous matrices, it would be advantageous to have both halogens available to prevent carbide formation and decompose a mineral matrix. In that respect, Freon-12 has the advantage of releasing chlorine and fluorine. When the furnace operates at low temperatures, all unused freon is destroyed moments later in the plasma. Moreover, in contrast to solid additives, gaseous modifiers can be obtained in very pure form, are easily manipulated and can be made available at any stage of the operating cycle, thus providing more complete control of the chemistry. In the future, when Freon-12 will not be available, other less volatile chloro-fluorocarbons under development should provide suitable substitutes.

In this study, we have tested the ability of Freon-12 to enhance the detectability of Zn, Pb, Cd, Cr, Mn, V, Cu, Ti and Ca for aqueous solutions with an emphasis on optimizing for the refractory elements. In addition, we have studied the effect of Freon-12 on a Zeolite sample which had been placed into the furnace in a slurried form. Zeolites, often used as molecular sieves, are crystalline aluminosilicates that contain appreciable amount of sodium, magnesium or calcium [24]. The AlO4 and SiO4 framework includes channels and voids occupied by the cations. Zeolites are widely used for their catalytic activities, selective adsorption and ion exchange properties. A simple and efficient analytical method for these materials would be of great interest, notably because of the various applications of zeolites in food, cosmetic and medical products [24] that requires the simultaneous determination of important trace elements. Their thermal and chemical stability makes them a difficult sample type to process, however, halogen assisted Slurry-ETV-ICP-AES may allow analysis without a laborious digestion.

2.3 Experimental

2.3.1 Instrumentation

The instrumentation and chemical suppliers are listed in Table 2-1, and the instrument operating conditions are provided in Table 2-2. The modifications to the ETV furnace can be found in reference [1]. The modifications allow the introduction of a sheathing and cooling gas flow (S/C gas) at the exit of the graphite furnace tube. When in use, this gas flow cools down the analyte vapor and provides a thin sheating layer between the wall of the transport tube and analyte laden gas stream (see Fig. 2-1) which prevents the analyte from contacting and condensing onto the tube walls.

Table 2-1. Instrumentation and material suppliers.

ICP RF Generator	Model 2500, 27.12 MHz crystal controlled with autotuning, Plasma-Therm, Kresson, NJ, USA.
Torch	Fassel type
Spectrometer	Model 90750, 0.75 M focal length, 2400 grooves/mm grating, Thermo Jarrell-Ash, Franklin, MA, USA.
Data acquisition hardware and software	Retrofit from Technical Service Laboratories, Mississaugua, Ontario, Canada.
Data processing software	Lab Calc, Galactic Industries, Salem, NH, USA. Quattro-Pro, Borland International, Inc.
Electrothermal vaporizer	Model HGA 2200, Perkin-Elmer, Norwalk, CT, USA.
Freon-12™	Du Pont, Wilmington, DE, USA.
1000 μg/ml reference standard solutions	Fisher Scientific, Fair Lawn, NJ, USA.
Milli-Q water system	Millipore, Bedford, Mass, USA.
Nitric acid	Fisher, Trace Metal Grade.
Zeolite NZ	Institute of Materials and Reagents,University of Havana, Cuba.

Metallic parts exposed to the chemically active carrier stream have been replaced with graphite parts. The solvent vapor evolved from the sample during the drying and charring stage was vented to the atmosphere by the sheath gas flowing through the furnace while a vent was open. About ten seconds before the end of the charring stage, a three-way valve controlling the vent port (located on the end of the furnace, opposite to the ICP) was manually switched to admit the carrier gas stream into the furnace, thus establishing the appropriate gas flow direction for the vaporization stage. The carrier gas was either pure argon or a mixture of argon and Freon-12. The dry-vapor resulting from the atomization of the sample was transferred to the plasma through a Teflon tube 15 cm long (3.5 mm i.d.) and a cylindrical glass tube 7 cm long (5 mm i.d.) that makes the connection to the plasma torch. The dosing hole of the graphite tube was permanently stopped with a graphite plug. The venting valve assembly was momentarily removed to deposit the sample by the tube end. Background correction was performed with a galvanically driven refractor plate. Movements of the refractor plate and signal integration were controlled by a program (SF20 written by Guy Légère of our laboratory) running on a 80386 PC at 40 MHz. The sampling time for each background corrected point was 420 ms, which included two 200 ms integration periods for the off-peak and on-peak measurements and two 10 ms settling times for the refractor plate.

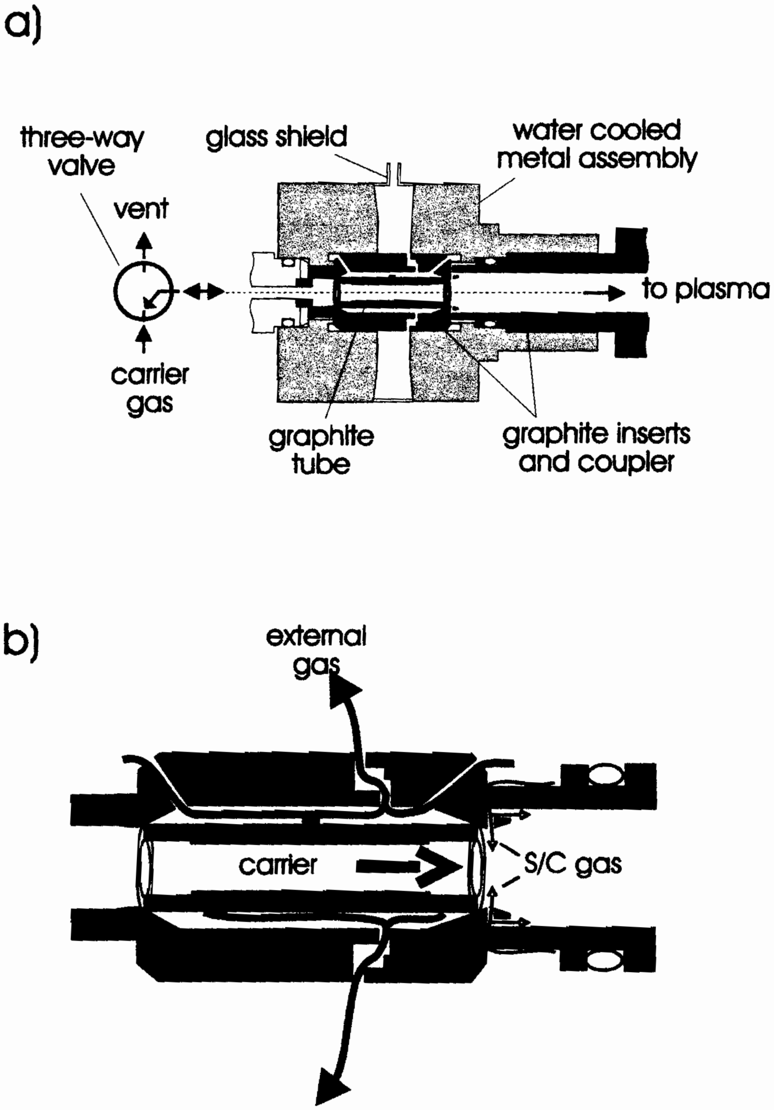

Figure 2- 1. The modified Perkin-Elmer HGA-2200 graphite furnace assembly (a) and the internal gas flows (b).

Table 2-2. Operating conditions and emission lines used for quantitation.

ICP	
Plasma Gas	Argon, 16 l/min
Intermediate Gas	Argon, 0.8 l/min
Central Gas	See text
Observation Height	See text
ETV Temperature Programming	
Drying	100°C, ramp time of 10 sec., hold for 30 sec.
Charring	200°C, ramp time of 10 sec., hold for 30 sec.
Vaporization	2400°C, ramp time of 10 sec., hold for 30 sec.
Elements and Analytical Emission Lines (nm)	
Ca (II)	393.3
Ti (II)	334.9
V (II)	311.0
Cr (II)	267.7
Mn (II)	293.9
Cu (I)	324.7
Zn (I)	213.8
Cd (I)	228.8
Pb (II)	220.3

2.3.2 Sample Preparation

High-purity water (18 MΩ) was obtained by passing distilled water through a Milli-Q ion exchange and membrane filtering system (see Table 2-2) and used throughout the experiments. Working multielement standard solutions were prepared from 1000 μg/ml reference standard solutions by serial dilution in 1% nitric acid solution.

The major components of the zeolite as determined by a routine flux digestion and X-ray fluorescence analysis are given in Table 2-3. The sample consists of particles having an average diameter of 5 μm. The zeolite slurry was prepared by adding the proper amount of the unmodified material to half the total volume of water. After mixing, nitric acid was added and the slurry was made up to the final volume with water (usually to 5 ml). The slurry had a final concentration of 1% w/v in 1% nitric acid solution and was thoroughly hand-shaken before deposition. Since partial leaching of analytes from the zeolite if it occurs would not affect analytical results, no attempt was made to evaluate any possible release of trace elements during slurry preparation. The slurry particulates were fine enough to provide a suspension stable over minutes after hand-shaking, without having to recourse to surfactants, or either vortex or ultrasonic sampling. The standards were prepared by spiking the slurry with a 10 µg/ml multielement stock solution (technique of standard additions) before completing the final dilution to volume. The final concentration was of 0.5 µg/ml of liquid standard and 1 µg/ml of the slurry. The method of standard additions was preferred since excitation conditions would be similar throughout.

Table 2-3. Major elements analysis of the Zeolite NZ by X-ray fluorescence.

Compound	Concentration
SiO2	66.35%
Al2O3	11.22%
CaO	3.48%
Fe2O3	2.11%
K2O	1.20%
Na2O	1.45%
MgO	0.48%

2.3.3 Procedure

Ten microliters of the multielement standard solution or the zeolite slurry were deposited into the furnace in the central part of the graphite tube with an Eppendorf™ pipette adapted with a bent tip to facilitate sample introduction in the vicinity of the end of the tube. The same sample loading procedure was used throughout. For liquid studies, the concentration of the solution ranged from 0.1 to 10 µg/ml of Ca, Ti, V, Cr, Mn, Cu, Zn, Cd and Pb. The three-way valve was then installed, the furnace was purged with argon and the sequence of drying, charring and vaporization was initiated. When pure argon was used as a carrier, solvent ventilation was effected as described in the instrumentation section. However, when freon was introduced as a vaporizing aid, no ventilation was performed and the solvent was directed to the plasma at the drying and charring stages. This avoids the pulse of freon gas in the plasma that occurs when we switch the carrier gas to the plasma. This gas pulse was produced by the sudden release of the pressure that builds up in the section of the carrier gas line located upstream from the three-way valve. This mode of operation preserved the stability of the plasma and improved the precision of results. No adverse effect on transient shapes caused by water condensing inside the transfer line have been observed.

2.4 Results and Discussion

Both carbide forming (Ca, Ti, V and Cr) and non carbide forming elements (Mn, Cu, Zn, Cd and Pb) were studied. The temperature of boiling or sublimation of the pure metals and their carbides and halides forms can be used as guidelines to compare the ease of vaporization for each element (see Table 2-4). In most cases, however, element emission was observed when the furnace surpassed the melting point [25]. Boiling points suggest the state of the element in the transfer line to the plasma and allow one to compare, at least within a restricted range of sample and matrix loadings, the efficiency of formation of dry aerosols [13]. The data shows that the temperature of boiling and sublimation for titanium, chromium and vanadium change drastically and decrease by more than 3000°C from carbides to halides. Comparatively, the calcium evolution temperature changes less than 500°C upon halogenation. Among the non carbide forming elements, zinc and cadmium are easily volatilized at low temperature. Thus, they can be considered as probe elements for the post-furnace condensation process. The other elements (Cu, Pb and Mn) are vaporized at more elevated temperatures (>1100°C) either as pure metals or as oxides [25]. Among those, manganese and copper signals may benefit from the presence of Freon-12 due to their ability to form volatile chlorides.

Table 2-4. Temperature ranges of boiling or sublimation points (in order of increasing temperatures in each subgroup).

Temperature Range	**Metals**	**Chlorides**	**Fluorides**	**Carbides**
<500 C		Cr, Ti, V	Ti, V	
500-1000 C	Cd, Zn	Zn, Pb, Cd		
1000-1500 C	Ca	Mn, Cu	Cu, Cr, Pb, Zn	
1500-2000 C	Pb, Mn	Ca	Cd	
2000-2500 C			Ca	Ca
2500-3000 C	Cu, Cr			
3000-3500 C	Ti, V			
3500-4000 C				Cr, V
4000-4500 C				
4500-5000 C				Ti

2.4.1 Operating Parameters with an Argon Carrier

The system was optimized in two steps. First the ETV settings were optimized with the plasma operating at 1 kW and an observation height of 15 mm above top of load coil. Integrated signals were used throughout because they represent the total amount of analyte reaching the plasma and are more independent of the kinetics of vaporization. To confirm the effect of the sheathing and cooling gas flow (S/C gas) on transients, argon was introduced in variable proportions as a carrier flow through the furnace and as S/C gas at the exit. Figure 2-2 presents the resulting cadmium, manganese and titanium transients recorded for a 1 μg/ml multielement solution. The argon carrier flow was reduced as the S/C gas was increased to keep the total flow of argon reaching the plasma constant at 0.7 l/min. Because the carrier stream merged with the S/C gas to form the central channel stream in the plasma, keeping this total flow constant was essential to preserve excitation conditions and thus generate transients that could be compared.

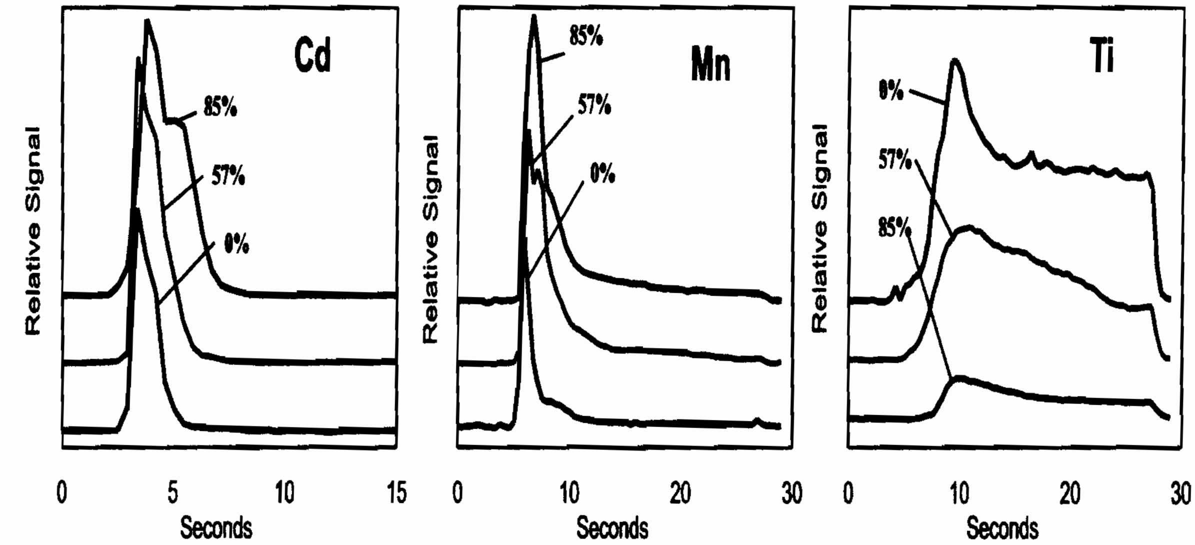

Figure 2-2. Effect of sheathing and cooling gas on cadmium, manganese and titanium. The proportion of argon flow diverted to the S/C gas stream is indicated as percentage. The total flow of argon was kept constant at 0.7 l/min.

Transients for cadmium and manganese both benefited from the diversion of argon into the S/C gas. The cadmium transient exhibited the same peak shape and area enhancements as observed previously on the same instrument in the work of Ren and Salin [3], and manganese more than doubled its signal with these conditions (see Fig. 2-2). In contrast, titanium was still vaporizing after 20 seconds of firing at 2400°C (following the initial 10 second ramp) and the signal was severely depressed on introduction of S/C gas. The signal improvement for manganese is unexpected given the relatively high boiling point for this metal (1962°C) when compared with cadmium (B.P. 765°C). Condensation of the vaporized manganese either into easily transported micro-particulates or on the surface of concomittants, should occur rather easily even in the absence of any S/C gas. Moreover, it was not anticipated that the titanium signal would be adversely affected by the S/C gas. This metal would be even less sensitive to changes in the condensation conditions. As a consequence, the question that begged to be answered was whether the changes observed for the refractory elements upon introduction of a S/C gas were due to a cooling effect at the furnace outlet, or were instead related to the change in the carrier stream velocity inside the furnace. Kántor [13] has postulated that the improvement in transport efficiency observed in some reports [26,27] after increasing the carrier flow rate, could be related to a combination of enhanced turbulencies and a cooling effect on the argon stream in the furnace.

To verify this point, data were collected using argon carrier flows above 1 l/min but without any S/C gas. Transients recorded for cadmium, lead, vanadium and titanium with these conditions are shown in Fig. 2-3. It is worthwhile mentioning that transient shapes were changed and that heights were increased for high boiling points elements when compared to the data taken under the same conditions as in Fig. 2-2 (after correction for the sample concentration of 5 μg/ml used in this measurement). In contrast, the comparison revealed a suppression of the signal for the more volatile elements. The cadmium transient shape was degraded but the peak tailing previously observed for titanium, vanadium and calcium were either greatly attenuated or suppressed. Titanium, in Fig. 2-3, was plotted on a relative scale to rule out any scaling effect due to the decrease of emission in the plasma. A significant decrease in tailing was observed. Considering these results, a compromise carrier flow rate of 1.5 l/min was selected for liquid studies and the use of a S/C gas was dropped. These results are in accordance with the optimal argon carrier flows for ETV-ICP-AES reported previously for non-volatile elements which tend to favor a flow over 1.1/min [17], while more volatile ones such as lead gave best results below 0.6 l/min [7,8]. Carrier flows higher than 1.5 l/min resulted in substantially depressed signals.

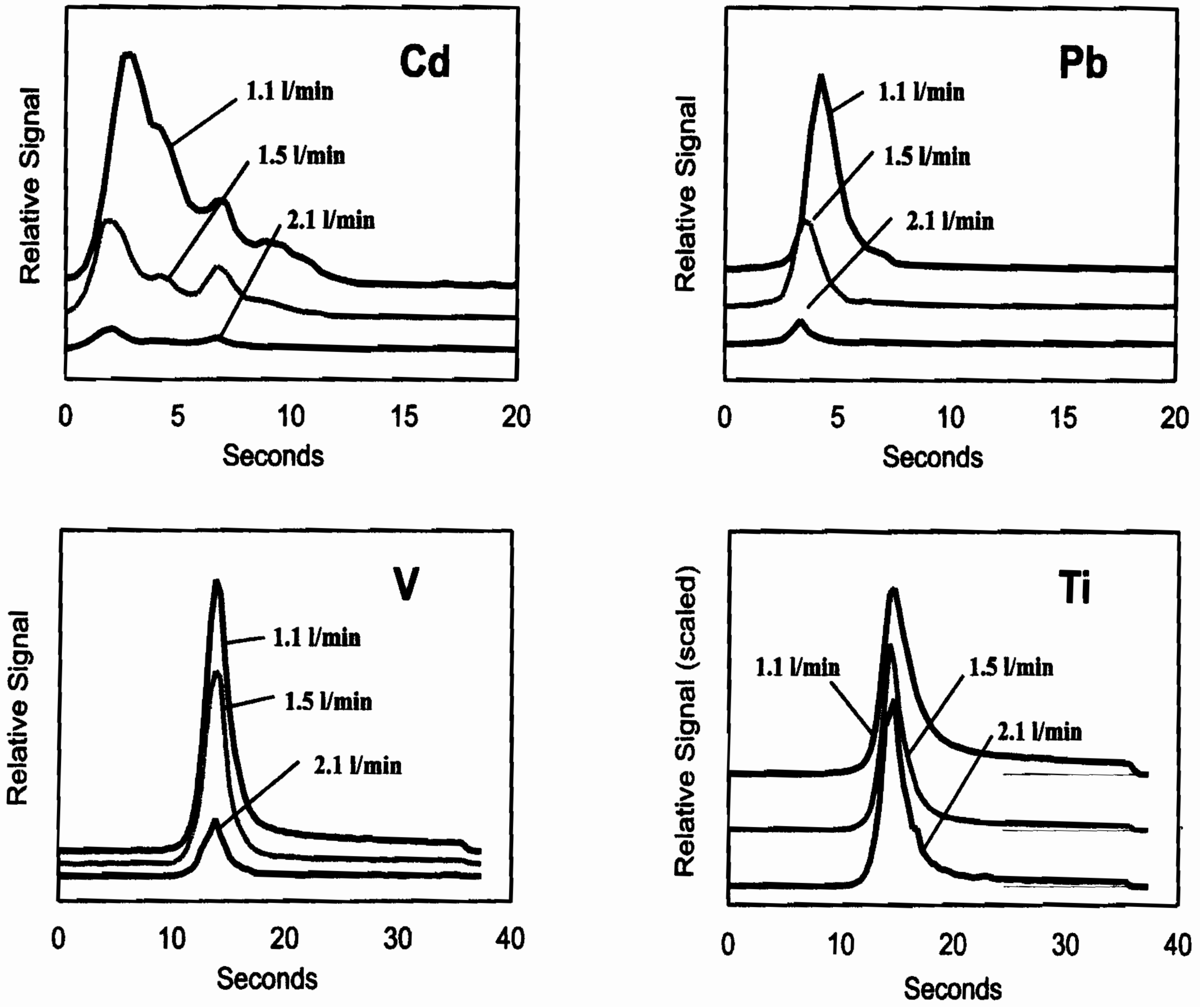

Figure 2-3. Effect of argon carrier flow rate on cadmium, lead, vanadium and titanium with suppressed S/C gas flow.

2.4.2 Optimization of Plasma Parameters upon Freon-12 Introduction.

A survey of the influence of the plasma parameters on the signal-to-baseline noise ratio (S/Nbl) revealed that for most elements, a low observation height and a reduced plasma power were the most appropriate when using pure argon as furnace carrier. The shape of the S/Nbl surface plots in relation to the plasma parameters are illustrated for cadmium and chromium in the upper part of Fig. 2-4. Copper and calcium are better observed at lower power and higher in the plasma. An observation height of 15 mm and a plasma power of 1 kW were selected as the best compromise when using pure argon as carrier. Even though these settings were obtained for a dry plasma, they are close to the optimal ones found with a wet plasma.

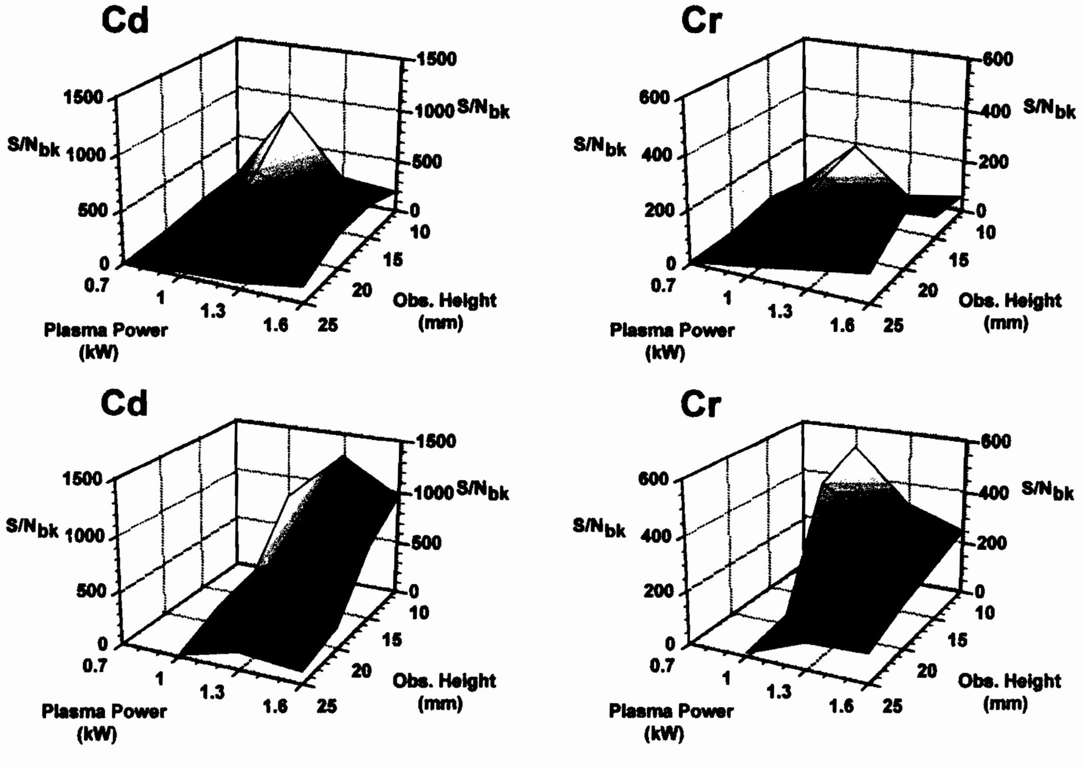

Figure 2-4. Effect of plasma power and observation level on the observed signal-to-background noise ratio (S/Nbl) for a pure argon carrier stream (above) and in an argon plus 25 ml/min of Freon-12 carrier stream (below).

Upon introduction of Freon-12 at a rate of 25 ml/min in the carrier stream, we observed a significant improvement in S/Nbl for refractory elements such as chromium, vanadium and titanium. Figure 2-4 illustrates the changes induced by the freon in the S/Nbl surface shapes in relation to the plasma operating parameters, for cadmium and chromium. The S/Nbl for chromium was substantially improved, particularly at low observation heights. This shift in the S/Nbl maximum toward lower observation heights for the Freon-12/argon ETV was observed with all elements and may be due to the ease with which halide forms can be dissociated in the plasma compared to the forms generated by argon ETV. The S/Nbl improvement is also observed to a lesser extend for the more volatile elements such as cadmium. Probably in that latter case the carbon soot generated from freon acted as physical carrier, as has already been observed for this metal in presence of CCl4 [20]. These S/Nbl improvements were achieved primarily through signal magnitude enhancement, as we should expect if such gains were related to a better transport efficiency. A plasma incident power of 0.7 kW was not investigated in the presence of freon because the plasma had the tendency to extinguish upon sample atomization. A compromise observation height and plasma power of 10 mm and 1 kW were selected. An incident power of 1.3 kW was used with the zeolite slurry to improve the plasma stability.

Figure 2-5 illustrates the effect of freon flow on cadmium and titanium at identical plasma settings. These results show the contrast between the different vaporization behaviors of the volatile and non-volatile elements. For the chosen plasma operating settings, cadmium suffered from the introduction of increasing proportions of Freon-12 (enhancements in S/Nbl were, however, observed for this element at different plasma powers and observation heights). In Freon ETV, vaporized cadmium can condense on carbon soot particulates generated from the halocarbon decomposition, thus improving the transport efficiency. Nevertheless, this element probably already benefited from a similar physical carrier effect in argon ETV from the concomitants of the multielement solution. In contrast, with freon titanium transients were narrower and appeared earlier in the temperature ramp (maxima are shifted down by about 700°C based on the time lag). Eventually, signals were depressed when over 25 ml/min of freon were added to the argon stream. This signal depression could be caused either by changes in plasma excitation conditions or by the formation of stable fluoride species in the plasma [23]. A Freon gas flow of 25 ml/min was selected in order to obtain the highest stochiometric ratio of Freon over the matrix in the furnace without affecting too severely the emission in the plasma.

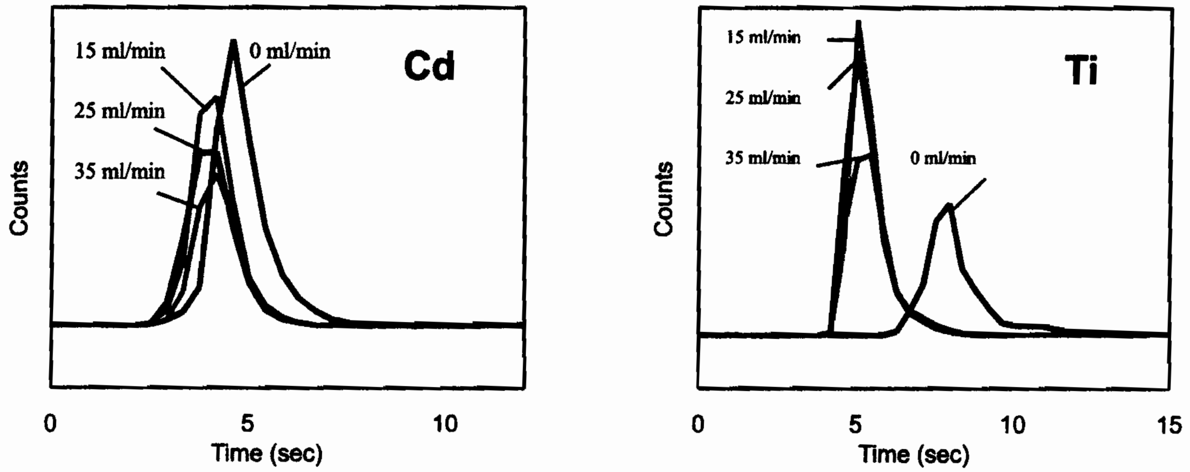

Figure 2-5. Effect of an increasing flow of Freon-12 (indicated gas flow) added to the argon carrier on transients obtained for cadmium and titanium, as observed in a 1 kW plasma at a level of 15 mm above coil.

2.4.3 Detection Limits with Liquids Standards

Detection limits (3σ) for the elements studied were measured for conventional nebulization and for ETV with pure argon and mixed argon/freon carrier. As shown in Table 2-5, these results verified that Freon ETV achieved better detection limits than argon ETV for the refractory elements titanium and vanadium. For these elements, the best overall detection limits (including nebulization) were obtained with Freon ETV. A similar improvement was also observed for manganese even though it does not form refractory compounds. For chromium, the detection limit previously obtained for nebulization was not fully recovered with Freon ETV, but was still almost five times better than the one observed with a pure argon carrier. A ten-fold improvement over pure argon was obtained for this element by Kirkbright and Snook [22] with 0.1% trifluoromethane, but the optimal conditions for their ETV-ICP-AES were obtained for a different set of elements. As a general rule, Freon-12 improved levels of detection for all elements except cadmium, and the linearities of calibration curves were rectified. This was true especially at the low concentration end of the scale where positive deviations were observed. It should be noted that the first firings of a newly installed tube generally revealed a substantial amount of zinc and copper. This contamination could usually be cleared out by a single high temperature firing with the usual amount of freon.

Table 2-5. Detection limits (ng/ml) for liquid standards obtained with conventional nebulization, argon ETV and Freon ETV, along with the improvement factor observed for ETV on introduction of freon. The Freon-12 flow rate was 25 ml/min.

Element	Nebulization	Argon ETV	Freon ETV	Improvement Factor[a]
Zn	2.3	5.0	0.5	4.6
Pb	60	13	27	2.2
Cd	10	5.6	7.2	1.4
Cr	10	77	17	0.6
Mn	23	89	5.8	4.0
V	14	180	5.2	2.7
Cu	6.5	6.5	2.2	3.0
Ti	2.9	8.0	1.8	1.6
Ca	2.4	0.2	0.3	8.0

[a] Freon ETV relative to nebulization.

2.4.4 Analysis of Zeolite and Detection Limits

Zeolite has been analyzed in various conditions of S/C gas and carrier flow. The presence of Freon-12 appeared to be essential for the determination of refractory elements such as titanium and vanadium and advantageous for chromium, as shown in Fig. 2-6. Generally, a shift toward a lower temperature of evolution was observed for all refractory elements in Freon ETV, as with liquid standards (see Fig. 2-5). It is an indication that an analogous vaporization process is involved in both cases. Signals for vanadium and titanium were severely depressed in argon ETV but with the addition of freon, transient shapes and magnitudes were restored to the appearances and levels observed with liquid standards. Titanium in the zeolite was not quantified because the signal saturated the detector of the corresponding channel. No visible residues were left inside the furnace tube after runs with freon.

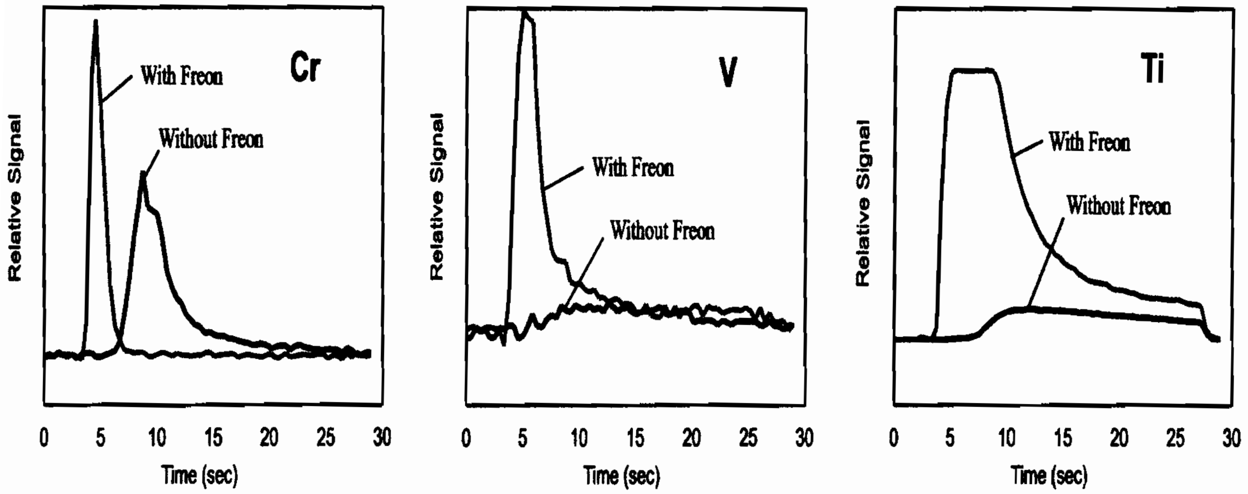

Figure 2-6. Transient signals obtained for chromium, vanadium and titanium for 10 µl of a 1% zeolite slurry in unspiked water, with and without a flow of 25 ml/min of Freon-12 added to the carrier stream.

The determination of six elements (Pb, Cd, Cr, Mn, V and Cu) in the zeolite was attempted in the presence and the absence of a S/C gas flow with mixed argon/freon carrier. Surprisingly, better results were obtained in the presence of a S/C gas, in contrast to the observations previously made for liquid samples in similar conditions. With a S/C gas flow, sensitivities were higher and both the linearity of the analytical curves and the reproducibility of transients were improved. With S/C gas, the percent relative standard deviations ranged from 3% (Cd) to 6% (Pb) for the zeolite slurry spiked with a 1 µg/ml multielement solution. The detection limits and the element levels found in the zeolite NZ with a S/C gas stream are shown in Table 2-6 with the results obtained using X-ray Fluorescence. In general, better detection limits were achieved in the presence of S/C gas flow. Lead was evaluated from transient peak heights since the large amount of aluminum released from the zeolite (see analysis results in Table 2-3) generated a spectral interference on the lead channel. Nonetheless, the vaporization of aluminum was slightly delayed as compared to lead and the peak signal for this later element was clearly observed on the transient. The comparison with the X-ray Fluorescence analysis results of Table 2-6 revealed that the cadmium level was correctly evaluated but that lead was overestimated. In the case of lead, some contribution from the rather massive aluminum interference was probably included in the analytical signal. Manganese and vanadium were underestimated in Freon ETV, for a unknown reason, although copper and chromium were both evaluated correctly.

Table 2-6. Element levels and detection limits for a zeolite slurry. The total argon flow was 0.7 l/min with 0.6 l/min diverted to the S/C gas. A Freon-12 flow of 25 ml/min was used. A single sample was evaluated and all spiked and unspiked slurries were measured in 5 replicates (standard deviations for Freon ETV determinations are shown between parenthesis).

	Freon ETV		**X-ray Fluorescence**	
Elements	**Concentration** (μg/g)	**Detection Limit** (μg/g)	**Concentration** (μg/g)	**Detection Limit** (μg/g)
Pb	49 (14)	6.9	10	3
Cd	1.2 (4)	0.6	2	2
Cr	77 (7)	1.4	83	2
Mn	690 (70)	7.4	341	30
V	31 (4)	0.3	19	10
Cu	73 (10)	1.1	64	15

2.4.5 Comparison with Literature Data

A comparison of detection limits obtained in previous works dealing with halogen assisted ETV or DSI ICP-AES as presented in Table 2-7, shows that the best sensitivities for titanium were achieved with either chlorine [17] or chlorinated freon (this work) in accordance with the thermochemical data already mentioned [23]. Freon-23, however, provided the greatest improvement over argon for titanium [21]. Matousek and Powell [16] obtained detection limits an order of magnitude lower for chromium and vanadium with chlorine assisted ETV. This notable difference can possibly be attributed to the significantly different furnace, which was using an upward stream carrier flow and had a lower internal volume. Kirkbright and Li-Xing [21] carried out optimization on individual elements for DSI-ETV-AES, which can explain why their improvement factors for Freon-23 were not significant for zinc, chromium and copper (although ultimate limits of detection for these elements were very good). This last point shows that one of the great advantage of Freon-12 ETV is that it removes most of the adverse effects of choosing compromise operational parameters in multielement determination, and thus provides very good sensitivities for an extended set of element. In addition, detection limits obtained for solids were not substantially altered when compared to the ones achieved with the same instrumentation in less difficult solid matrices [2]. The improvement factors in that later case were very high since no or few signal for trace elements were recorded for the zeolite in argon ETV.

Table 2-7. Limits of detection for graphite ETV or DSI coupled with ICP-AES in presence of a gaseous halogenating agent, with improvement factors when compared to limits of detection obtained with an inert gaseous carrier (between parentheses). All results are expressed in nanograms.

lements	**This work**		**Matousek** *et al.* [16] [a]	**Ren and Salin** [19] [b]	**Kirkbright and Li-Xing** [21] [c]	**Kirkbright and Snook** [22] [d]
	Liquids	**Solids**				
Zn	0.01 (10)			3.2	0.004 (1)	
Pb	0.5 (0.5)	1.4				
Cd	0.14 (0.8)	0.12				
Cr	0.34 (4.5)	0.28	0.03	0.1	0.020 (1)	0.05 (10)
Mn	0.12 (15)	1.5		1.4		
V	0.1 (35)	0.06	0.006			
Cu	0.04 (3.0)	0.22		0.02	0.0073 (1.5)	
Ti	0.04 (4.4)		0.03		0.89 (124)	
Ca	0.01 (0.7)					

[a] ETV, Cl_2/Ar with liquid samples.
[b] ETV, Freon-12/Ar with solid samples.
[c] DSI, Freon-23/Ar with liquid samples.
[d] DSI, Freon-23/Ar with liquid samples.

2.5 Conclusion

It was found that Freon-12 was an efficient vaporization enhancer for the determination of carbide forming elements with a graphite furnace. Detection limits were improved for the refractory elements titanium, vanadium and chromium. Manganese, which has a relatively high evolution temperature also had a better detection limit with Freon-12. Moreover, the effective determination of volatile elements was not affected by the changed conditions in the plasma and comparable detection limits were obtained for elements such as cadmium and lead through a proper choice of operating conditions. The connection with a direct reading ICP-AES instrument, technically easy to achieve, permitted the simultaneous determination of a set of elements with low detection limits. Additionally, it appeared throughout this study that a background correction performed with a galvanically driven refractor plate was essential for dealing with the rapid changes induced in the plasma at the vaporization stage.

The true power of Freon ETV appears to be its applicability in slurry based analysis of solid samples which are difficult to digest or to vaporize in a conventional furnace. The thermal decomposition of freon in the furnace delivers on site and with the proper timing the chemically aggressive species that digest the matrix. Furthermore, the freon forms halides that are easily transported to the plasma. Although the exact chemistry involved still has to be confirmed, the technique shows potential for the accurate determinations of elemental trace levels in difficult solid matrices. With such materials, this method could be an interesting alternative to less sensitive and more matrix dependent analytical techniques such as X-ray fluorescence.

2.6 References

[1] J. A. C. Broekaert and P. W. J. M. Boumans, *Sample Introduction Technique in ICP-AES*, in *Inductively Coupled Plasma Emission Spectrometry Part I. Methodology, Instrumentation, and Performance,* Ed. P. W. J. M. Boumans, pp. 297, John Wiley & Sons, New York 1987.

[2] B. Docekal, J. A. C. Broekaert, T. Graule, P. Tschöpel and G. Tölg, *Fresenius' Z. Anal. Chem.* **342,** 113 (1992).

[3] H. Matusiewicz, *J. Anal. At. Spectrom.* **1,** 171 (1986).

[4] J. M. Ren and E. D. Salin, *J. Anal. At. Spectrom.* **8,** 59 (1993).

[5] P. Verrept, L. Galbács, L. Moens and R. Dams, *Spectrochimica Acta* **48B,** 671 (1993).

[6] S. A. Darke, C. J. Pickford and J. F. Tyson, *Anal. Proc.* **26,** 379 (1989).

[7] I. Ida, H. Yoshikawa, Y. Ishibashi and N. Gunji, *Anal. Sci.* **5,** 615 (1989).

[8] K. C. Ng and J. A. Caruso, *Analyst* **108,** 476 (1983).

[9] D. E. Nixon, A. F. Fassel and R. N. Kniseley, *Anal. Chem.* **46,** 210 (1974).

[10] H. Nickel and Z. Zadgorska, *Spectrochimica Acta* **48B,** 25 (1993).

[11] T. Kántor, *Spectrochimica Acta* **43B,** 1299 (1988).

[12] B. Hu, Z. Jiang and Y. Zeng, *J. Anal. At. Spectrom.* **6,** 623 (1991).

[13] B. Hu, Z. Jiang, Y. Zeng and H. Zhu, *Anal. Sci.* **7,** 433 (1991).

[14] J. P. Matousek and H. K. J. Powell, *Spectrochimica Acta* **43B,** 1167 (1988).

[15] J. P. Matousek, R. T. Satumba and R. A. Bootes, *Spectrochimica Acta* **44B,** 1009 (1989).

[16] J. P. Matousek and H. K. J. Powell, *Spectrochimica Acta* **41B,** 1347 (1986).

[17] R. K. Skogerboe, D. L. Dick, D. A. Pavlica and F. E. Lichte, *Anal. Chem.* **47,** 568 (1975).

[18] J. M. Ren and E. D. Salin, *Spectrochimica Acta* **49B,** 555 (1994).

[19] J. M. Ren and E. D. Salin, *Spectrochimica Acta* **49B,** 567 (1994).

[20] T. Kántor, *J. Anal. At. Spectrom.* **7,** 219 (1992).

[21] G. F. Kirkbright and Z. Li-Xing, *Analyst* **107,** 617 (1982).

[22] G. F. Kirkbright and R. D. Snook, *Anal. Chem.* **51,** 1938 (1979).

[23] W. Schrön, *Spectrochimica Acta* **44B,** 965 (1989).

[24] D. W. Breck and R. A. Anderson, *Molecular Sieves*, in *Kirk-Othmer Encyclopedia of Chemical Technology*. pp. 638-669 (1980).

[25] D. L. Styris and D. A. Redfield, *Spectrochimica Acta Rev.* **15,** 71 (1993).

[26] C. J. Park, J. C. Van Loon, P. Arrowsmith and J. B. French, *Can. J. Spectrom.* **32,** 29 (1987).

[27] G. F. Kirkbright, D. L. Millard and R. D. Snook, *Anal. Proc. (Chem. Soc. London)* **17,** 16 (1980).

Chapter 3

RAPID SAMPLE PRECONCENTRATION BY SPRAY DEPOSITION FOR ELECTROTHERMAL VAPORIZATION INDUCTIVELY COUPLED PLASMA SPECTROMETRY

This chapter describes the spray deposition of liquid samples inside a modified commercial electrothermal vaporization (ETV) unit. Sample preconcentration was achieved by spraying the sample and simultaneously heating the tube in such a way that the sample water was continuously vented to ambient, while the dried analytes stay on the graphite surface. The idea was to apply to ETV the spray deposition concept that had already been implemented with direct insertion (DSI) using graphite probes. Once sprayed in the furnace, the concentrated sample is then submitted to a typical ETV temperature program including drying and ashing stages, and ending with the vaporization of the sample at high temperature (>2000°C). The ETV is attached to an ICP torch and the vaporized sample is analyzed by atomic emission spectrometry. It was expected that an unlimited volume of sample could be concentrated this way if sufficient time was allowed for sample spraying. The results presented in this section were rather preliminary although they confirmed the feasibility of the concept. It is noteworthy that the detection limits obtained from a small element set improved in direct proportion with the volume of sprayed sample.

This paper appeared in a special issue of *Spectrochimica Acta Part B on Sample Introduction in Atomic Spectrometry*. The title of the paper was *"Rapid Sample Preconcentration by Spray Deposition for Electrothermal Vaporization Inductively Coupled*

Plasma Spectrometry", by Jean-François Alary and Eric D. Salin, Department of Chemistry, McGill University, Montreal, Quebec, Canada H3A 2K6. It appeared in *Spectrochimica Acta*, **50B**, 405 (1995). J.-F.A made the experimental setup and conducted the experiments under the supervision of E.D.S. The paper was jointly written by the two authors.

3.1 Abstract

The deposition of aqueous sample in an electrothermal vaporization unit (ETV) is implemented by spraying onto a graphite tube heated at 160°C. The water is evaporated continuously and vented by a flow of argon, leaving the analytes on the inner walls of the graphite cuvet. The analytes are later atomized at high temperature and directed to an inductively coupled plasma for atomic emission spectrometry (ICP-AES). The effects of observation height, argon flow in the furnace unit at atomization, and plasma energy on the signal-to-noise ratio were studied. The combination of the advantages of ETV with a sample volume of 1 ml provides detection limits for Cd (0.06 ng/ml), Pb (0.3 ng/ml), Zn (0.02 ng/ml) and Cu (0.04 ng/ml) which are an improvement of two order of magnitude when compared to conventional nebulization. Moreover, the ETV allows a more convenient interface to the plasma than similar Direct Sample Insertion experiments.

3.2 Introduction

In a previous paper [1] we discussed a liquid sample introduction technique for ICP-AES that demonstrated detection limit improvements of approximately 600 in two minutes compared to conventional nebulization on the same spectrometer. The technique utilized a Meinhard nebulizer to spray liquid sample directly into a heated graphite cup which was subsequently inserted into a plasma using direct sample insertion (DSI) methodologies. The technique appears to have almost 100% transfer efficiency. In addition to the obvious detection limit improvements, the technique also eliminates solvent from the system, which should provide a reduction of isobaric interferences for ICP-MS [2,3]. While DSI offers a number of advantages, including 100% sample delivery, it does not provide certain conveniences that would appear to be offered by electrothermal vaporization (ETV) for ICP-AES or ICP-MS. In particular, the ability to use conventional torches will appeal to those in the user community that wish to switch often between sample introduction techniques. The DSI-ICP system inserts the sample carrying probe directly into the center of the plasma and consequently requires a torch without a central injector tube. For some, another advantage of ETV interfaces will be their commercial availability, particularly for ETV-ICP-MS. All of this must be balanced against potential transport problems [4,5]. Finally, it is possible that a DSI configuration will place more carbon into the mass spectrometer than an ETV arrangement.

Aerosol deposition for furnace atomic absorption was first reported by Matousek [6]. Matusiewicz and Barnes [7] later reported aerosol deposition for ETV-ICP-AES. In these cases "aerosol" indicates that a nebulizer and spray chamber were used so that only the smaller droplets were transferred to the ETV system. Matusiewicz and Barnes used a FASTAC commercial aerosol deposition system originally developed for furnace atomic absorption [8,9]. The FASTAC system generated an aerosol using a conventional nebulizer and then transported the aerosol to a hot furnace (typically 140°C). The aerosol was dried on the furnace tube and subsequently vaporized using a dry-ash-atomize cycle. The relative (ng/ml) detection limits [7] were a factor of 2-20 times poorer than those obtained with the same equipment but without the FASTAC equipment [10]. They used 50 µl discrete nebulization injections and reported signals comparable to direct deposition of 5 µl of sample, indicating 10% transfer efficiency.

Given the high degree of success achieved by the DSI-ICP-AES system using spray deposition, it seemed appropriate that these principles be tested on an ETV system. The test elements chosen were cadmium, lead, zinc and copper. It was realized that there might be transport problems, however the commercial success of these units for ICP-MS would suggest that these are not debilitating. Our hope would be that ETV improvement factors similar to those obtained with DSI could be achieved providing ICP-MS detection limits on ICP-AES instruments. In later experiments we will investigate the applicability of the technique with ICP-MS. One should keep in mind that our recent work in this area [1] was motivated by a desire for a 100% efficient ICP-AES and ICP-MS interface for flow injection based preconcentration [11]. ETV based front-ends for flow injection preconcentration should provide most of the advantages of the DSI system while offering the commercialization advantages suggested above.

3.3 Experimental

The electrothermal apparatus used is illustrated in Fig. 3-1. The manufacturers of various system components are listed in Table 3-1. The furnace is controlled by a FORTH language system in EPROM allowing it to be run as an autonomous sub-system. Suitable FORTH programs were written to control the ETV. The operating parameters are listed in Table 3-2. The Meinhard nebulizer was mounted on the sample tube arm of the

Thermo-Jarrell Ash furnace, placing it under computer control. One end of the furnace tube was coupled to the ICP torch by a Teflon insert and a 40 cm section of Tygon tube. The opposite end of the furnace tube was configured with a glass tube and a valve, allowing it to be used for venting. The ETV furnace tube was maintained at 160°C during the deposition process. This temperature was determined by using a tungsten-halogen lamp to observe any mist emerging from the end of the furnace tube. Too high a temperature resulted in boiling or sputtering and mist generation, while too low a temperature resulted in flooding. A warm-up stage was introduced in the operating procedure before the sample deposition step. The cooling water flow to the electrodes was stopped and the furnace was run briefly to bring the contact rings above room temperature. If this was not done, vapor from the spray deposition processes would condense on the cool outer parts and then be revaporized during the furnace atomization cycle. The water affected precision and could cause the plasma to be extinguished. Cooling water flow was re-established before the ash stage. Gas flow was directed away from the ICP through the furnace during the deposition process by opening up the vent valve and restricting the argon gas flow into one side (left side in Fig. 3-1) of the furnace. This venting configuration was maintained during the traditional drying and ashing process to eliminate water deposition in the transfer tubing [12]. The nebulizer was operated with nitrogen (to reduce costs) using a gas flow rate of 1.2 lmin^{-1}. A pumped liquid flow rate of 200 μl/min was used throughout these studies. After drying, the gas flow is inverted by closing the vent valve and introducing gas from the vent side (left in Fig. 3-1) of the furnace. The sample was then ashed and vaporized in a traditional manner with the conditions listed in Table 3-2.

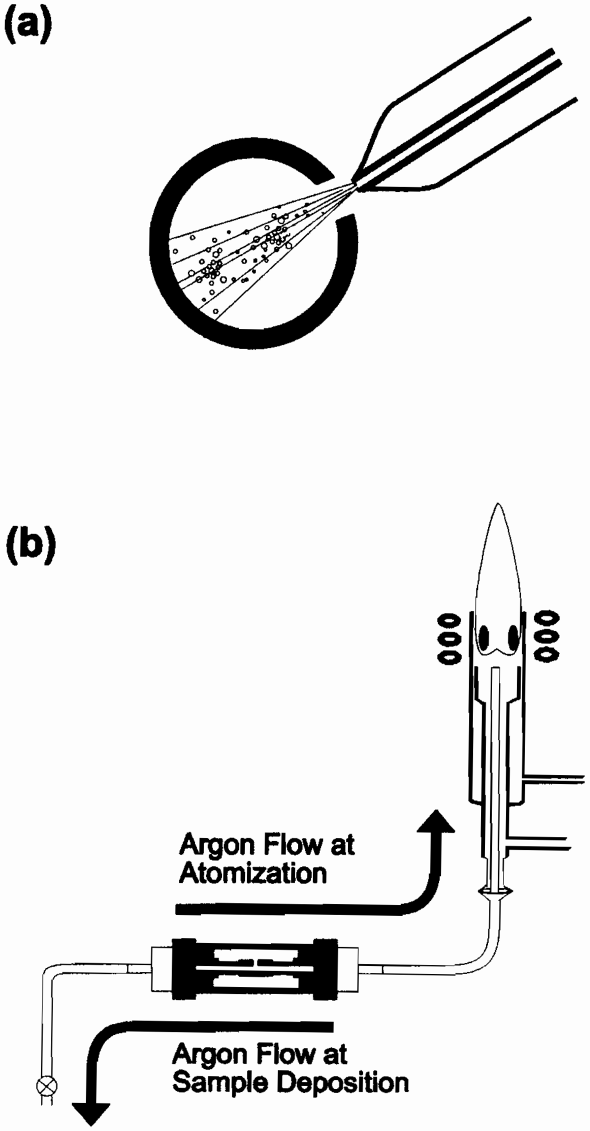

Figure 3-1. Spray deposition in the pyrolytically coated graphite cuvet: (a) cutaway view showing the position of the Meinhard nebulizer over the dosing hole during sample deposition; (b) overview of the system and gas flow pathways.

Table 3-1. Equipment and Supplies.

ICP Spectrometer	Modified Jarrell Ash Model Atomcomp 750	Franklin, MA, USA
Data Processing Software	Borland International, Quattro Pro	Scotts Valley, CA, USA
	Galactic Industries, Lab Calc	Salem, NH, USA
Spray Nebulizer	J.E. Meinhard (Type A)	Santa Ana, CA, USA
Nebulizer	J.E. Meinhard (Type A)	Santa Ana, CA, USA
ICP standards	Spec Industries	Edison, NJ, USA
	Fisher Scientific	Fair Lawn, NJ, USA
Furnace	Thermo-Jarrell Ash Model CTF 188	Franklin, MA, USA
Entrance slit width	25 μm	
Exit slit width	50 μm	

Table 3-2. Electrothermal Vaporization Unit (ETV) Operational Parameters for Calibration Experiments.

Stage	**Temperature**	**Duration**	**Internal Argon Flow ($\mathrm{lmin^{-1}}$)**
Warm-up	550°C	45 sec.	0.2
Spray Deposition	160°C	5 min.	0.65
Drying	200°C	2 min.	4-6
Ashing	300°C.	2 min.	0.65
Vaporization	2200°C	10 s. (including a 2 sec. ramp)	0.65
Cleaning	2400°C	3 sec.	0.2

The spectrometer (Table 3-1) data and spectral acquisition capability has been improved by installation of a rapid scanning refractor plate based background correction system [13] from Trulogic. Two hundred one-sided background corrected data points were collected at 17 Hz simultaneously for each of the four elements. Optimizations were carried out using the Simplex Method [14] using a program written in our laboratory by Douglas Webb. The spectrometer is controlled by SF20 software written by Guy Légère Data was postprocessed by Lab Calc (Galactic Software) and Quattro Pro (Borland International). The spectrometer and torch are physically independent so they were aligned by reverse-path laser imaging as described previously [15]. The spectrometer system utilized a mirror collection system with 2:1 imaging and was operated under conventional operating conditions as listed in Table 3-3 for the nebulization based sample introduction experiments.

Table 3-3. Operating Conditions for Nebulizer Experiments.

Power	1.0 kW
Nebulizer Flow Rate	1.2 ml/min
Observation Height	15 mm above load coil
Integration Time	10 seconds
Lines Used	
Cu	324.7 nm
Zn	213.8 nm
Cd	228.8 nm
Pb	220.3 nm

Solutions were prepared by dilution of 1.0 mg/ml standards in Milli-Q (Millipore, Bedford, Mass.) doubly deionized water and 1 % Fisher Trace Metal Grade nitric acid. Nebulizer based detection limits were taken under the conditions listed in Table 3-3.

3.4 Results and Discussion

Blank noise was determined by using the noise extracted from the later portion of the background corrected data acquisition cycle. This was determined to be valid by mathematical correlation studies [16] in which two independent blank signals for a given element, either Cd or Pb (since they exhibit no trace level contaminants) were correlated in the first five seconds of the transient signal. The analyte always appears during the first five seconds. These studies demonstrated that there were no regular features in the transient segment that includes the ramp to the atomization temperature. In summary, a series of blank runs were, on average, completely flat when background corrected. It is worth noting that they are not flat without background correction due to the well known "pressure pulse" phenomena [10]. This methodology was assumed to be valid for Zn and Cu, although the optimized system does show traces of these elements in the blanks. In fact, on an unoptimized spectrometer system on which the first experiments were conducted, all elements exhibited flat baselines using the methodology described above.

The signal/blank-noise (S/σ_{Blk}) ratio was optimized by the Simplex Method [14] by varying observation height, plasma power and carrier gas flow rate. In essence, we are optimizing the detection limits by using this methodology. The carrier gas is combined with a 0.56 $lmin^{-1}$ Ar flow separately introduced in the furnace enclosure. Experiments measuring the total input to the furnace and output to the torch indicate that the gas input into the system will be approximately 20% higher than the flow reaching the plasma due to leakage in the assembly. Figures 3-2 and 3-3 provide relative optimization data for Cd and Cu respectively. The heavy trace in each of the figures represents the element being optimized in this set of experiments while the other three traces are the other elements monitored during the study. It becomes immediately apparent that Cd, Zn and Pb are highly sensitive to optimization parameters while Cu is relatively insensitive. Zn, at the extreme, varies by a factor of 14. Figures 3-2(a) and 3-3(a) provide information on the parameters. Rather than plotting the new simplex value, which provides a very "noisy" appearing plot, we have plotted the vertex of the simplex. This provides a smoothing effect and allows one to see the trends much more easily as the simplex converges to an optimum. Since it takes four data sets before one has the first vertex, the vertices are offset by three values to align properly with the data in Figures 3-2(b) and 3-3(b). It is particularly interesting to watch the simplex plateau for two variables in Fig. 3(a) while the convergence process continues for the last variable. Analysis of the optimization data revealed that background noise remained relatively constant for Cd, while the signal increased. On the contrary, for Cu, optimization was achieved primarily by finding conditions which reduced the background noise. It is not surprising that Cd (228.8 nm), Zn (213.8 nm) and Pb (220.3 nm) would display similar sensitivity to parameters while Cu (324.7 nm) would optimize somewhat differently. Since Cu was relatively insensitive to operating parameters the optimum conditions for Cd was selected as a suitable compromise for all subsequent measurements.

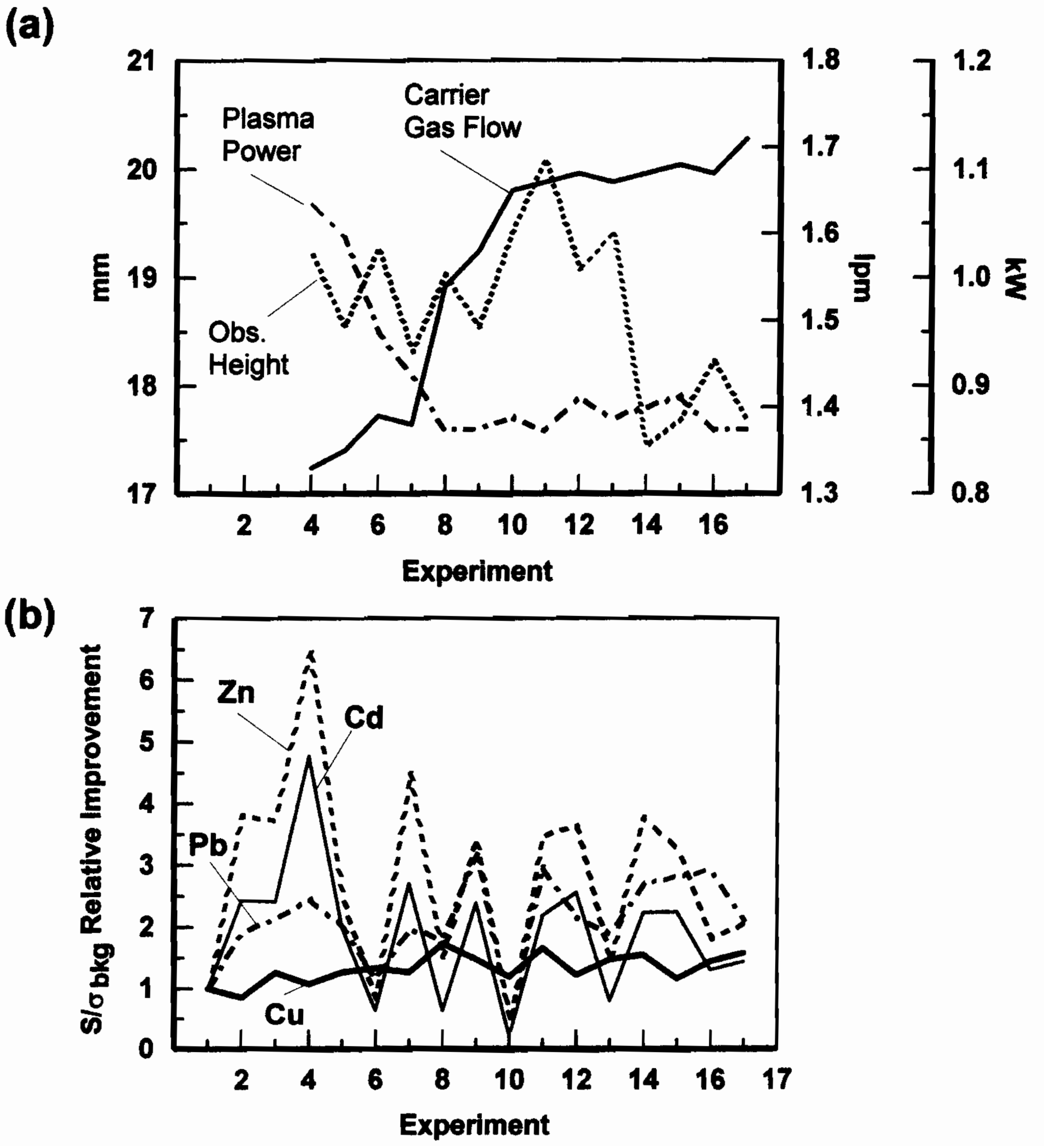

Figure 3-2. Simplex optimization for copper. The optimization was carried out for the integrated signal to background noise ratio by varying the observation height, plasma power and carrier gas flow, with a 100 ng/ml multielement solution deposited for 15 seconds at each experiment. Transient signals for cadmium, zinc and lead were recorded simultaneously: (a) Evolution of the geometrical centers of parameter vertices in the course of optimization (see text); (b) Relative improvement of S/σ_{Bkg} *for copper, zinc, cadmium, and lead.*

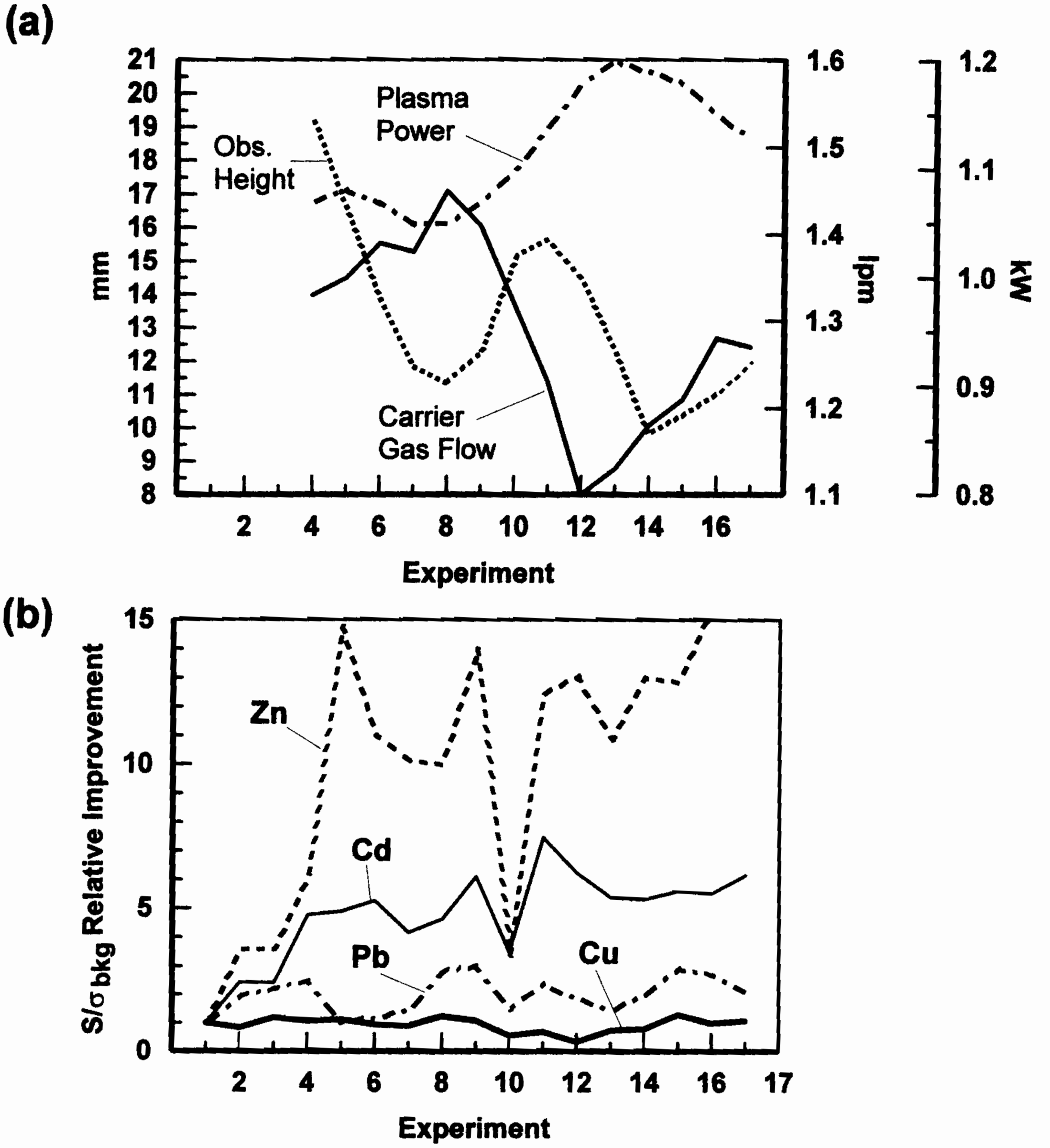

Figure 3-3. Simplex optimization for cadmium. The optimization was carried out for the integrated signal to background noise ratio by varying the observation height, plasma power and carrier gas flow, with a 100 ng/ml multielement solution deposited for 15 seconds at each experiment. Transient signals for copper, zinc and lead were recorded simultaneously: (a) Evolution of the geometrical centers of parameter vertices in the course of optimization (see text); (b) Relative improvement of S/σ_{Bkg} *for cadmium, zinc, copper and lead*

Figure 3-4 presents time profiles for 1 ng/ml solutions of the elements included in these studies. The structure observed for certain elements (e.g. double humps for Cd and Zn) are highly reproducible over the concentration range. The lower traces are the blank signals. Note that the Zn and Cu scans reveal significant levels of the analyte in the blank. ICP-MS analysis verify that these traces are not directly related to the nitric acid used to generate the 1% levels which were maintained in all solutions.

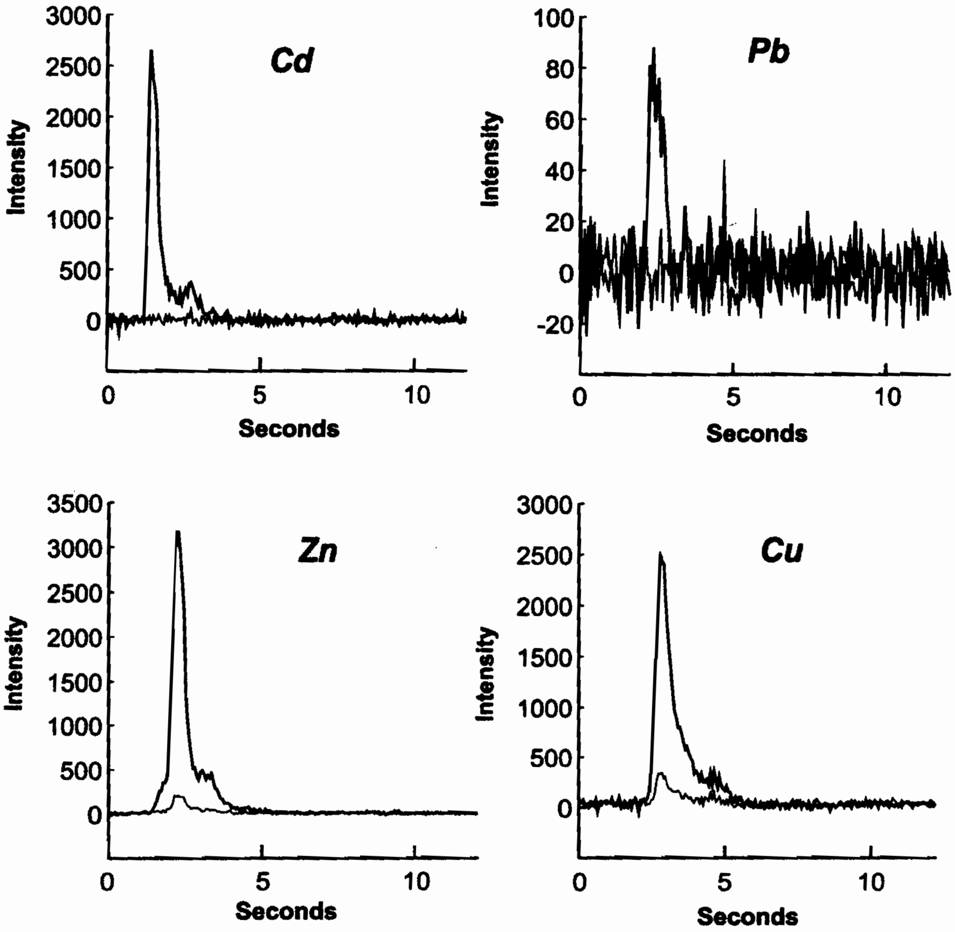

Figure 3-4. Transient signals for cadmium, lead, zinc and copper, after background correction. Top traces (thick lines); 1 ng/ml multielement solution: bottom traces (thin lines); blank signals. All signals were obtained after a sample deposition time of 5 minutes at a rate of 200 μl/min.

Log-log blank corrected calibration curves are presented in Fig. 3-5. Cd and Pb provide linear performance and consequently are not illustrated; however, both Zn and Cu deviate from linearity below 1 ng/ml. We believe that these deviations may result from environmental contamination, however further work will be necessary for a definitive statement. Despite these deviations, calibration curves for all elements show correlation coefficients above .99 when blank corrected.

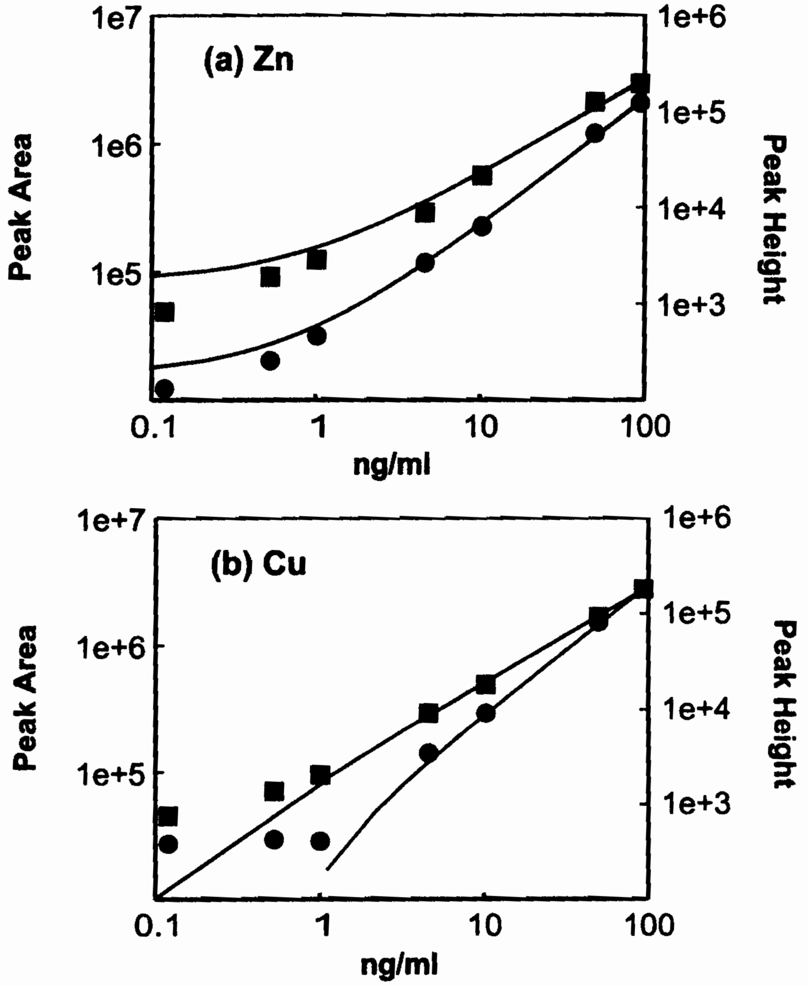

Figure 3-5. Calibration curves: (a) Zinc; (b) Copper. ● *Peak height.* ■ *Peak area. The solid lines illustrate the linear regressions through data points.*

As expected from our previous DSI work [1], the integrated signal vs. deposition time for Cu and Cd are highly linear. In fact, Matousek [6] reported similar performance for atomic absorption in 1977. Since the blank noise is independent of deposition time, this indicates that detection limits can be, within limits, selected by choosing a deposition time.

Detection limits for the system are presented in Table 3-4. All ETV and nebulizer data from this table were taken on the same instrument. Detection limits were determined as the concentration whose signal was three times the blank noise. Spray-ETV-ICP-AES detection limits are very similar to those obtained using rapid spray deposition DSI-ICP-AES. These detection limits are presented in Table 3-4 along with the detection limits obtained on the same system first with an ETV system using a traditional 20 μl sample injection and then using a conventional Meinhard nebulizer and Scott type spray chamber.

Table 3-4. Detection Limit Data. All detection limits in ng/ml

Technique	**Element**	**Detection Limit**		**Approximate Improvement Factor**[a]	**Matusiewicz and Barnes** [10]	**DSI-ICP-AES-DSI** [1]
		Area	Height			
Nebulizer	Pb	150				
Nebulizer	Zn	4				
Nebulizer	Cd	11				
Nebulizer	Cu	7				
ETV-Pipette	Pb	10	9	15		
ETV-Pipette	Zn	0.8	0.7	5	0.05	
ETV-Pipette	Cd	2	2	6	0.2	
ETV-Pipette	Cu	2	3	4	0.07	
ETV-Spray	Pb	0.3	0.4	500		0.07
ETV-Spray	Zn	0.02	0.02	200		0.12
ETV-Spray	Cd	0.06	0.07	180		0.1
ETV-Spray	Cu	0.04	0.05	180		0.05

[a] Relative to nebulization using area.
[b] Detection limits (5 µl) using area.
c Detection limits (0.5 ml deposited) using area.

In general, we are observing expected trends. When going from a 20 µl injection to a 1.0 ml spray deposition one would expect a detection limit improvement of 50 if one had 100% deposition efficiency. We observe, in fact, an improvement of 40 (working to one significant figure). Since all values were acquired on the same instrument, they may, as a first approximation, reflect what may be obtained "relatively" on other spectrometer systems assuming that one does not become quantum noise (light level) limited. The detection limits that we obtained for ETV-ICP-AES are similar to those reported previously by a number of researchers [5,17-19] but are about an order of magnitude poorer than those reported by Ida [20] and Matusiewicz and Barnes [10], who used an ETV-ICP-AES arrangement with a modified graphite platform. Our detection limits with the spray-ETV-ICP-AES system show a factor of 100 improvement compared to conventional nebulization on the same system. The spray-ETV-ICP-AES shows roughly an improvement factor of 10 compared to conventional ETV-ICP-AES in our own work and those of others with several notable exceptions as mentioned above. This leads us to consider the work of Matusiewicz and Barnes [10] more closely. While their spectrometer (1 meter), operating frequency (40 MHz) and power level (0.55 kW) are quite different from ours, our speculation is that the major factor in their excellent detection limits is a graphite platform design which they utilized after investigating a wide variety of electrothermal sample vaporization configurations. Other than the external arrangements described above, our electrothermal design has not been modified in any way. Given that our theoretical improvement (50) and experimentally determined improvements (40) for the transition from spray-ETV-ICP-AES match closely, one could reasonably extrapolate that even lower detection limits, perhaps as much as 200 (1 ml vs. 5 μl) might be possible with an electrothermal vaporizer such as theirs and a spray deposition technique.

Our precision averaged at the 7% RSD level with either manual pipetting or spray deposition. These are a factor of two to three poorer than those reported by others [5,17-19]. We believe that the poor precision is caused in some major part by variable gas leakage in the ETV system which may cause irregular flow through the rather complex flow system (including sheathing flows) provided by this commercial arrangement. Since both pipetting and spray deposition gave similar RSDs, there is no indication that the spray deposition technique is inherently imprecise. On the contrary, one would expect it to be more reproducible than manual injection, which can provide RSDs of 2% [10].

3.5 Conclusion

The concept of 100% spray deposition seems to be applicable to ETV-ICP-AES as well as the previously demonstrated DSI-ICP-AES. Detection limits for ideal samples are approaching the ICP-MS range and are a factor of 100 better than those achieved on the same system with conventional nebulization. There are indications from the literature that the detection limits could be considerably lower. These experiments have not addressed any of the matrix problems which can occur with ETV-ICP-AES, and indeed, one might expect those problems to be exacerbated due to the accumulation of concomitants along with the analyte. We believe that this may be an inordinately pessimistic view given that the analyte is evenly deposited over a larger surface area. Certainly, the question requires investigation.

3.6 References

[1] R. Rattray, J. Minoso and E. D. Salin, *J. Anal. At. Spectrom.* **8,** 1033 (1993).

[2] J. M. Carey, E. Hywel Evans, J. A. Caruso and W.-L. Shen, *Spectrochimica Acta* **46B,** 1711 (1991).

[3] V. Karanassios and G. Horlick, *Spectrochim. Acta Rev.* **12,** 1387 (1989).

[4] T. Kántor, *Spectrochimica Acta* **43B,** 1299 (1988).

[5] D. L. Millard, H. C. Shan and G. F. Kirkbright, *Analyst* **105,** 502 (1980).

[6] J. P. Matousek, *Talanta* **24,** 315 (1977).

[7] H. Matusiewicz and R. M. Barnes, *Spectrochimica Acta* **40B,** 41 (1985).

[8] J. J. Sotera, L. C. Cristiano, M. K. Conley and H. L. Kahn, *Anal. Chem.* **55,** 204 (1983).

[9] H. L. Kahn, R. G. Schleicher and S. B. Smity Jr. *Ind. Res.* **20,** 101 (1978).

[10] H. Matusiewicz and R. M. Barnes, *Spectrochimica Acta* **40B,** 29 (1985).

[11] P. Moss and E. D. Salin, *Appl. Spectrosc.* **45,** 1581 (1991).

[12] J. M. Ren and E. D. Salin, *J. Anal. At. Spectrom.* **8,** 59 (1993).

[13] G. Légère and P. Burgener, *ICP Inf. Newsl.* **13,** 521 (1982).

[14] J. A. Nelder and R. Mead, *Computer Journal* **7,** 308 (1964).

[15] J. M. Ren, G. Légère and E. D. Salin, *Appl. Spectrosc.* **47**, 1953 (1993).

[16] G. M. Hieftje, *Anal. Chem.* **44,** 69A (1972).

[17] R. M. Barnes and P. Fodor, *Spectrochimica Acta* **38B,** 1191 (1983).

[18] K. C. Ng and J. A. Caruso, *Anal. Chem.* **9,** 1513 (1983).

[19] A. M. Gunn, D. L. Millard and G. F. Kirkbright, *Analyst* **103,** 1066 (1978).

[20] I. Ida, H. Yoshikawa, Y. Ishibashi and N. Gunji, *Anal. Sci.* **5,** 615 (1989).

Chapter 4

QUANTITATION OF WATER AND PLASMA DIAGNOSIS FOR ELECTROTHERMAL VAPORIZATION-INDUCTIVELY COUPLED PLASMA-MASS SPECTROMETRY; THE USE OF ARGON AND ARGIDE POLYATOMICS AS PROBING SPECIES.

When an attempt was made to implement the spray deposition technique to ETV-ICP-MS, it was noticed that adverse effects were caused by water vapor being vaporized concurrently with the analytes. These effects were, however, more pervasive than just causing the extinction of the plasma as in Spray ETV-ICP-AES. Noisy and irreproducible results were obtained due to the random level of water expelled by the graphite furnace at the high temperature stage. Clearly, the successful application of the Spray ETV technique to ICP-MS required a better understanding of the fundamental principles involved, especially in regard to the effect of water on the ability of the instrumentation to efficiently generate and collect ions for quantitation.

A literature survey had revealed that some argides derived from the dissociation of water could be used as rough estimates of the water content of the plasma [1-6]. It was rationalized that if a linear relationship could be established between the level of some argides species and the water introduced in the plasma through the injector flow, that information could eventually guide the optimization of the spray deposition technique. In the course of this work, however, the study became more ambitious and was extended to include other plasma species. The effect of basic operational parameters, including the water plasma content, were explored using experimental design theory as mathematical framework.

Enriching the plasma with controlled amounts of water was also attempted as a way of enhancing transient signals. However, fluctuations in water level from other sources within the instrumentation, chiefly from the furnace, introduced an important - often predominant - source of noise in the recorded signal for several elements. The use of plasma species as internal standard to at least partially counteract the effect introduced by changing plasma conditions has already been reported for ICP-MS [7-12]. These studies, however, dealt with matrix effects inducing signal suppression. It was expected that the technique of using a plasma argide as ratioing species in ETV-ICP-MS [9], could be used to correct unwanted signal amplification as well.

This paper was submitted to *Spectrochimica Acta Part B*. The title of the paper was *"Quantitation of Water and Plasma Diagnosis for Electrothermal Vaporization-Inductively Coupled Plasma-Mass Spectrometry; The Use of Argon and Argide Polyatomics as Probing Species"*, by Jean-François Alary and Eric D. Salin, Department of Chemistry, McGill University, Montreal, Quebec, Canada H3A 2K6. It is currently being peer reviewed. J.-F.A was responsible for the experimental setup and conducted the experiments under the supervision of E.D.S. The paper was jointly written by the two authors.

4.1 Abstract

The water content of the carrier flow originating from an electrothermal vaporization unit (ETV) attached to an inductively coupled plasma mass spectrometer (ICP-MS) is monitored by following the argon hydride ion (ArH^+) at m/z 37. The goal is to measure the water expelled by the ETV at sample vaporization and evaluate the influence of this parameter on the ion generation efficiency. Linear responses from the argon hydride were obtained when the water loading in the plasma injector flow was increased from 0 to 3.3 mg/min. Other argides and water derived species (Ar^+, Ar_2^+ and O_2^+) were also monitored simultaneously and the effects from operating parameters have been calculated for each species. The magnitude of these effects can eventually be used as diagnosis tools. It was also found that signals for Zn, Cu, Pb, Sb and As were greatly influenced by slight variations in water loading at low water levels. These signal fluctuations are greatly attenuated and transients shapes restored by ratioing each element transient with the ArH^+ or Ar_2^+ signal that were recorded simultaneously. Envisioned applications that would benefit from a water enhanced signal include spray electrothermal vaporization, direct sample insertion (DSI), and laser ablation for inductively coupled plasma-mass spectrometry. The argon dimer Ar_2^+ seems more appropriate for making the correction since it provides a direct insight on the plasma temperature and provides a robust signal.

4.2 Introduction

In a previous paper we have presented a Spray Deposition Technique [13] involving spraying a liquid sample into a warm (160°C) electrothermal vaporization unit (ETV). Close to 100% of the sample is retained in the ETV. The dried sample is then vaporized and introduced into an inductively coupled plasma-mass spectrometer (ICP-MS). Improvements in detection limits are achieved through the accumulation of milliliter sample volume. Although good recovery of analytes is obtained, the evaporation of large quantities of water in the furnace assembly (in typical ETV applications only from 10 to 50 µl of sample is evaporated) generates several problems. The main problem encountered in Spray ETV-ICP for atomic emission spectrometry (AES) [13] was the sudden release of condensed water into the plasma during the ETV high temperature stage, often resulting in solvent overloading and extinction of the plasma. This problem was solved by modifying the temperature program and shutting down the cooling water flow to the furnace electrodes during spraying, however, the optimum furnace operating conditions were found by trial and error. A direct measurement of the water released into the plasma during all stages of the sample spraying and vaporization would be useful for fine tuning the analytical sequence.

Another reason for measuring the water level in the plasma is the influence this parameter has on analyte signals recorded by the instrument, either through modifications to the basic properties of the plasma [3,5,14-16], or through formation of oxides, argides and doubly ionized metals [3,5,14,17-19] that may cause interferences. It was found that with conventional nebulization, desolvating droplets located low in the plasma have a large effect on ion-atom equilibrium and polyatomics formation by local cooling of the plasma [20,21]. Since we are dealing instead with a dry plasma or a plasma enriched with small amount of water vapor, the conditions are similar to those studied in several investigations in which some hydrogen is leaked to the plasma [22-24]. The effect of adding hydrogen usually resulted in a better transfer of energy from the plasma outer layers to the central core through enhanced thermal conductivity. It was observed that upon introduction of hydrogen, the electron density (n_e) as monitored by the continuum emission [25] or by Stark broadening of H_β lines [26] increased significantly. The effect of water vapor is more complex owing to the high heat capacity exhibited by water in the 3000-4000 K range caused by the dissociation of the molecule [24]. As a consequence, the central channel temperature is inhibited from rising above this value as long as the water is not fully dissociated. When this process is completed, the released hydrogen can produce its benefits. It was also recently observed that this enhancement is linked to the total energy available to the plasma [27], and that in low energy conditions e.g. with low plasma power and high injector flow, a net decrease in electron density can be seen upon introduction of water vapor. Adding water vapor to a stream of argon with volatilized ferrocene [15] revealed that the iron ion signal maximum shifted from inside the coil in dry conditions, to 13 mm above coil with 11 mg/min of water vapor. The signal maximum decreased in intensity but could be restored with higher plasma power. By comparison, 30 to 40 mg/min of water are typically introduced in the plasma with a conventional nebulizer and a significant part of the water is in the form of droplets. Clearly, water vapor introduced in small proportion in a dry plasma can have a significant impact on the various ionic balances and their positioning in the plasma. In view of these findings, it was expected that releasing uncontrolled amount of water to the plasma would randomly modify the transient signal in Spray-ETV-ICP-MS. Some sort of water monitoring as well as a diagnostic of the plasma state using selected argides species should help decipher the plasma behavior at sample vaporization. The solvent derived argides and the argon ion and dimer were examined as possible candidates for these purposes.

Mechanistic studies of the plasma indicate that argide polyatomic species such as ArH^+ and Ar_2^+ may originate in cooler conditions more likely to be found at the ion extraction process [9,28,29]. High levels of argides are also associated with the presence of an important secondary discharge generated by the use of an inverted or unshielded load coil [1,28,30,31]. The argides are considerably reduced in intensity by suppressing this discharge with proper coil arrangement although they remain at appreciable level [28,30]. The exact zone of creation of the argides that are not related to the secondary discharge is still debated. Nonose *et al.* [28] have determined that ArH^+ abundance correlates well with the electron density (n_e) observed within the interface zone but not with the densities observed in the plasma, an observation that lead the authors to infer that the argon hydride is formed inside the expansion jet. They also determined that the observed ratio of ArH^+ to ArO^+ is compatible with a temperature of formation of 2000-2500°K. In contrast, Tanner [1] has concluded that solvent derived argides, except for the argon dimer, are very likely to be sampled as such from the plasma based on the fact that these polyatomic species show a behavior similar to other species that are already known to originate from the plasma. Both authors agreed however, on the fact that the argon dimer is formed by condensation in the expansion region.

Nevertheless, a direct correlation with levels of argide oxide or hydride with water content has been experimentally observed in several studies [1-6] and will be explored in detail in this work. We have also studied the effect of various plasma parameters on the ArH^+ signal and their correlation with the amount of water introduced into the plasma. In addition to ArH^+, the oxygen and argon dimers plus the baseline noise recorded at m/z 197 were included in the experimental design. The purpose of this study was to find a way of quantitatively monitoring the low water loading of the plasma typically encountered with ETV applications, in order to include this parameter in an optimization routine. The knowledge of this parameter would help greatly in the adjustment of the operational parameters for Spray ETV-ICP-MS. Argon and oxygen dimers were monitored as probe species for providing an insight on the plasma state. It appeared during this study that with a suitable experimental strategy coupled with computations involving simple linear relationships, a basic plasma diagnosis can be established based on polyatomic species found in argon plasmas.

The argon hydride $^{36}ArH^+$ at m/z 37 was selected as the water monitoring species because the relatively low abundance of the ^{36}Ar isotope can be measured without detector saturation. The main interferences encountered at m/z 37 are $^{37}Cl^+$ and possibly SH^+ formed from the rare isotope ^{36}S. The chlorine interference can be corrected for by simultaneously measuring ^{35}Cl. Other isotopic variations of the argon hydride found at m/z 39 and 41 are overshadowed by ^{40}Ar on quadrupole mass spectrometers with low resolution such as those routinely used for ICP-MS and therefore they cannot be used. Another likely candidate would be $^{40}ArD^+$ at m/z 42, especially if an HCl matrix is used, but this species would suffer from Ca interference and was not evaluated in this study. The choice of an argon hydride instead of an oxide is preferred since virtually all hydrogen found in the central zone of the plasma is derived from the dissociation of the water matrix [5,32]. Additionally, all ArO^+ isotopic species interfere with metals of interest. OH^+ was not selected because its low mass makes it sensitive to space charge effects.

4.3 Experimental

4.3.1 Instrumentation and Sample Preparation

A SCIEX/Perkin-Elmer Elan 250/500 inductively coupled plasma mass spectrometer was used for this study (see Table 4-1). This instrument is equipped with a center-tapped load coil that greatly reduces the occurrence of the secondary discharge (or "pinch"), when compared to other coil geometries that distort the ion kinetic energy distribution downstream from the sampler aperture and as a consequence perturb the level of polyatomic species [30]. Data were collected using the "Graphics" application of version 2.0 of the Elan 5000 software with the plasma and ETV operating in conditions listed in Table 4-2. Two torch models were used. The outer quartz tube extended 9 and 18 mm respectively from the top of the load coil (TOLC) for the medium and long torch. On the Elan 250/500, the coil and torch support mechanism move from a minimal sampler to TOLC distance of 16 mm, a setting obviously not attainable when the long torch was mounted. Medium and long torches were used to minimize mixing of the plasma gases with the atmosphere, particularly atmospheric water. A standard Meinhard (Type A) nebulizer with a double pass spray chamber was used for the nebulization experiments. Lens optimization was conducted according to the manufacturer instructions with a 200 ug/L solution of Mg, Cd and Pb. The same lens settings were used for the dry plasmas. Mass calibration on the spectrometer were checked daily since this particular instrument has shown sudden and unpredictable deviations from calibration, especially for the high masses.

Table 4-1. Equipment and Supplies.

Description	**Model**	**Manufacturer**
ICP Mass Spectrometer	Elan 250/500 coupled to an UNIX based PS/2 running the Elan 5000 software	SCIEX/Perkin-Elmer Thornill, Ontario, Canada
Concentric Nebulizer	Type A	J.E. Meinhard Santa Ana, CA, USA
ETV Furnace	CTF 188	Thermo Jarrell Ash Franklin, MA, USA
Concentric Nebulizer Used for Spray Deposition	Type A	J.E. Meinhard Santa Ana, CA, USA
Water Purification System	Milli-Q System	Millipore Bedford, MA, USA
ICP Standards	QC19 multi-elements standard (including Sb, As, Be, Cd, Ca, Cr, Co, Cu, Fe, Pb, Mg, Mn, Mo, Ni, Se, Tl, Ti, V, Zn) in a 5% HNO_3 matrix	SCP Sciences Lasalle, Québec, Canada

A saturated stream of argon was generated by bubbling the gas through a porous (fine) glass frit in a flask containing deionized water immersed in a regulated temperature bath (regulated to ±1°C). The gas flow was regulated at the exit with a needle valve and monitored with a Matheson ball flow meter. Condensation in downstream gas lines was prevented by maintaining the water bath temperature below room temperature. A glass wool plug placed in the insulated exit of the flask blocked any droplets from being carried by the gas flow. The saturation of the argon was checked by weighing the water vapor trapped on a silica gel column and also by following the weight loss of the flask over an extended period of time. Both measurements showed that the argon water contents were close to the values predicted by the partial vapor pressures of water at various temperatures.

Table 4-2. ICP-MS and Spray-ETV-ICP-MS Operational Parameters.

	ICP-MS with moistened argon central flow	**Spray-ETV-ICP-MS**
ICP		
Plasma Power (Watts)	900 or 1100[a]	1100
Distance Top of Load Coil (TOLC) to sampler cone (mm)	16 or 19[a]	16
Plasma Argon Gas Flow (dm^3/min)	15	15
Secondary Argon Gas Flow (dm^3/min)	1	1
Central Argon Gas Flow (dm^3/min)	1.0 or 1.2[a]	1.0
Plasma Water Loading (mg/min)	0 to 3.3[a]	Variable
Mass Spectrometer		
Dwell Time (msec)	200	10
Points across Peak	1	1
Numbers of Replicates	100	80
Spray-ETV		
Warm Up		
Furnace Temperature		2000°C
Electrodes Cooling Water Flow		On, then off
Spray Deposition		
Furnace Temperature		160°C
Nebulizer Pressure		28 psi (N_2)
Deposition Time		30 s
Sample Volume		100 μL
Venting Flow To Atmosphere		1 dm^3/min (Ar)
Electrodes Cooling Water Flow		Off
Furnace Drying		
Furnace Temperature		200°C
Time		30 s
Venting Flow To Atmosphere		2.8 dm^3/min (Ar)
Electrodes Cooling Water Flow		Off
Furnace Ashing		
Furnace Temperature		400°C
Time		30 s
Carrier Flow To Plasma		1 dm^3/min (Ar)
Electrodes Cooling Water Flow		On
Vaporization		
Furnace Temperature		2200°C
Time		10 s
Carrier Flow To Plasma		1 dm^3/min (Ar)
Electrodes Cooling Water Flow		On
Furnace Cleaning		
Furnace Temperature		2600°C
Time		3 s
Carrier Flow To Plasma		1 dm^3/min (Ar)
Electrodes Cooling Water Flow		On

a) Respectively low and high settings for the 2^4 matrix design.

Consequently, full saturation of the argon was assumed throughout this work. Varying fluxes of water in the injector gas flow were obtained by combining an appropriate proportion of the saturated argon flow with a make-up gas flow of dry argon.

The ETV experiments were conducted with a Thermo Jarrell Ash furnace model CTF 188 (see Table 4-1) using commercially available pyrocoated graphite tubes. The furnace has been modified to accommodate spray deposition as previously described [13]. Since then, several improvements have been introduced to the spray ETV program, the most important being the addition of a dummy high temperature stage for drying thoroughly the furnace assembly just before spray deposition. None of these modifications imply any fundamental change to the general principle of spray deposition. The ETV furnace was linked to the ICP torch through a 60 cm section of tygon tubing with an internal diameter of 6 mm, and the wet argon was introduced into the furnace as the carrier gas.

Solutions were prepared from 1000 mg/L multi-element standard solutions diluted in Milli-Q water (18 MΩ) (See Table 4-1 for details on standards and water purification system).

4.3.2 Factorial Design and Experimental Strategy

A four parameter, two level, full factorial design [33,34] was used to explore in an organized manner the effects of controlled introduction of water into the central plasma gas, and effects from other operating parameters such as plasma power, injector plasma flow rate and sampling depth. The signal from water derived polyatomics and other species of interest were simultaneously measured. The signals were recorded for $^{36}ArH^+$ (at m/z 37), $^{36}Ar^+$, $^{40}Ar_2^+$ (at m/z 80), $^{17}O_2^+$ (at m/z 34) and the baseline noise at m/z 197, which corresponds to

$^{197}Au^+$. Argon 36 and the argon dimer were included for probing the energetic state of the plasma. A design matrix including the 2^4 possible combinations of parameters (full factorial), shown in Table 4-3 with the range investigated for each parameter, was constructed and the experiments were run according to the strategy described in the following section. A particular effect e_i^k, defined as the variation in the signal of species k caused by a change in parameter i, is extracted from the data set using Eqn (4-1).

$$e_i^k = \bar{y}_+^k - \bar{y}_-^k \qquad (4-1)$$

Where $\bar{y}_+^k$ is the average response obtained when parameter i is set to its high value (+) and $\bar{y}_-^k$ when parameter i is set to its low value (-), irrespective of the settings of the other parameters. Calculations were done on responses normalized to unit variance (within the same species), in order to offset the differing abundance of each species. Calculated effects are thus directly expressed as a fraction of the total variance observed for each species over the parameter set, which makes trend comparison between species much easier. The combined effect for two parameters was obtained by subtracting the average response obtained when both parameters are set high or low, minus the average response when the two parameters have opposed signs. Two parameter effects are actually an evaluation of the non-additivity, or the non-orthogonality, of the net effect that the parameters involved have on the system. Higher order effects were used as noise estimate's assuming that three and four parameter interactions measure differences arising from experimental errors. It can be seen from eqn (4-1) that all the observations supply information in the calculation of each of the effects, thereby providing a significant signal-to-noise improvement (in this case a factor of

$\sqrt{8}$). For a two-level factorial design, linear responses are assumed over the explored parameter range.

Table 4-3. 2^4 Matrix Design.

Parameter Set	**Water Loading** ("-" = 0.0 mg/min "+" = 3.3 mg/min)	**Plasma Power** ("-" = 900 watts "+" = 1100 watts)	**Sampling Depth** ("-" = 16 mm "+" = 19 mm)	**Central Flow Rate** ("-" = 1.0 dm^3/min "+" = 1.2 dm^3/min)
1	-+[a]	-	-	-
2	-+	-	-	+
3	-+	-	+	-
4	-+	-	+	+
5	-+	+	-	-
6	-+	+	-	+
7	-+	+	+	-
8	-+	+	+	+

a) The matrix design shown in this table was subsequently randomized for plasma power, injector flow rate and sampling depth, thereby excluding the water loading parameter. Low and high water loading were evaluated for each combination of the other parameters (see text for experimental strategy).

A randomization of the experimental sequence was applied on a subset of the matrix design that included plasma power, sampling depth and injector gas flow. For each parameter set, the water load was ramped in five evenly spaced fixed increments, beginning with a zero water loading and ending with a water loading of 3.3 mg/min. A steady state was obtained for each increment. The calculation of the water loading effects in the parent design used the zero and the high water load levels as low and high settings, while intermediate loading results served in establishing the linear relationship of each species with water level. Each trace took 15 minutes to record and the whole design was acquired within three hours, a time frame short enough to minimize instrumental drift. The impact of any long term drift on the final results is however greatly attenuated by the random order in which the experiments are conducted.

4.4 Results and Discussion

For the four species selected, the traces in Fig. 4-1 show the effect of introducing water in increments as described in the experimental section, with three different combinations of plasma power, injector flow rate and sampling depth. The parameter set numbering refers to the matrix design of Table 4-3. The relationship between water loading and $^{36}ArH^+$ response, in curve (a), seems to be directly proportional to the water loading. An apparent linear response was also observed from the curves obtained with the other parameter sets (not shown). Moreover, the $^{36}ArH^+$ sharply responded to the water load and a steady state was rapidly achieved after sudden changes in plasma loading. Sets 1 and 4 were selected for graphing because they gave the highest and the lowest response slope respectively. $^{17}O_2^+$ also has a direct response to water loading although the response is noisier and less sensitive than $^{36}ArH^+$. In contrast, the argon and argon dimer respond sluggishly to changing conditions in the plasma, and appeared to be very sensitive to transient fluctuations when gas flow adjustments were done. The $^{36}Ar^+$ response seems dominated by long term drift that might result from surface charging effects characterized by a longer response time. A similar drift is apparent for $^{40}Ar_2^+$ although the response to change in water loading was sharper. The origin of this drift remains unexplained but can be nulled out as we will see in the next section.

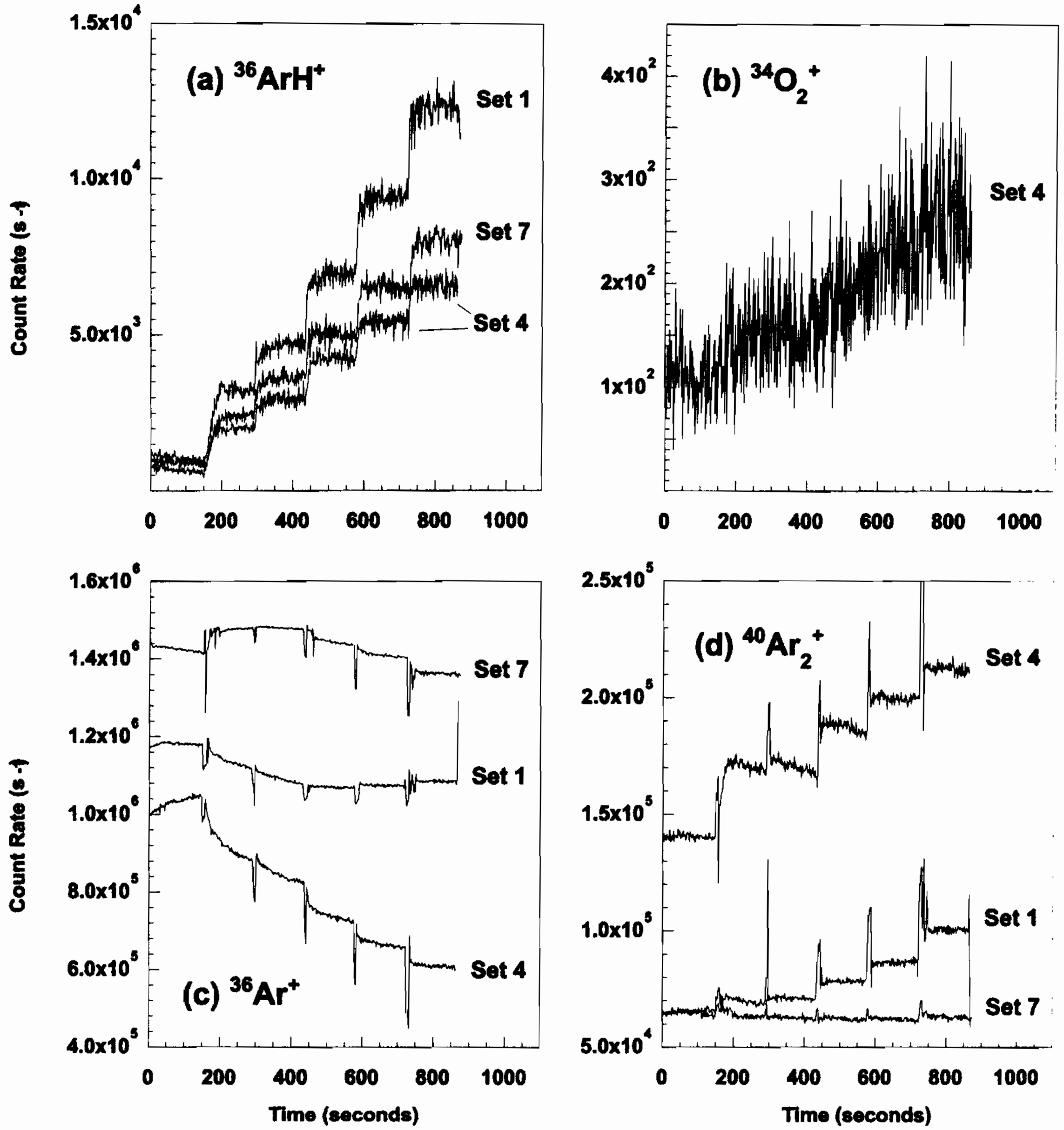

Figure 4-1. Signal recorded for (a) $^{36}ArH^+$, (b) $^{18}O_2^+$, (c) $^{36}Ar^+$ and (d) $^{40}Ar_2^+$ using operating parameters Sets 1, 4 and 7 as described in Table 4-3, except for $^{18}O_2^+$ for which just Set 4 is shown. The plasma was loaded with increasing amount of water starting from 0 mg/min up to 3.3 mg/min, in steps of 0.7 mg/min.

Correlation values above 0.99 (0.9992 in the best case) are obtained for the argon hydride response in function of water loading when linear regression is applied to separate curves. The mean intercept value corresponds to a plasma load of 0.3 mg/min in water (σ=0.1) which was attributed to contamination from atmosphere.

4.4.1 Slope of Response and Energy Transfer Efficiency

The parameter sets can be categorized according to the response of $^{36}ArH^+$ to water loading and seem to be correlated with the efficiency of energy transfer to the central channel. Set 1 is a situation of low plasma power with a low injector flow rate. With this combination of parameters, the instrument generated the highest response slope for $^{36}ArH^+$ (see Fig. 4-1(a)). In contrast, Set 4 produced the lowest response when the sampling depth and injector flow were set high and the plasma power was at its low setting. Lower energy transfer efficiency (compared to Set 1) is expected since the plasma is cooled by the high injector flow, even though ions are collected further away from the coil that allows more energy to be transferred. The net effect was a sharp decrease in argon hydride levels while the linearity with water loading was preserved. Interestingly, the oxygen dimer response is minimally affected by these changes. Just one experimental set is illustrated in Fig. 4-1(b) for this species as the others overlap. Set 7 (high plasma power and sampling depth, low injector flow) presents an interesting situation in which the argon hydride gave slightly below average response, however, the argon ion was the highest recorded and the argon dimer was second lowest. The combination of high power and low injector flow generated more "robust" conditions of excitation [35] and poor survival conditions within the plasma for molecular species such as argides. The opposite of Set 7 in term of plasma robustness was Set 2 with low plasma power, short sampling depth and high injector flow (not shown), which gave a high response for the argon dimer and a low one for the argon ion.

The effect on noise as recorded at m/z 197 proved to be insignificant over the parameter range explored and was ignored.

4.4.2 Calculated Effects

The parameter effects calculated using Eqn 4-1 for the matrix design from Table 4-3 are summarized in Table 4-4. Main and second order effects representing more than three times the error associated with the unit variance response of each species (as evaluated from the high order terms) are printed in bold. Only one of the second order effects exhibits a small contribution to the total variance for the argon hydride, which tends to confirm the initial hypothesis about linear response to water loading over the parameter ranges covered. Of great interest is the contribution of water loading to the total variance for $^{36}ArH^+$ and $^{34}O_2^+$, which account for respectively 91% and 92% of the total variance observed for each of these species. Also, the contrasted behavior of $^{36}Ar^+$ and $^{40}Ar_2^+$ are clearly revealed by effect values of opposed sign for the two species, upon changes of plasma power, water loading and injector flow. When the availability of energy to the central channel is increased by increasing plasma power (with all other parameters fixed), the energy probing species ($^{36}Ar^+$) becomes more abundant. Conversely, decreasing the injector gas flow also has a positive effect on argon (the calculated effect has a negative value because it corresponds to an *increase* in the parameter). The same conditions deplete the argon dimer sampled by the instrument. The calculated effects associated with the water vapor loading are indicative of a net cooling effect on the plasma.

Table 4-4. Calculated Effects.

Factors	**Effect (in variance units) on:**				
	$^{36}ArH^+$	**$^{34}O_2^+$**	**$^{36}Ar^+$**	**$^{40}Ar_2^+$**	**Dimer Temperature[a]**
Main Factors					
Water Loading (W)	**1.91**	**1.92**	**-0.94**	**0.78**	**-0.78**
Plasma Power (P)	0.00	-0.10	**1.14**	**-1.07**	**1.21**
Sampling Depth (S)	**-0.39**	-0.19	0.31	0.15	-0.13
Injector Flow (I)	-0.10	0.32	**-1.13**	**1.19**	**-1.30**
Second Order Factors[b]					
P/W	-0.03	0.17	0.25	**-0.43**	0.20
S/W	**-0.36**	-0.10	-0.05	-0.10	0.12
I/W	-0.06	-0.10	-0.37	**0.51**	**-0.27**
S/P	0.16	0.16	0.20	0.06	0.03
I/P	0.05	-0.09	0.15	**-0.51**	0.00
I/S	0.07	-0.02	0.30	-0.07	0.19
Standard Deviation on Factors[c]	0.06	0.12	0.14	0.11	0.09
Total Signal Variance (in count/sec or Kelvin)	4350	106	261000	52300	1440 K

a) As calculated using the equation derived from statistical mechanics by Cleland and Meeks [29] for the argon dimer equilibrium in the plasma (see text).

b) Second orders effects show correlated response of signal for simultaneous changes in two parameters.

c) Evaluated from third and fourth orders factors according to the equation $SD_k = \left(\sqrt{\sum F_i^2}\right) / N$ where SD_k is the standard deviation of effects for species k, as estimated using the N selected high order effects F_i. The three effects involving three parameters and the one involving all four parameters were used to calculate SD_k for each species.

4.4.3 Multiparametric Equation for Evaluating the Water Load

An attempt was made to evaluate the water level in the plasma from the recorded argon hydride signal. Since we have also introduced the effects from other operating parameters, the factorial design arithmetic should allow one to recover this information in various operating conditions. The signal for each species can be estimated back at each vertice of the design by using Eqn (4-2) [33].

$$\hat{y}^k = \bar{y}^k + \tfrac{1}{2}(e_1^k x_1 + e_2^k x_2 + e_3^k x_3 \ldots + e_{12}^k x_{12} + e_{13}^k x_{13} \ldots) \qquad (4\text{-}2)$$

Where $\hat{y}^k$ is the estimated signal for the species k, $\bar{y}^k$ the average signal recorded, e_1^k the main effect and x_1 the design factor for parameter 1 over species k, e_{12}^k the cross-effect and x_{12} the design factor for parameter 1 and 2 and so on. The factor 1/2 appears before the parenthesis term because each design factor represents two units of change (-1 to +1) for any parameter. In fact, the estimated signal $\hat{y}$ is extrapolated from the central point (0,0,0,0) where all parameters are at mid position and to which we assign the average signal recorded. We can include all high order effects in Eqn (4-2) but usually only the main effects and most significant second order (cross) effects are needed. A vertice is defined as being one of the 2^4 parameter sets generated in the design presented in Table 4-3. We used Eqn (4-2) to interpolate the amount of water at varying values of plasma power, sampling depth and injector flow, using the factors calculated from the $^{36}ArH^+$ response. The design factor x_W for water level can be isolated from Eqn(4-2), which gives after selection of the most significant effects:

$$x_W = \frac{2(y^{^{36}ArH^+} - \bar{y}^{^{36}ArH^+}) - (e_P x_P + e_S x_S + e_I x_I + e_{SP} x_{SP})}{e_w + e_{SW} x_S} \qquad (4\text{-}3)$$

Where the main factors for plasma power, injector flow and sampling depth (as denoted by subscripts *P*, *I* and *S*) as well as the cross-effects of sampling depth with plasma power (*SP*) and water level (*SW*), are used for evaluating the actual water load. The two cross-effects e_{SP} and e_{SW} were included in the model because they significantly reduced the error on predicted values. It is noteworthy that the cross-effect that includes the water loading (e_{SW}) can be used without any prior information about the water level. The quantity $y^{^{36}ArH^+}$ is the signal recorded for $^{36}ArH^+$ while $\bar{y}^{^{36}ArH^+}$ retains the same meaning as in Eqn (4-2). With this method of calculation, the real values for the operating parameters are first translated into corresponding design factors by ratioing. The calculated factors are then introduced into Eqn (4-3) along with the recorded signal for $^{36}ArH^+$. The value of water loading is restored from the calculated x_W using the low and high limits of water loading originally used to compute the model. For example, a plasma power of 950 Watts, an injector flow of 1.18 dm^3/min and a sampling depth of 17 mm will translate into design factors $x_P = -0.5$, $x_I = 0.8$ and $x_S = -0.33$ respectively, given the range of value spanned for each of these parameters (see Table 4-3 for actual ranges). If the recorded signal for argon hydride is 4000 count/sec, the design factor for water resulting from the computation of Eqn (4-3) is equal to 0.25. This factor value corresponds to a measured level of water of 1.20 mg/min since a design factor of -1 means 0 mg/min and +1 means 3.3 mg/min in the original model. The fact that all design factors (including the one derived by calculation) are within the interval -1 to +1, implies that the calculated water loading has resulted from an interpolation. Incidentally, it is possible to extrapolate the model, although with caution, for one or several parameters including the water loading parameter. With this method of calculation, the parameter values are moved from the "real" to the "factorial design" world by ratioing and are restored using the inverse transformation. It should be noted that the effects e in Eqn (4-2) and (4-3) are those obtained from original signals and not from data normalized to unit variance that were presented in Table 4-4 solely for discussion purposes. The original magnitude of each effect can be obtained simply by multiplying the normalized effect by the total signal variance observed for the species.

The intermediate values of water loading for the 8 parameter sets were estimated using Eqn (4-2) with a standard deviation of 0.15 mg/min from the real values. The argon hydride signal recorded in a different day can be related to the water loading using the model. The signal recorded for the Mg, Ag and Pb test solution used for mass alignment allows one to correct for daily variations in the instrument sensitivity. The day to day precision in measurement of water loading is of the order of 15%-20% but the linearity of the response is preserved. This value can be used as an internal standard to correct for daily variations in water loading.

4.4.4 The Argon Dimer as Temperature Probe

Although the argon and argon dimer taken separately seem to give a fairly good overview of the energetic state of the plasma, a more fundamental diagnosis can be obtained by calculating the temperature of formation of the dimer according to the equilibrium proposed by Cleland and Meeks [29].

$$Ar^{+} + Ar \Leftrightarrow Ar_2^{+} \quad (4\text{-}4)$$

An equation relating the observed ratio of intensity of Ar_2^+ to the intensity of Ar^+ with the equilibrium temperature was derived by Cleland and Meeks from partition functions of the involved species. The calculated temperature obtained using this relationship is representative of the ratio observed at the detector level. It probably does not reflect the actual equilibrium as it exists in the plasma (or in the ion extraction subsystem) but includes as well distortion introduced at various stages of the ion extraction and transmission processes. For this reason, it is probably more accurate to speak of an "instrumental" temperature. The $^{36}Ar^+$ and $^{40}Ar_2^+$ intensities determined previously were introduced into the equation after correction for isotopic abundances, to obtain the temperature of formation of the dimer for the various set of experimental parameters. An evaluation of the ion transmission efficiency and spectrometer sensitivity at different m/z values was done using the Mg, Ag and Pb test solution, and the argon and argon dimer intensities were corrected accordingly. Although, as we discussed above, we had no intention of determining the true value of the ratio as it actually exists within the plasma, the observed ratio is expected to be accurate enough to reveal internal trends and be used as a comparison between similar instruments.

In Fig. 4-2, the "dimer temperature" curves were calculated from the corresponding Ar^+ and Ar_2^+ curves of Fig. 4-1. A striking feature immediately apparent in the resulting curves is that the slow drift that was observed in the response curves for Ar^+ and Ar_2^+, as observed after a sudden change in the water loading, is almost totally corrected with the new indicator. Neat steps resembling those seen for argon hydride are instead generated. The dimer temperatures were introduced in the experimental design calculations, after normalization to unit variance, and the various effects were evaluated using Eqn (4-1). The resulting values are listed in Table 4-4 and mirror the Ar^+ behavior, but with a greater sensitivity to plasma power and injector flow as revealed by the magnitude of respective effects. In contrast, the response is less sensitive to sampling depth. The small negative value for the sampling depth effect means that the plasma temperature, as sensed by the dimer equilibrium, is very slowly decreasing as the load coil is moved away from the sampling cone. The unexpectedly low magnitude of change related to this key parameter might be explained by the fact that we are observing the top of the temperature maxima, however, this point was not verified experimentally. The low numerical values obtained for cross-effects indicates that the dimer temperature reacts more independently, or in other word exhibit more orthogonality, to a variation of a given operating parameter. In contrast, $^{40}Ar_2^+$ and to a lesser extent $^{36}Ar^+$ exhibits several significant cross-effects that render the picture more complex.

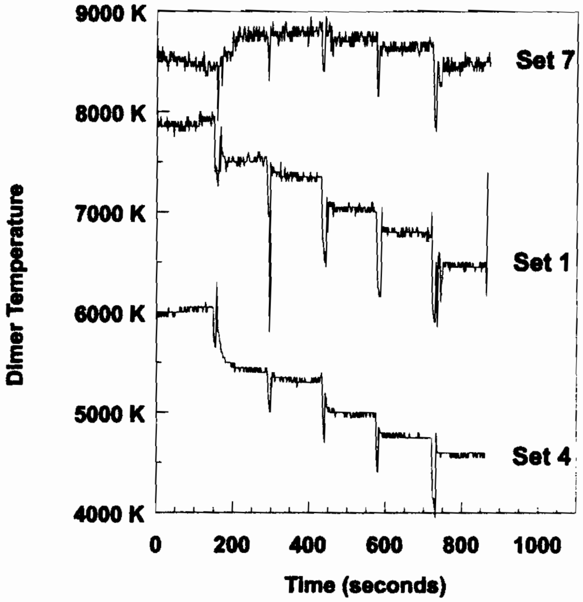

Figure 4-2. Plasma temperature as calculated from the argon dimer equilibrium [29] $Ar + Ar^+ \Leftrightarrow Ar_2^+$ using data from Fig. 4-1(c) and (d). The plasma water load was varied over time in the same manner as in Fig. 4-1 and the parameter sets 1, 4 and 7 refer to the operational parameters of Table 4-3.

The instrumental temperatures recorded are in general much greater than the ones usually found in plasmas with conventional nebulization. In their communication [29], Cleland and Meeks have reported a temperature of 2400 K for a plasma of 1300 Watts with an injector flow of 0.85 dm^3/min, which are more energetic conditions than the one found in this work. Also, Nonose *et al.* [28] have found a plasma temperature of 3500 K based on observed ratio of argides polyatomics using similar statistical mechanic arguments. Our measurements covered a plasma temperature range of 4100-9000 K just by varying the plasma power and the injector flow within a relatively narrow range. Adding water vapor in low amount also changed the plasma temperature but not as much as the two previous parameters. The conditions within a dry plasma appear to be more sensitive to operational parameters than within a wet plasma.

Measuring the argon ion to argon dimer ratio with an acceptable accuracy is a tedious task not easily done routinely. In Fig. 4-3, the signal recorded for $^{36}Ar^+$ and $^{40}Ar_2^+$ in various conditions of water loading and other conditions used for the experimental design (48 observations in all) were plotted against the calculated temperature for the dimer equilibrium. A reasonable relationship between the argon dimer signal and the dimer temperature appears between 4000 K and 7000 K, a temperature range that excludes very dry plasma conditions.

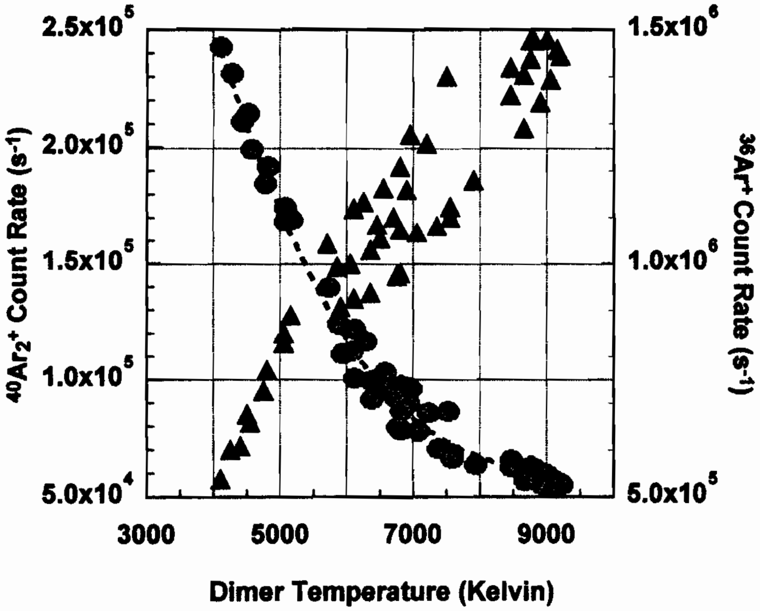

Figure 4-3. Signals for $^{36}Ar^+$ and $^{40}Ar2^+$ with the plasma temperature as calculated from the argon dimer equilibrium. Data shown were obtained for each discrete water load (as illustrated in Fig. 4-2) using all 8 parameter sets.

4.4.5 Spray ETV Experiments

To evaluate the effect of varying the water vapor loading on the signal generated by Spray-ETV, we have done several runs using the spraying parameters and ETV temperature programming listed in Table 4-2. The water evaporated from the tube at spraying is collected in internal parts of the furnace, particularly within the porous structure of the graphite inserts that form the contact electrodes. At sample vaporization, this condensed water is released to the plasma with the analytes as vapor. The monitoring of the $^{36}ArH^+$ has permitted to modify the temperature sequence to reduce the collection of water at spraying. The residual water from the previous run is expelled using a dummy high temperature stage at 2000°C just before sample deposition, as mentionned earlier. An additionnal advantage is that following this stage, the furnace assembly becomes hot enough to prevent internal condensation of water at sample spraying. The cooling water flow to the electrode rings is interrupted until the ashing stage, after most of the sample water has been dried away to atmosphere. The instrument therefore vaporizes the sample with minimal evaporation of water. The evaporation of water vapor during the high temperature stage is illustrated on Fig. 4-4 for Spray-ETV experiments with 100 μL of a 10 ng/L sample prepared from the multistandard solution of Table 4-1 (1 ng of each element is deposited). Figure 4-4 show traces obtained with a dry argon carrier flow and with an argon carrier flow moistened with 0.5 mg/min of water vapor. The carrier flow of the furnace becomes the injector flow when it forms the central channel in the plasma since no make-up gas flow was introduced between the ETV and the plasma torch. The argon hydride and argon dimer included in the analytical procedure show that the sample vaporization is characterized by two phases. During the first 4 seconds after the initiation of the furnace firing, the water content of the plasma is low and controlled by the amount of water introduced as vapor in the argon carrier. The plasma temperature as determined from Ar_2^+ and data from Fig. 4-3 is of about 7500 K at that stage. The second stage is characterized by a rise in the plasma water load which as consequence lower the plasma temperature to below 4000 K for the experiment done with 0.5 mg/min of water. The rise in water loading is much less severe with a dry carrier and the plasma temperature is more stable over the vaporization stage. The abrupt rise in water loading that we see in Fig. 4-4(f) has also been observed for the other experiments done with a moistened carrier. This suggests that some water build up within graphite inserts are promoted even in presence of low proportion of water vapor in the carrier. This water accumulation probably arises at the ashing stage when the cooling water flow is resumed and cool spots appear in the inserts. At the onset of the vaporization stage, the temperature surge in the furnace is restricted to the graphite tube, but within seconds the inserts are heated up rapidly by heat conduction and therefore release the water trapped in their porous structure. This delayed heating of the inserts explains why the water surge is observed after the volatile metal peaks. It can be added in proof that the ArH^+ signal plateaus at a level directly proportional to the amount of water in the carrier flow at ashing (data not shown), and that there is no long term drift, that is, no apparent drying off of the inserts from run to run. Also, all experiments done with a dry carrier show a response very similar to the one of Fig. 4-4(f), which indicates that little water recondensed from the sprayed sample is released to the plasma. Running the same experiments with D_2O samples (or DOH to minimize costs) and recording ArD^+ at m/z 42 to distinguish it from the carrier moistening water, would help determine the very source of the water expelled by the furnace at vaporization.

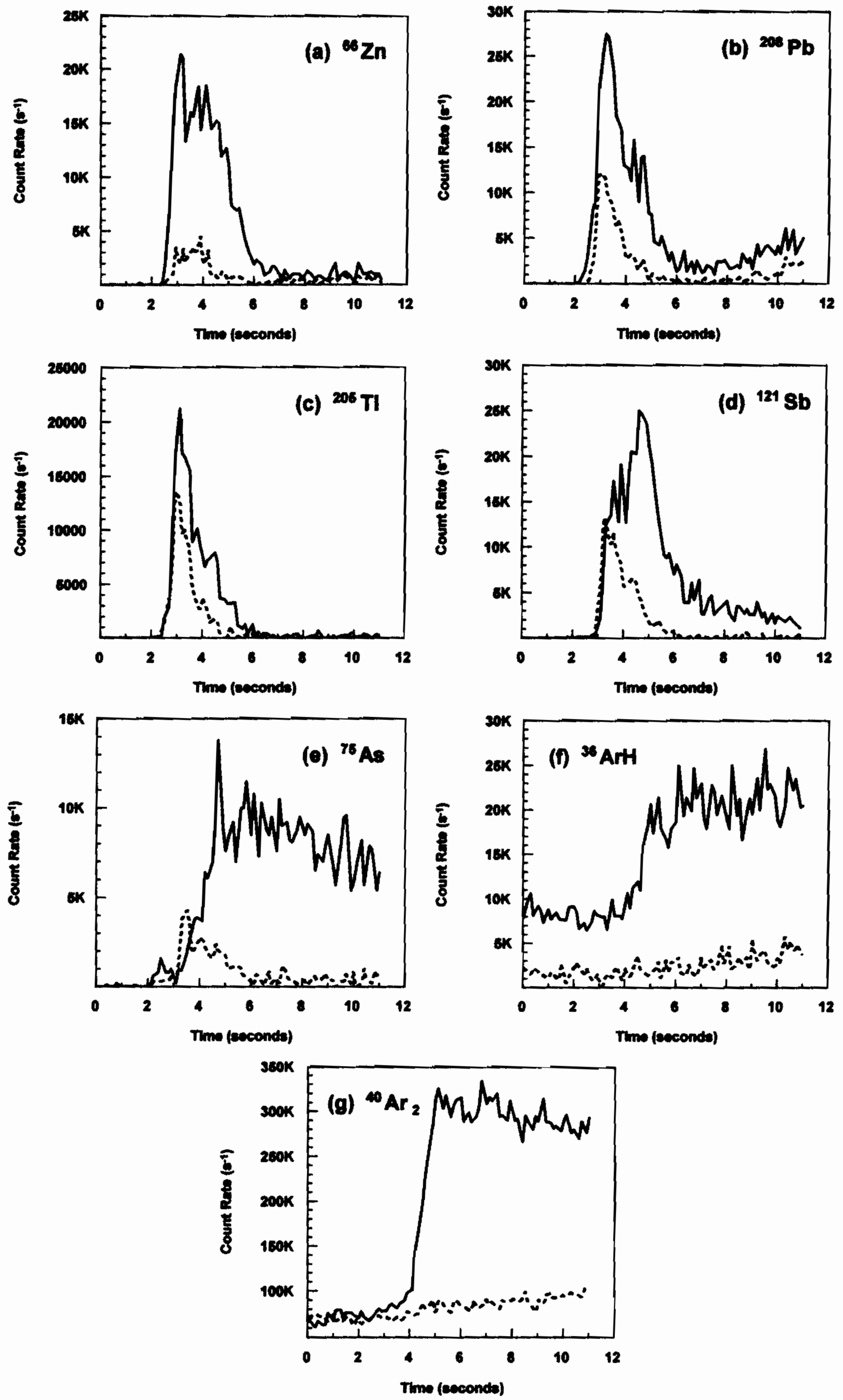

Figure 4-4. ETV transients recorded for 1 ng of (a) Zn, (b) Pb, (c) Tl, (d) Sb and (e) As, sprayed in the furnace, with signals for (f) $^{36}ArH^+$ and (g) $^{40}Ar_2^+$ recorded simultaneously. Transients were obtained for a dry plasma (— — — —) and for a plasma water loading of 0.5 mg/min (————).

The transients for zinc, lead, antimony and thallium illustrated in Fig. 4-4 appear to be greatly influenced by the amount of water present in the plasma. A comparison of transients for these metals obtained in a dry plasma (broken lines) with transients obtained in a water enriched plasma (solid lines) shows a significant increase in signal strength which seems to be in direct proportion with the plasma water load (all other operating parameters being equals). Most of the transients appear in the first phase of the vaporization stage, that is, when the observed water comes mostly from the carrier. When the surge of water hits the plasma, the trailing parts of the transients are greatly amplified. This leads to the appearance of double humps and apparent high tailings for metals that are still entering the plasma at this moment. In the literature, signal quenching by a similar water surge at mid-course of sample vaporization was proposed to explain the appearance of two maximums for the Pb I 405.78 nm emission line in ETV-ICP-AES [22]. The effect and length in time of the surge was deduced from peak shape changes but was, however, not observed directly.

The nearly identical enhancement in signal obtained for elements showing different chemical and thermal properties is an indication that the amplifications take place within the plasma, with the notable exception of arsenic. It is suspected that the presence of water within the carrier altered the chemistry of vaporization for this element [36] allowing it to escape at sample ashing. In addition, the high tailing increased as water level was increased in the furnace gas (for the same amount of sprayed element). These suggest that the tailing signal might be due to interference by $^{40}Ar^{35}Cl^{+}$ formed from traces of chlorine in the sample matrix, and promoted by the lower temperature of the plasma as more water vapor is introduced.

4.4.6 Transients Ratioing Using Ar_2^+ and ArH^+ Responses

The use of argon polyatomics as monitoring species for evaluating matrix effect in ICP-MS has been advocated in several studies [7-12]. Some workers used the argon dimer [10,11] and also other argides and polyatomics [8] as internal standards to correct for high matrix loading in ICP-MS with conventional nebulization. Grégoire *et al.* [7] used the argon dimer signal to select the proper calibration strategy for analysis of slurries in ETV-ICP-MS, based on the observed modifications in the Ar_2^+ transient induced by the sample matrix reaching the plasma. Another interesting application of the argon dimer monitoring for ETV-ICP-MS was proposed by Vanhaecke *et al.*[9] in which biological and environmental samples in solid form were vaporized and analytes transients were ratioed to the dimer signal on a point-to-point basis to restore linearity in calibration curves. All these studies attempted to correct for space-charge effects and, in general, the correction worked well for elements with masses close to the species used as internal standard. The studies on ETV have in common the monitoring of the rapidly changing conditions for ion generation and ion transmission that is observed throughout the vaporization stage.

Although we are dealing with the opposite effect (signal amplification), we felt that the approach of Vanhaecke *et al.* [9] would be of great use to deal with the rapid fluctuations in ion generation efficiency. A ratioing of the element transients illustrated in Fig. 4-4 was done using the argides transients that had been simultaneously recorded. The resulting transients ratioed with argon hydride and argon dimer for a moistened carrier are presented in Fig. 4-5. It is immediately apparent that in both cases, the peak shapes are restored or at least greatly improved using either argide as correcting species while the signal to noise ratio is ameliorated. The hump and peak tailing are almost totally corrected for lead and greatly attenuated for antimony and zinc. The peak for thallium is narrowed. Overall, the argon dimer appears to apply a more efficient correction over transients probably owing to the fact that it is more sensitive to plasma changes. In addition, its recorded abundance is much higher than for the hydride and as consequence, the ratioing operation introduces less noise in the resulting signal. The transients obtained in dry plasma did not gain any significant improvement from the ratioing and were not shown.

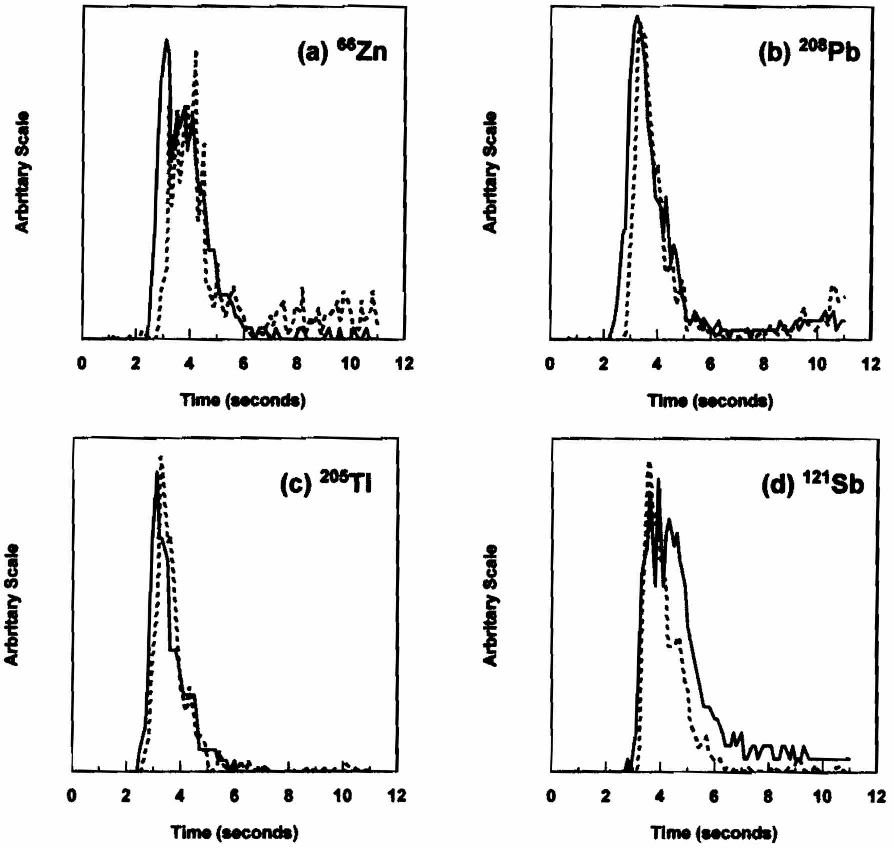

Figure 4-5. ETV transients of Fig. 4-4 for (a) Zn, (b) Pb, (c) Tl and (d) Sb, using $^{36}ArH^+$ *(———) and* $^{40}Ar_2^+$ *(— — — —) as ratioing species.*

Figure 4-6 illustrates the evolution of the integrated signals obtained from similar spray-ETV experiments carried out with the same sample, as the water loading is increased. In Fig. 4-6(a), the transients are not corrected and the various elements show a relative signal increasing ranging from a factor 2 for Sb to a factor of above 6 for Cu, when the water load reaches a relatively low value of 0.7 mg/min. Arsenic is not shown on these figures. Figure 4-6(b) and (c) illustrate the same data but after ratioing with the argon hydride (b) and argon dimer (c) transients. The argon dimer introduces an overcorrection while the hydride undercorrects the deviation caused by a varying water load. Nevertheless, while the uncorrected signals see variations of a factor over 6, the deviations over corrected data are restricted to a range of about ±35%. Therefore, the argon dimer can probably be used as an internal standard to minimize signal drift due to limited fluctuations in water load from runs to runs.

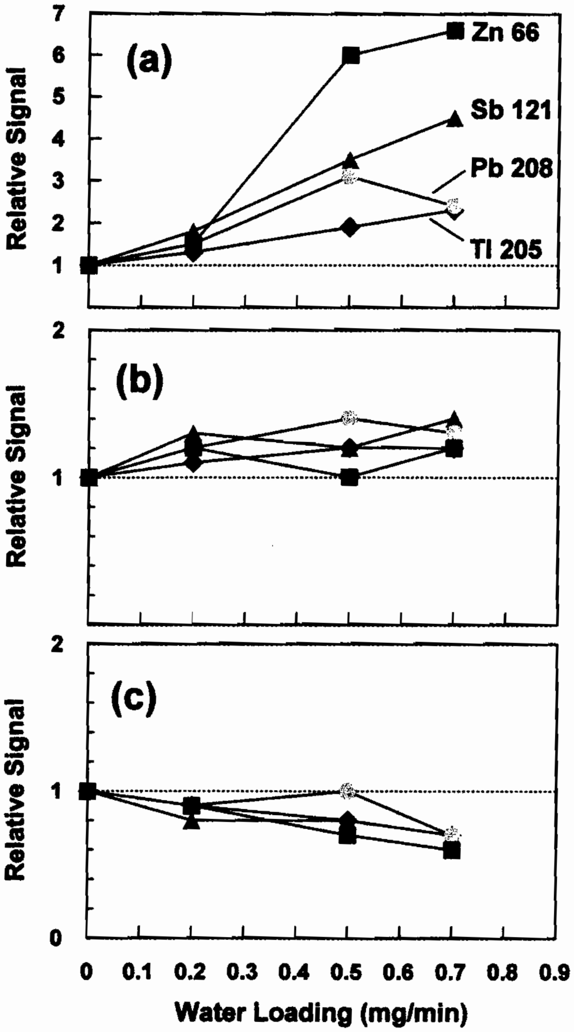

Figure 4-6. Integrated signals for Zn, Pb, Sb and Tl obtained when the plasma water loading is increased from 0 to 0.7 mg/min, as calculated from (a) unratioed transients, (b) transients ratioed with $^{36}ArH^+$ and (c) transients ratioed with $^{40}Ar_2^+$ (Note the Y scale expansion for graphs (b) and (c)).

4.5 Conclusion

An exploration of the variability of argon species derived from water has shown a linear response of the argon hydride ^{36}ArH$^+$ to the controlled introduction of water vapor in the plasma injector flow. A model derived from factorial design was applied in order to evaluate the water loading from the argon hydride response and from the plasma operating parameters. Moreover, the examination of the main and cross-effects calculated from the factorial design gives us a unique view of the sensitivity of the plasma to one or another parameter or their combination, and this with a minimal set of experiments.

The signal enhancement generated by introducing small amount of water vapor in ETV-ICP-MS seems to be usable if we correct the transients of Cu, Pb, Sb and Zn using the signal from an appropriate probing species. This species should be selected to give an adequate monitoring of short term fluctuations in the plasma during sample vaporization, and especially those induced by water. It appeared that the argon dimer provides the necessary sensitivity to rapid fluctuations in characteristics of dry plasmas. These conditions are typically found when electrothermal vaporization or laser ablation are used as sample introduction systems. The dimer also acts as a crude thermometric indicator. As an alternative, the argon hydride can be used as ratioing species.

These findings have an immediate application for Spray-ETV-ICP-MS as the commercial ETV we used was not designed to accommodate more than a few tenths of microliter of sample water. Therefore, when over half a milliliter of sample is sprayed in the ETV, some water recondensed and is released at varying pace at sample vaporization. The information we get from the water loading and the energetic state of the plasma can be exploited to improve the temperature sequence and the gas flow pathways in the furnace during the analytical sequence. We were able this way to minimize greatly the water released to the plasma at sample vaporization.

4.6 References

[1] S. D. Tanner, *J. Anal. At. Spectrom.* **10,** 905 (1995).

[2] V. Hernandis, J. L. Todoli, A. Canals and J. V. Sala, *Spectrochimica Acta* **50B,** 985 (1995).

[3] N. Jakubowski, I. Feldmann and D. Stuewer, *Spectrochimica Acta* **47B,** 107 (1992).

[4] D. C. Grégoire, *Prog. analyt. Spectrosc.* **12,** 433 (1989).

[5] R. C. Hutton and D. K. Eaton, *J. Anal. At. Spectrom.* **2,** 595 (1987).

[6] A. Gray, *Spectrochimica Acta* **41,** (1986).

[7] D. C. Grégoire, N. J. Miller-Ihli and R. E. Sturgeon, *J. Anal. At. Spectrom.* **9,** 605 (1994).

[8] X. Chen and R. S. Houk, *J. Anal. At. Spectrom.* **10,** 837 (1995).

[9] F. Vanhaecke, L. Galbács, S. Boonen, L. Moens and R. Dams, *J. Anal. At. Spectrom.* **10,** 1047 (1995).

[10] J. W. McLaren, D. Beauchemin and S. S. Berman, *Spectrochimica Acta* **43B,** 413 (1988).

[11] D. Beauchemin, J. W. McLaren and S. S. Berman, *Spectrochimica Acta* **42B,** 467 (1987).

[12] R. W. Fonseca and N. J. Miller-Ihli, *Spectrochimica Acta* **51B,** 1591 (1996).

[13] J.-F. Alary and E. D. Salin, *Spectrochimica Acta* **50B,** 405 (1995).

[14] H. Niu and R. S. Houk, *Spectrochimica Acta* **B51,** 779 (1996).

[15] N. Jakubowski, I. Feldmann and D. Stuewer, *J. Anal. At. Spectrom.* **8,** 969 (1993).

[16] J. W. Olesik and S.-J. Den, *Spectrochimica Acta* **45B,** 731 (1990).

[17] E. Poussel, J.-M. Mermet and D. Deruaz, *J. Anal. At. Spectrom.* **9,** 61 (1994).

[18] R. Tsukahara and M. Kubota, *Spectrochimica Acta* **45B,** 779 (1990).

[19] G. Zhu and R. F. Browner, *J. Anal. At. Spectrom.* **3,** 781 (1988).

[20] S. E. Hobbs and J. W. Olesik, *Spectrochimica Acta* **48B,** 817 (1992).

[21] J. W. Olesik, L. J. Smith and E. J. Williamsen, *Anal. Chem.* **61,** 2002 (1989).

[22] J. P. Matousek and J.-M. Mermet, *Spectrochimica Acta* **48B,** 835 (1993).

[23] M. Murillo and J.-M. Mermet, *Spectrochimica Acta* **42B,** 1151 (1987).

[24] Y. Q. Tang and C. Trassy, *Spectrochimica Acta* **41B,** 143 (1986).

[25] M. Murillo and J.-M. Mermet, *Spectrochimica Acta* **44B,** 359 (1989).

[26] S. E. Long and R. F. Browner, *Spectrochimica Acta* **43B,** 1461 (1988).

[27] D. G. Weir and M. W. Blades, *Spectrochimica Acta* **49B,** 1231 (1994).

[28] N. S. Nonose, N. Matsuda, N. Fudagawa and M. Kubota, *Spectrochimica Acta* **49B,** 955 (1994).

[29] T. J. Cleland and F. R. Meeks, *Spectrochimica Acta* **51B,** 1487 (1996).

[30] B. M. Ross, P. Yang, D. M. Chambers and G. M. Hieftje, *Spectrochimica Acta* **46B,** 1667 (1991).

[31] D. J. Douglas, *Spectrochimica Acta* **41B,** 197 (1986).

[32] G. H. Vickers, D. A. Wilson and G. M. Hieftje, *Spectrochimica Acta* **45B,** 499 (1990).

[33] G. S. P. Box, W. G. Hunter and J. S. Hunter, *Factorial Designs at Two Levels*, in *Statistics for Experimenters. An Introduction to Design, Data Analysis, and Model Building*. pp. 307-351, John Wiley & Sons, New York 1990.

[34] R. A. McLean and V. L. Anderson, *Applied Factorial and Fractional Designs. 1*, (1984).(Abstract)

[35] J.-M. Mermet, *Anal. Chim. Acta* **250,** 85 (1991).

[36] D. L. Styris and D. A. Redfield, *Spectrochimica Acta Rev.* **15,** 71 (1993).

Chapter 5

SPRAY DEPOSITION FOR ELECTROTHERMAL VAPORIZATION INDUCTIVELY COUPLED PLASMA-MASS SPECTROMETRY

5.1 Introduction

The adaptation of the spraying deposition technique to ICP-Mass Spectrometry required only small modifications to the commercial Atomic Absorption ETV unit used for this purpose. Moreover, as illustrated in the preceding chapter, mass spectrometry allows the monitoring of plasma species giving direct information on several key aspects of the plasma state during sample vaporization. The linear relationship of the plasma water loading with the observed abundance of argon hydride (ArH^+) was explored in details in the preceding chapter. This relationship will be used for monitoring the water vapor originating from the ETV and entrained to the plasma in the argon carrier flow. It was found that a small amount of water vapor greatly influenced the response of several elements during sample vaporization, and the most likely explanation for this would be the shifting of the ion signal maximum away from the load coil but within reach of the sampling cone [1,2]. In a sequence of measurements the water loading will cause random variations and this will affect the reproducibility of the transient signal. The analytical sequence of the electrothermal unit was improved so as to minimize the water evaporation from the graphite inserts used as contact electrodes. These parts are thought to collect some part of the water vapor generated during sample spraying.

The ICP-MS technique is more prone to matrix effect than optical ICP [3]. In ICP-MS, matrix effects are often caused by space charge effects occurring in the ion extraction and ion transmission subsystems. For dry sample introduction systems such as ETV, spark ablation, as well as laser ablation, space charge effects can be more problematic for two reasons. First, the sample is introduced in the plasma as a transient burst of matter comprising the analytes and the dried matrix, generating an instant loading of the plasma several time greater than that observed with the continuous stream of pneumatic nebulization. Second, the plasma is much dryer than with conventional nebulization and it is therefore not exposed to the cooling effect from the evaporation of water droplets and from the dissociation of the vapor. The ion generation conditions are in fact so favorable that the ion abundance peak was observed within the load coil as mentioned above, which indicates that the vaporization of sample particulates and the subsequent free atoms ionization occur on a short time scale. The argon cation, the most abundant ionized atomic species in the plasma, is one order of magnitude more abundant in a dry plasma than in a plasma with pneumatic nebulization. The argon ion is primarily responsible for the electrical flux observed in the extracted ionic beam [3]. Its higher abundance in the ion beam promotes analyte losses by increasing the local concentration of charge. With conventional ETV-ICP-MS, these problems are diminished as just a few tenths of a microliter of sample, representing usually less than 50 ng of solid material (including the matrix) if we exclude slurries or solid samples, are typically introduced in the furnace. The total mass of solid sample deposited during a Spray ETV experiment is, however, several times greater than with ETV-ICP-MS, and it is expected that matrix effects will appear even for matrices of low concentration.

In Table 5-1, an estimate of the various fluxes of matter entering the plasma through the central channel is presented, as categorized by species. Estimates related to each sample introduction technique were calculated for a 100 ng/ml solution of 19 metals having an average molecular weight of 78 g/mole. The metals used for this calculation are those found in the multielement standard stock solution used to prepare the standard solutions used in this part of the study. The ETV transients were assumed to last for 3 seconds and the analyte and matrix mass loading were averaged over this time frame. As such, the calculated values should underestimate the true value of the actual loading of the plasma/spectrometer at the transients apex.

Table 5-1. Calculated fluxes of matter entering the plasma through the injector channel. Calculations were done assuming an argon injector flow of 1 dm^3/min and with a 100 ng/ml multistandard (19 elements) solution with an average molecular weight of 78 g/moles. All quantities are expressed in µmoles/min.

	Conventional Nebulization[a]	**Drop ETV**[b]	**Spray ETV**[c]
Argon	45,000	45,000	45,000
Water [d]	1,100	-	-
Metals	3.4×10^{-4}	2.4×10^{-2}	1.25×10^{-1}
NaCl 100 µg/ml	3.4×10^{-2}	3.5	17.5

[a] For a sample feed rate of 1 ml/min with a sample transfer efficiency of 1% and a water transfer rate of 2%.
[b] For a 50 µL sample and a transient signal lasting 3 seconds.
[c] For a 250 µL sample and a transient signal lasting 3 seconds.
[d] Not dissociated.

The calculations were made by taking into consideration a matrix of NaCl 100 µg/ml. We reasoned in term of the number of atoms or molecules (µmole/min) reaching the plasma per unit of time at any moment of the transient signal. It is readily apparent from examination of Table 5-1 data that there is a difference of two orders of magnitude when comparing the analyte and dry matrix loading for ETV and that for pneumatic nebulization. Moreover, the water load constitutes more than 99.9% in the species introduced in the plasma for this latter technique, when the argon of the injector flow is excluded. There is a fundamental difference between the effects since the dried sample matrices generally include atoms that dissipate the energy of the plasma through radiative cooling (*e.g.* the easily ionized elements such as alkaline metals). Water, once dissociated to its atomic constituents, promotes the energy transfer from the hot external layers of the plasma to the central regions [4-6]. In the case study of Table 5-1, the dry matrix loading temporarily imposed to the plasma by vaporizing 250 µl of sample containing 100 µg/ml of NaCl from a high temperature furnace (as in the Spray ETV example), is equivalent to continuously nebulizing a 50,000 µg/ml (5%w/v) matrix of NaCl with a conventional spray chamber/nebulizer. Sea water, a usually troublesome matrix, has a total salt concentration of about 3.5%w/v.

In this chapter, several aspects of Spray ETV-ICP-MS are discussed. The operational parameters of sample spraying and of ion determination at the plasma level are carefully examined and both steps are optimized independently. A significant reduction of water vaporization during the high temperature stage is achieved by modifying the temperature programming of the furnace. Small amounts of water vapor are also bled into the carrier stream to improve the strength of the signal. Detection limits for several elements are determined and compared to detection limits obtained with a conventional spray chamber/pneumatic nebulization system and drop ETV. The transient ratioing using either ArH^+ or Ar_2^+ as presented in Chapter 4 is applied, and the improvements in analytical figure of merits were discussed. Freon-12 is introduced as a gaseous modifier to help determine the carbide forming elements of group IVA, VA and VIA of the periodic table. Finally, the interference on ^{63}Cu due to the polyatomic species $^{40}Ar^{23}Na$ is studied. The Cd and Bi transients as observed after formation of the chlorides from interaction with the NaCl matrix, are compared with the transients observed in a sodium sulfate matrix of similar concentration. An estuarine water reference sample is measured using Spray ETV. A severe signal suppression is observed for the metals determined due to the high salt content, but the transients can be partially restored by signal ratioing with Ar_2^+.

5.2 Experimental

5.2.1 Instrumentation and Sample Preparation

Experimentally, this section is a direct continuation of the work presented in Chapter 4. The same SCIEX/Perkin-Elmer Elan 250/500 ICP-MS and Thermo Jarrell Ash electrothermal unit (ETV) model CTF 188 described in Chapter 4 was used for this study. The physical attachment of the two instruments is identical as well as the spraying device. The medium length ICP torch described in that chapter was used throughout in order to reach a sampling depth of less than 18 mm. Lens optimization and mass alignment on the mass spectrometer were conducted in the same manner and with the same frequency as described previously.

Controlled amounts of water were introduced in the furnace carrier argon flow, which forms the injector flow at the plasma level, using a fritted glass bubbler at fixed temperature. The same precautions for preventing condensation in the tubing and for blocking droplets were applied. A given water loading was achieved by mixing a flow of argon saturated with water vapor with a make up gas flow of dry argon in variable proportion, using ball flowmeters equipped with needle valves.

The reader is referred to Fig. 3-1 for an illustration of the Spray Deposition basic principle and instrumentation. The direction of the carrier and venting gas flow at each stage of the analytical sequence is illustrated and the description provided in the text explains in detail the modifications made to the Thermo Jarrell Ash model CTF 188 electrothermal vaporizer. This ETV unit used pyrolytically coated graphite tubes that were systematically changed after about 200 runs, even though their expected useful lifetime is typically twice as long. The plasma and ETV operational parameters as well as the temperature programming of the furnace are discussed in details in the sections on signal optimization. The solutions were prepared by dilution of a 100 mg/L multielement standard stock solution in distilled water, deionized to a residual resistivity of 18 MΩ, and preserved in 1% Fisher Trace Metal grade nitric acid. Origin of standards and the water purification system are listed in Table 4-1.

5.3 Results and Discussion

5.3.1 Optimization of Operational Parameters

Signal optimization for the Spray ETV-ICP-MS was achieved in steps owing to the complex interactions between operational parameters. Figure 5-1 illustrates the coupling of the instrumentation and the parameters selected for optimization. Lead was chosen as a test metal for its intermediate thermal volatility, average first ionization potential (7.4 eV) and good sensitivity in mass spectrometry. The high masses of its isotopes are well above those of most molecular species causing major interferences. Moreover, double ionization is negligible for this metal [7].

The first group of operating parameters are related to the efficiency of the sample spraying in the tube and encompass the formation of the spray and the continuous evaporation of the water from the furnace tube. During this optimization, the sample feed rate, spraying gas pressure, venting gas flow rate and the temperature of the graphite tube at spraying were introduced into a Simplex method. A separate optimization was conducted on

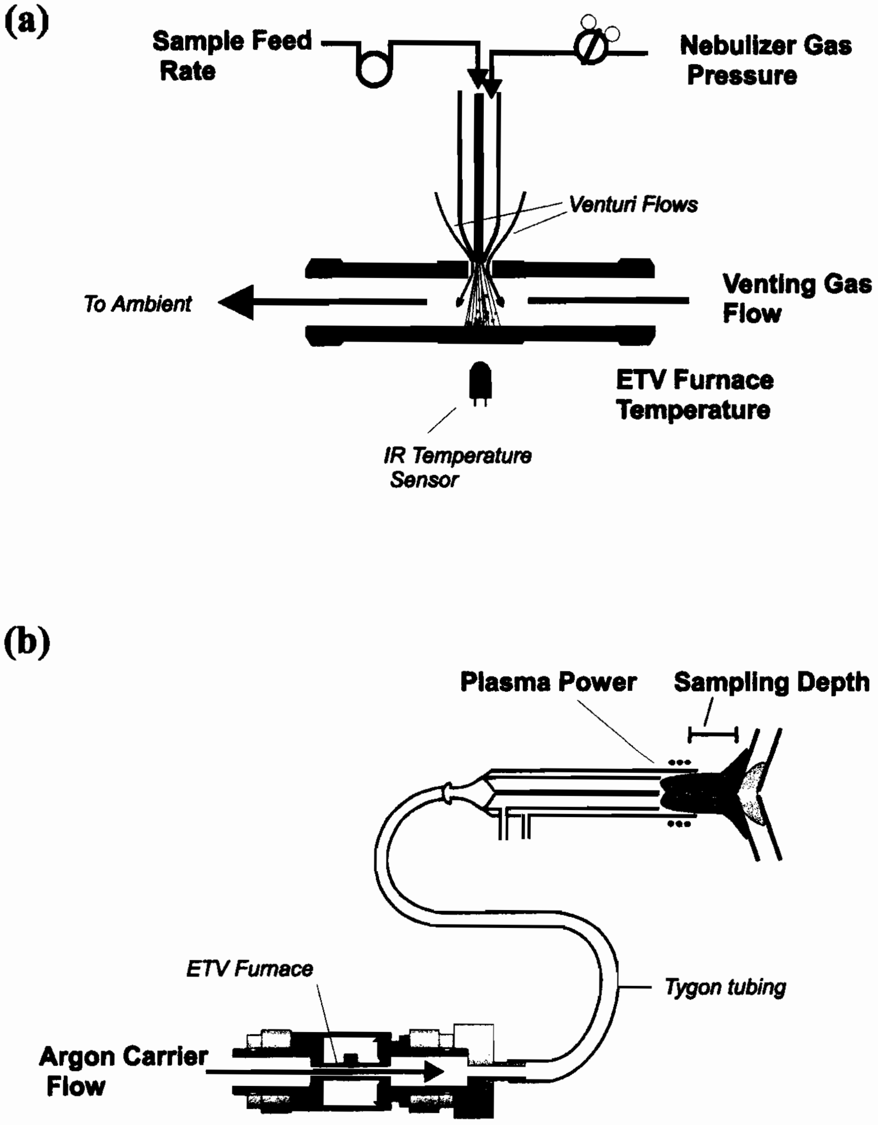

Figure 5-1. Operational parameters (in bold) selected for signal optimization for (a) Spray Deposition and (b) sample vaporization and determination.

the ion generation conditions, which are controlled primarily by the radio-frequency (RF) power applied to the plasma and the sampling depth of the sampling orifice relative to the top of the load coil (TOLC). Finally, the carrier gas flow rate at the high temperature stage was included in the Simplex optimization as this parameter modified the condensation conditions for particulates formed from the vaporized sample, which in turn influenced the transportation efficiency of the dry aerosol thus formed [8]. Since the furnace carrier flow later forms the plasma injector flow, this parameter will also modify the vaporization and ionization of metals in the plasma. A high carrier flow during sample vaporization should improve the condensation of the easily transported particulates from the metal vapor, especially for metals with low boiling points. However, a high injector flow cools the plasma and consequently inhibits the ionization process in the plasma. Since interest was primarily in the total net effect, no attempt was made to isolate these effects by using a make up gas flow for example.

This grouping of operational parameters corresponds to two well separated stages in the programming of the ETV. The signal of ArH^+ at *m/z* 37 was also followed as a direct indicator of the amount of water evaporated from within the furnace assembly and entrained to the plasma during the spraying, drying, ashing and vaporization of the sample. Changes were introduced in the program in order to regulate and minimize as much as possible the amount of released water.

5.3.1.1 Optimization of Spray Deposition Parameters

The spraying of sample and the continuous evaporation of water (or any other solvent) is the heart of the spray preconcentration technique and of the improvement in detection limits it provides. It is therefore critical that this stage be performed with good reproducibility and efficiency. The operational parameters controlling the spray deposition can be separated in two distinct subgroups. The first group includes the parameters of operation of the concentric nebulizer (gas pressure and sample feed rate) leading to the formation of the droplets thrown against the furnace wall. According to the theory describing liquid nebulization processes [9,10], small droplets are formed from the differential velocity of the liquid and gaseous stream emerging at the nozzle face. In Spray ETV, we can neglect the evaporation of water from freshly formed droplets as they are projected toward the inner graphite furnace wall since their path is very short (less than 5 mm). Also, the droplets are not size selected through surface impacting and differential settling as they are within a spray chamber. The size distribution of droplets arriving at the graphite surface is therefore expected to be very similar to the log-normal distribution predicted by the Nukiyama-Tanasawa equation [10]. This suggest that droplets covering a large range of size will cross the inner space of the furnace tube perpendicular to the venting gas flow. Also, a droplet having a small diameter is not expected to impact the graphite surface in the same manner as a bigger one, since surface tension of the liquid will exert a greater effect as the droplet diameter diminishes. Moreover, kinetic energy is predominant for big droplets and their aerodynamic properties (their mass to cross-section ratio) make them less susceptible of being slowed down by the surrounding gas, and as consequence less susceptible to entrainement with the venting gas.

The venting gas flow and furnace temperature come into play at this stage. Since the aim was to achieve 100% deposition efficiency in the furnace while simultaneously evaporating the solvent, the graphite tube needs to be heated up somewhat and the solvent vapor swept away as it gets formed. However, the "cross-wind" generated by the venting gas flow can carry away some of the finest droplets before they reach the opposite wall and deliver their dissolved content onto it. In addition, the temperature of the graphite furnace should be set within a critical range. Using too high a temperature, the biggest droplets can experience a "frying pan" effect that would generate a secondary fine mist, evacuated to ambient and therefore lost to the analysis. Using too low a temperature, the solvent is not evaporated at the required pace. In that respect, the ETV instrument used in this study appeared to be well adapted for spray deposition, as it incorporated an infra-red thermal sensor and the associated feedback circuitry for precise temperature control. Moreover, the sensor is aimed at the opposite face of the sprayed area (see Fig. 5-1) and the instrument can therefore maintain the programmed temperature in that part of the tube through feedback control. It is expected that ETV instruments using the mean resistivity of the graphite tube for temperature control would not be as adequate for Spray ETV as they can not compensate for the rather intense cooling effect locally induced by the evaporating water.

Since these parameters influence each other in a complex way, it was hoped that a Simplex optimization would help to find the optimal combination of spraying parameters with the minimal set of experiments. The nebulizer gas pressure, sample feed rate, venting gas flow and furnace temperature were introduced in the Simplex method previously used (see Section 3.4). Figure 5-2(a) illustrates the changes in Simplex parameters as the Simplex evolves from its starting point. The explored range was 20 to 35 psi for the nebulizer gas pressure, 2 to 6 RPM (rotating speed of the peristaltic pump head) for the sample feed rate, 0.2 to 1.4 dm^3/min for the venting gas flow and 120°C to 190°C for the furnace temperature. The plasma power was 1100 W and the carrier/injector flow 1 dm^3/min. In Fig. 5-2(a), these parameters are scaled relatively to these limits. The nebulizer gas pressure and pump speed were converted to nebulizer gas flow and sample feed rate, respectively. Instrumental drift was checked periodically by inserting the starting parameter set in the course of the Simplex, but the observed variations was found to be less than the signal variability initially measured. The parameters showed on Fig. 5-2 all oscillated around their respective center position, a fact that strongly suggest that the deposition parameters just marginally influenced the efficiency of deposition. Examination of the signal of some of the other metals simultaneously recorded, as illustrated in Fig. 5-2(b), shows a concerted fluctuation with the argon dimer. However, the Pb signal which was the test element, was quite insensitive to varying plasma conditions. Since we know that the argon dimer is, in dry plasma conditions, a good indicator of the plasma temperature, we concluded that varying plasma conditions were introducing more variance in signal than the sample deposition parameters. It should be noted that this optimization was conducted before several improvements were brought to the ETV temperature programming, improvements that greatly reduced the collection of water in contact electrodes (see next section).

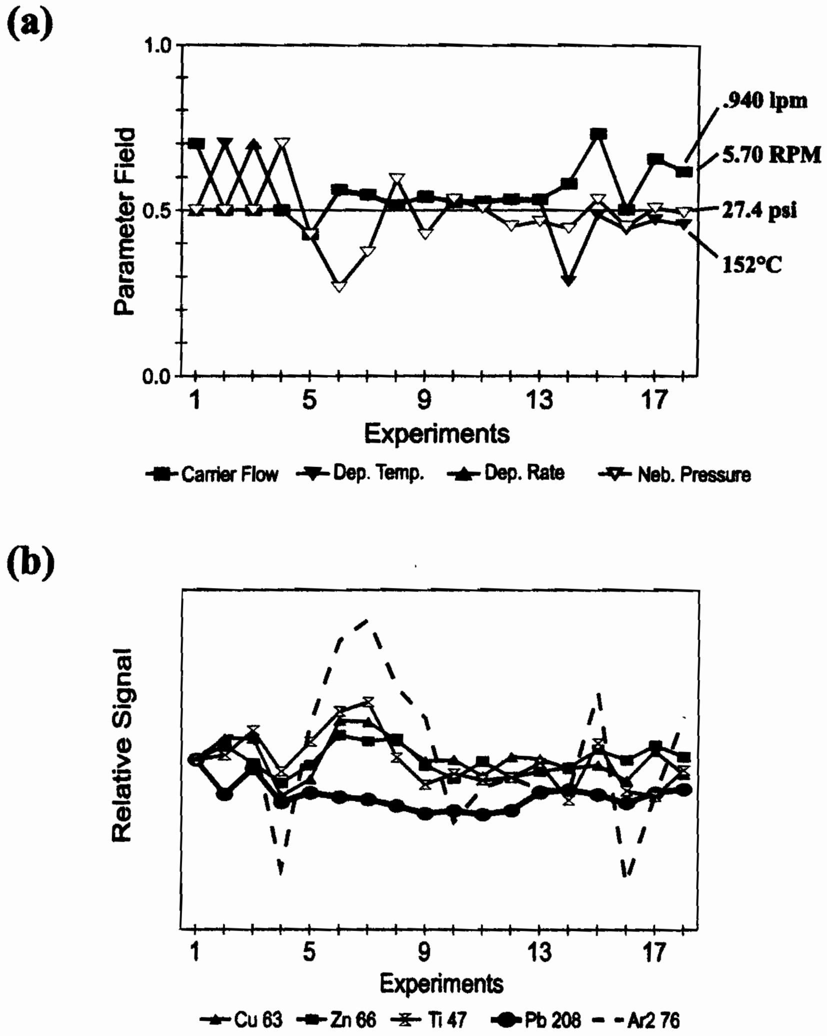

Figure 5-2. Evolution of (a) operational parameters during the optimization of Spray Deposition and (b)signal recorded for copper, zinc, titanium, lead and the argon dimer ($Ar_2{}^+$). Final values for each parameter are illustrated on the right side of graph (a).

These results revealed the good reproducibility of the spray deposition technique, although they are not direct proof of a 100% deposition efficiency. Rattray and Salin [11] have determined by Neutron Activation Analysis of deposited Mn that a Spray DSI system operated with graphite cups inductively heated to 170°C exhibits a 90% recovery factor. Increasing the nebulizer gas pressure resulted in a reduction of Mn recovery, suggesting that the more intense gas swirling observed in the cup lead to partial sample loss at spraying. No such adverse effect was observed with Spray ETV. The cylindrical geometry of the ETV furnace can be an advantage over Spray DSI in that respect, since it contains the spray within a closed volume. It was also observed in a previous optimization campaign that moving the nebulizer tips away from the dosing hole, even over a small distance (2 mm), greatly reduced the signals recorded for a multielement solution. It is supposed at this stage of the study that the nebulizer tip location used throughout *i.e.* flush with the outer surface of the graphite tube, created a venturi effect that aspirated the surrounding air that formed a shielding gas around the spray (see Fig. 5-1(a)). This shield would make the spray insensitive, to some extent, to the venting gas flow. Finally, used spray ETV tubes exhibited a sharp, circular dark spot of deteriorated graphite at the sprayed area. No evidence of sample sputtering or spot tailing in the direction of the venting flow was observed.

Another indication that the spray deposition is not very sensitive to operational parameters is the good reproducibility in the transients shape obtained in different spraying conditions, as illustrated in Fig. 5-3 for three sprayings with signal recorded for Pb. Similar results were obtained for the other metals of varying volatility in the multielement solution.

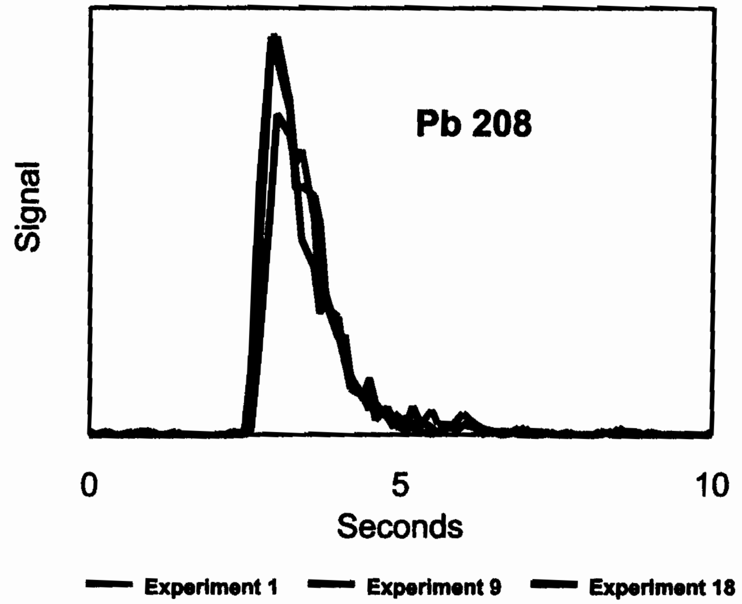

Figure 5-3. Pb transients recorded at beginning, mid-course and ending of the spray parameters optimization.

5.3.1.2 Improvement to the ETV Temperature Programming

The initial temperature programming of the ETV furnace had to be somewhat modified in order to accommodate spray deposition, especially to avoid condensation of the water in the cooled metal electrodes. Using the original graphite furnace atomic absorption (GF-AA) program, even spraying as little as 200 μL of sample eventually lead to plasma extinction at the high temperature stage after just several depositions, because of water overcharge of the plasma. It was in this fortuitous manner that the water accumulation problem was noticed and, as a consequence, appropriate modifications were brought to the temperature sequence (see Chapter 3). They initially consisted in introducing a warm-up stage (~400C for 30 seconds) before spraying , and interrupting the cooling water flow to the electrodes at sample spraying and drying. These improvements were sufficient to allow the plasma to survive repeated furnace firings, and no adverse effects on the atomic emission signals were noticed from the residual water evaporated at sample vaporization.

The pervasive effects of varying water plasma level on transients signal that were observed in Spray ETV-ICP-MS (see Chapter 4), called, however, for a further reduction in the amount of condensed water at sample spraying. The argon hydride signal recorded at *m/z* 37 has proved to be a faithful indicator of the water loading of the plasma and it was used extensively to improve the temperature programming in that respect. Figure 5-4 illustrates the argon hydride signal recorded during the analytical sequence for three spray depositions done using similar spraying conditions, but with different temperature programming. In Run 1, which used the modified program, the amount of evaporated water reaching the plasma was very low during the initial stages since the venting flow was directed toward ambient (see Fig. 3-1 and Fig. 5-1 for an illustration of the gas flow pathways). However, entrained water vapor reached a significant level when the carrier flow was diverted to the plasma at the onset of the ashing stage. The water level slowly decreased as the furnace dried but a further increase was seen at the high temperature stage. As discussed earlier, it is believed that the porous graphite inserts hosted some condensed water that was later evaporated as the graphite inserts heat up from thermal contact with the hot furnace tube. Using the original GFAAS program, however, as in Runs 2 and 3, the water level in the plasma reached higher values during the high temperature stage. Moreover, the condensed water was not totally expelled from the instrument and it accumulated from run to run, ending up eventually with the extinction of the plasma at sample vaporization. This problem occurred after just two runs in the example illustrated in Fig. 5-4 (plasma extinction on Run 3).

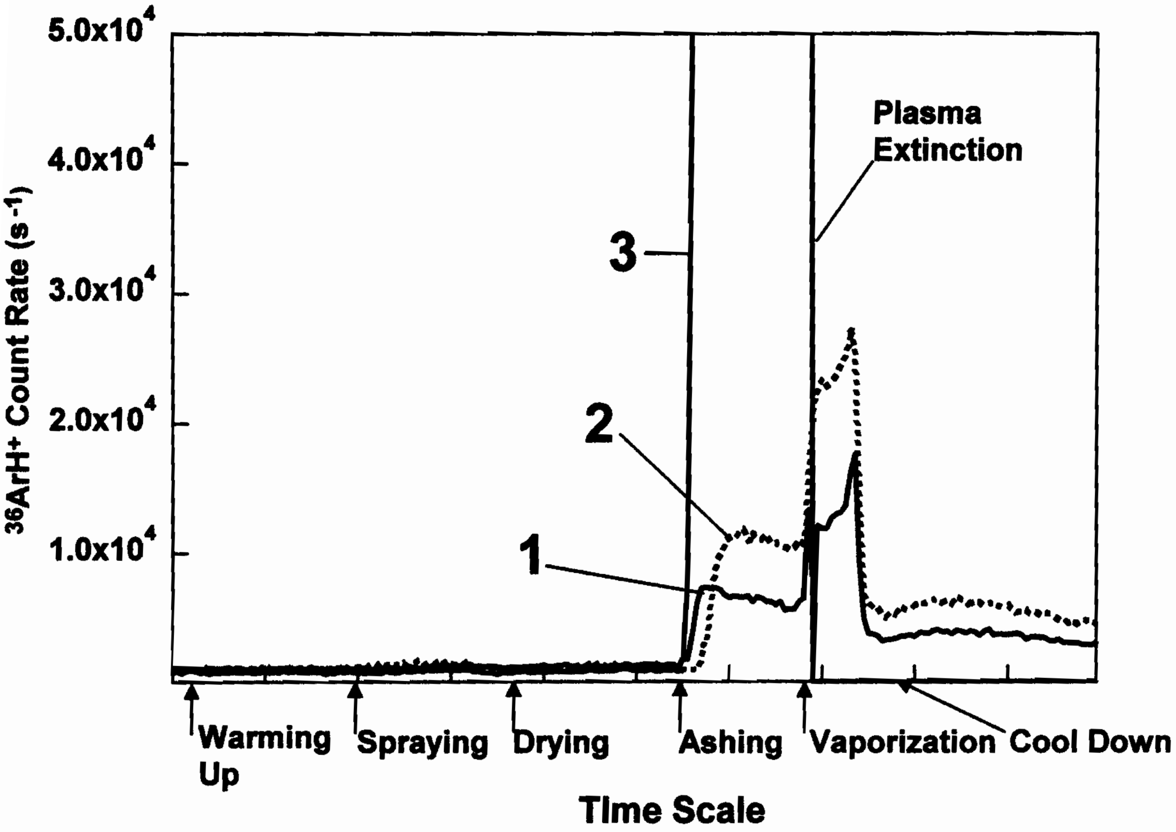

Figure 5-4. Argon hydride signal recorded at different stages of the sample spraying and analysis sequence. The first run (1, solid line) was done with the modified temperature programming that included an initial warm-up stage and a temporary interruption of the electrode cooling flow, the second (2, dotted line) and third runs (3, gray line) were done using the original GF-AA program.

The best temperature programming found is described in Table 4-2 and was used throughout for Spray-ETV-ICP-MS, unless stated otherwise. It consisted in heating up the furnace to 2000°C in the presence of an argon gas flow to prevent oxidation of the furnace, and then to revert to deposition temperature and simultaneously cut off the electrode cooling water flow. The sample is then sprayed and the cooling flow is resumed at the ashing stage. The modifications introduced to the original ETV FORTH program in order to implement this new sequence are listed in Appendix. With this sequence, no accumulation of water was observed even over an extended number of spray depositions, although water recondensation and releases at sample vaporization was not totally avoided. Another unsolved problem was the condensation from the water vapor added to the carrier flow as a signal enhancer. This condensation presumably occurred when the cooling water flow was reintroduced during sample ashing.

5.3.1.3 Optimization of Sample Vaporization and Determination by ICP-MS

The optimization of ICP parameters related to the ion generation and transmission efficiency was conducted using a three parameter Simplex. Figure 5-4 illustrates the evolution of plasma power, carrier flow and sampling depth, as the Simplex progressed. The injector flow and plasma power appeared to be the sole sensitive parameters. The optimal parameters resulted in values approaching those found in "cold" plasmas [3,12]. Cold plasmas are generally formed with a combination of high injector flow (>1 lpm) and a low plasma power (600 W) [12]. As a plasma gets colder, the dominant species flip from Ar^+ to NO^+, O_2^+ and H_3O^+ [3,12,13]. The ionization of metals from these molecular species is less dependent on the electronic level resonance than with Ar^+. Matrix effects arise from ionization suppression rather than from space charge effect as in normal ICP-MS situations [12]. It is of particular interest for Spray ETV-ICP-MS since matrix suppression, which is expected to be of significant importance for that technique, should affect all analytes rather independently of their *m/z* ratios. A plasma argide species used as internal standard is more likely to correct for fluctuations in plasma conditions over a larger domain of mass. Our optimized values for plasma power and injector flow placed us still far from true cold plasma conditions and those benefits are not expected to appear clearly in the analytical figure of merit. However, figures directly related to the signal enhancement obtained through signal optimization should be significant (such as detection limits).

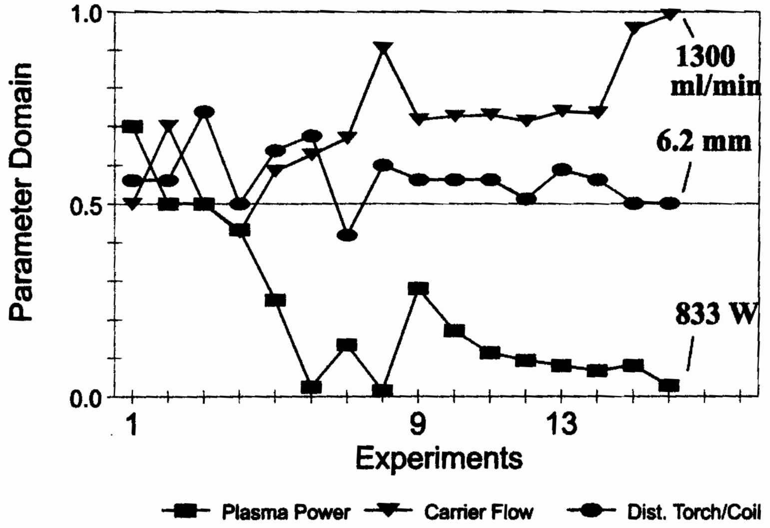

Figure 5-5. Evolution of operational parameters during the optimization of sample vaporization and determination with ICP-MS, using Pb as test element. The final values for each parameter are illustrated on the left end of corresponding curves.

A factorial design survey including the plasma power and injection gas flow, as well as the water plasma load, was applied to several metals to evaluate the effect of these operational parameters for multielement determination (Table 5-2). The mathematics involved are described in detail in section 4.3.2, and the parameter range were selected in the vicinity of the optimized values. From examination of Table 5-2, it can be seen that an increase in plasma water generally improved integrated signals for all elements. Zinc is particularly sensitive to the level of water. As expected, the injector flow and plasma power have contrasting effect for all metals transients; however, the sign of the induced changes were not consistent. A first group of element (Zn, Pb, Tl and Sb) exhibited improvement in signal when the injector flow was increased and the plasma power was decreased. Among those, lead showed the highest sensitivity to plasma power, which explains why this operational parameter optimized rapidly to low values as illustrated in Fig. 5-4. Arsenic and copper form the other group of elements that responded marginally to changes in plasma power but negatively to an increase in injector flow.

Table 5-2. Effects of water level in argon carrier, argon injector/carrier flow and plasma power on several metals transients and on argon hydride and argon dimer, as determined by Spray ETV-ICP-MS. Measurements and calculations were based on a 3 parameter full factorial design.

Parameter[a]	**As 75**	**Cu 63**	**Zn 66**	**Pb 208**	**Sb 121**	**Tl 205**	**ArH 37**	**Ar_2 80**
Water Load (W)	+[b]	+	++	+	+	.	.	.
Injector Flow (I)	--	-	+	+	.	+++	.	.
Plasma Power (P)	.	.	--	---	-	--	.	.
W/I	--	-	-	-	-	.	++	++
W/P	.	+	.	.	.	.	--	--
I/P	.	-	.	.	++	.	--	--
W/I/P	.	-	.	.	.	.	.	.

[a] The parameter low and high values were for; Water loading: 2.3 and 3.4 mg/min; Injector flow: 1.0 and 1.2 lpm: Plasma power: 800 and 900 W.

[b] The effect values were scaled relatively to the total standard deviation observed in the signal recorded for each element (σ). An operational parameter marked with a + sign induced a positive change of at least 0.5 σ in the corresponding metal signal when this parameter was increased by one unit (for example adding 100 W to plasma power), with a ++ sign if the induced change is of 1.0 σ and with +++ for a change above 1.5 σ. Negative effects were expressed using- signs. A dot indicated no significant effect (less than 0.5 σ of absolute change).

In short, the studied metals were responding to a cooling of the plasma in the following order:

$$\mathrm{Tl} > \mathrm{Pb} > \mathrm{Zn} > \mathrm{Sb} > \mathrm{Cu} > \mathrm{As} \qquad (5\text{-}1)$$

With an important signal enhancement observed for Tl at one end, and some signal suppression for As at the other end, the pivot point being located between Sb and Cu. It should be remembered at this point that any change in the injector flow was also mirrored in the furnace carrier gas flow, and that some part of the net effect observed for this parameter included a contribution from varying conditions in the sample vaporization and transport processes at the furnace level. These data strongly suggest that different optimized conditions would have been found if a different test element had been chosen.

The argides species behaviors were surprising, however, especially in regard to data collected in Chapter 4. The argon hydride and argon dimer exhibited a minimal sensitivity to main operational parameters but responded rather strongly to any simultaneous changes of two parameters. From previous experiments, it was expected that both species would favor low plasma power and high injector flow and water content. Instead, a combined increase in water level and injector flow (W/I) was required to significantly raise their signals in the plasma. In contrast, an important negative effect was obtained by simultaneously increasing the water level with the plasma power (W/P), or by increasing the injector flow with the plasma power (I/P). These data look credible as the calculated third order effect (W/I/P) was low. At this point, it is supposed that the differences noticed between the argides behavior observed in this experimental design and in the preceding design, can be ascribed to the different parameter domain covered. The plasma power was significantly lower, at 800-900 W as opposed to 900-1100 W in the experimental design of section 4.3.2, with an identical injector flow however. The plasma can be in an transition regime toward a true cold plasma, which might introduced non-linearities in the argides responses to parameter changes. Nevertheless, it is comforting to observe that any increase in plasma power seemed to favor the dissociation of argides in the plasma. Conversely, augmenting the injector flow while bleeding more water vapor in the injector flow cooled down the plasma and increased the survivability of the argides. These behaviors appear to be a logical continuity to our preceding observations and should not constitute a negative argument for using the argides as ratioing species.

5.3.2 Analytical Figures of Merit

5.3.2.1 Calibration Curves

Calibration curves for several elements are illustrated in Figure 5-6(a) and (b) on a log-log scale, with an ideal calibration curve having unity slope shown as a small dotted line for comparison. In general, these calibration curves bend at both ends of the concentration scale. Arsenic, copper, and lead (in Fig. 5-6(a)) and nickel, manganese and molybdenum (in Fig. 5-6(b)) exhibited a significant leveling off for the integrated signal over 100 ng/ml. Also, high blank levels were observed for all elements with the equivalent concentration for each element amounting to approximately 0.01 ng/ml for manganese, lead and cadmium, and 0.1 ng/ml for arsenic, copper, zinc and nickel.

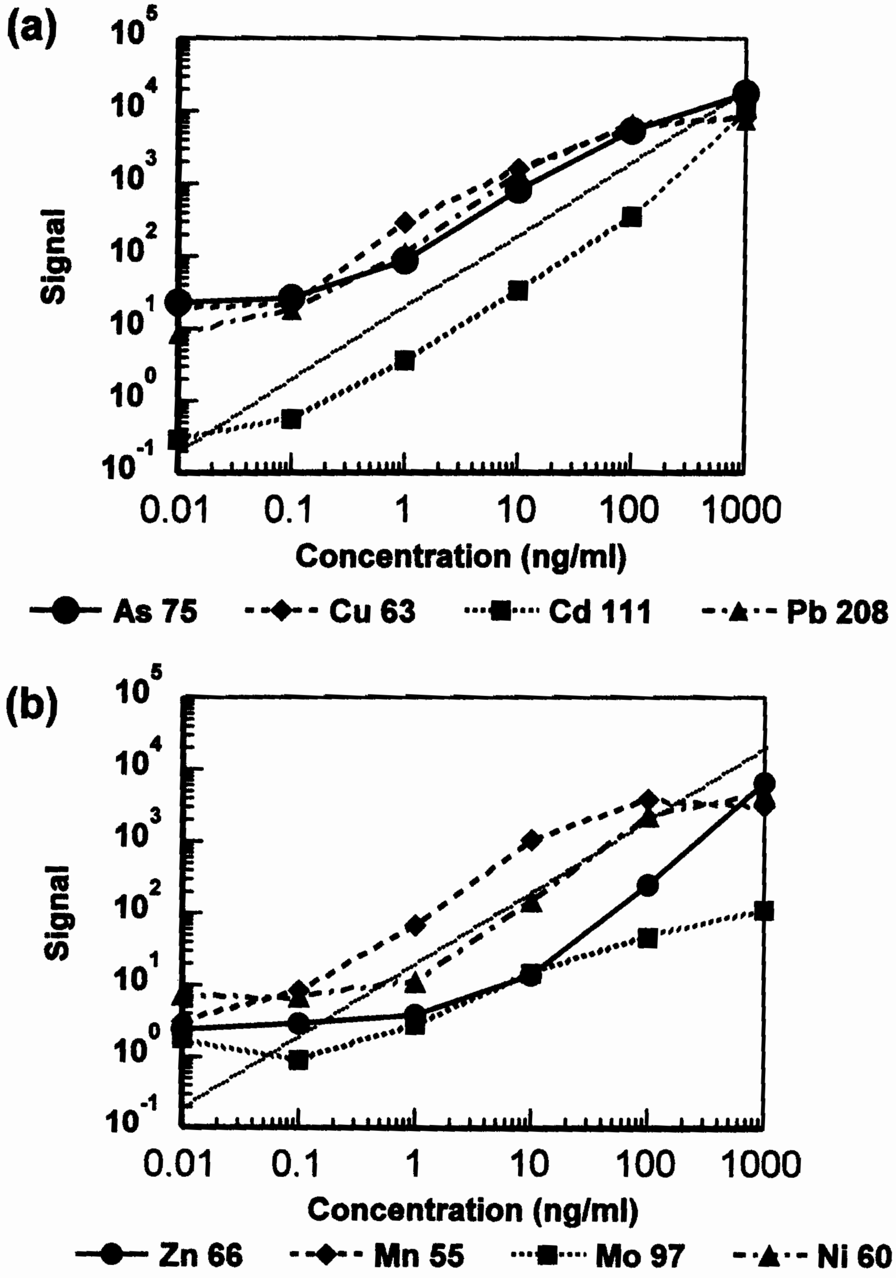

Figure 5-6. Calibration curves obtained from integrated signal for (a) arsenic, copper, cadmium, lead and (b) zinc, manganese, molybdenum and nickel as obtained with Spray ETV_ICP-MS. Standard multielement solutions in HNO_3 1% were sprayed for 250 seconds at 215 μl/min resulting in a sample size of 0.9 ml. The thin dotted line illustrates an ideal calibration curve with unity slope.

When translated into mass, an equivalent concentration of 0.1 ng/ml corresponded to 0.8 ng of each element given the high volume of sample deposited. Such a contamination level is of considerable concern. It is likely that a concentration of the blank contamination occurred. The laboratory in which the experiments were done was not a clean room and ICP-MS class blanks were difficult to maintain at the degree of purity required for very sensitive determination. Moreover, air suspended dust could have been entrained with the venturi flow (see Fig. 5-1) and, as a consequence might have been accidentally incorporated within the spray. This problem was not as severe on other occasions, however, for Spray DSI-ICP-MS experiments conducted in the same environment and on the same instrumentation [11] in previous years. In Fig. 5-7, Fig. 5-8 and Fig. 5-9 are illustrated the traces obtained with the blank and standard solutions with 0.01, 1 and 1000 ng/ml of cadmium, manganese and zinc. In the upper graph of each figure (graphs a), the blank traces (dotted lines) were illustrated along with the traces obtained for the 0.01 ng/ml standard (solid lines). Both traces were plotted on an identical scale for comparison purpose. For cadmium, it is readily apparent that both traces exhibited the same noisy appearance and that no discernible transient could be obtained from the low concentration standard. The apparently high blank of cadmium was therefore caused by a lack of sensitivity of the Spray ETV-ICP-MS for this element. However, blanks for zinc and manganese (Fig. 5-8(a) and Fig. 5-9(a)) as well as for copper, lead and nickel (not shown) all exhibited a discernible transients at the expected time location and so the initial hypothesis about blank contamination is confirmed. Zinc even showed a higher blank signal than the 0.01 ng/ml standard.

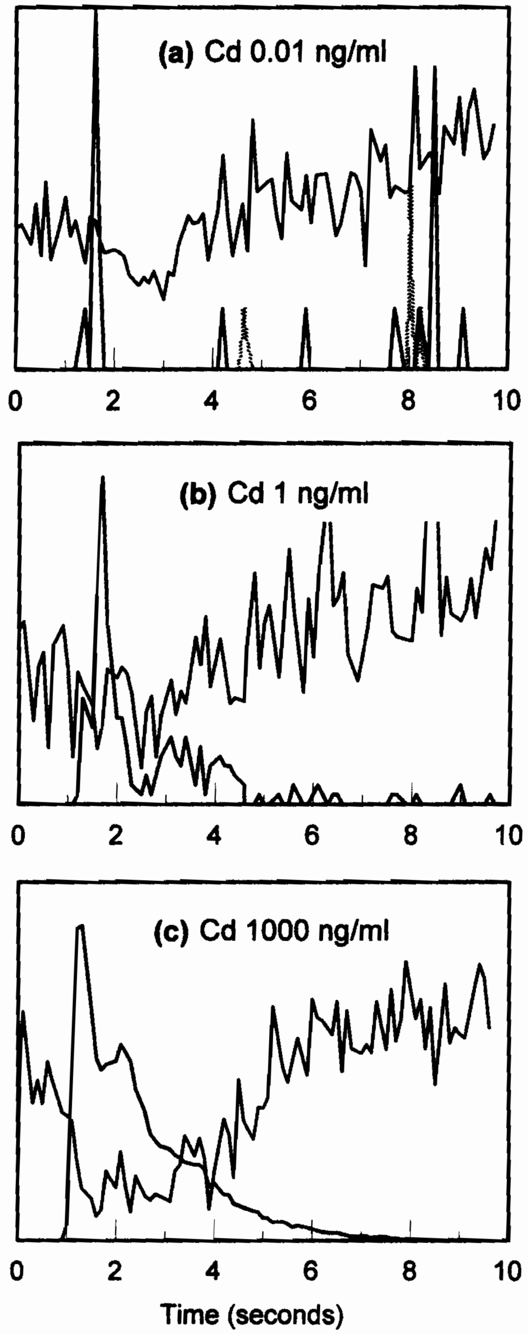

Figure 5-7. Transients obtained for cadmium for the blank (dotted line, on graph (a) only) and 0.01 ng/ml standard (solid line) (a), for the 1 ng/ml standard (b) and for the 1000 ng/ml standard (c). The argon hydride (ArH^+) recorded simultaneously at m/z 37 is also illustrated (gray lines). All argon hydride traces can be directly compared as they are plotted to the same scale.

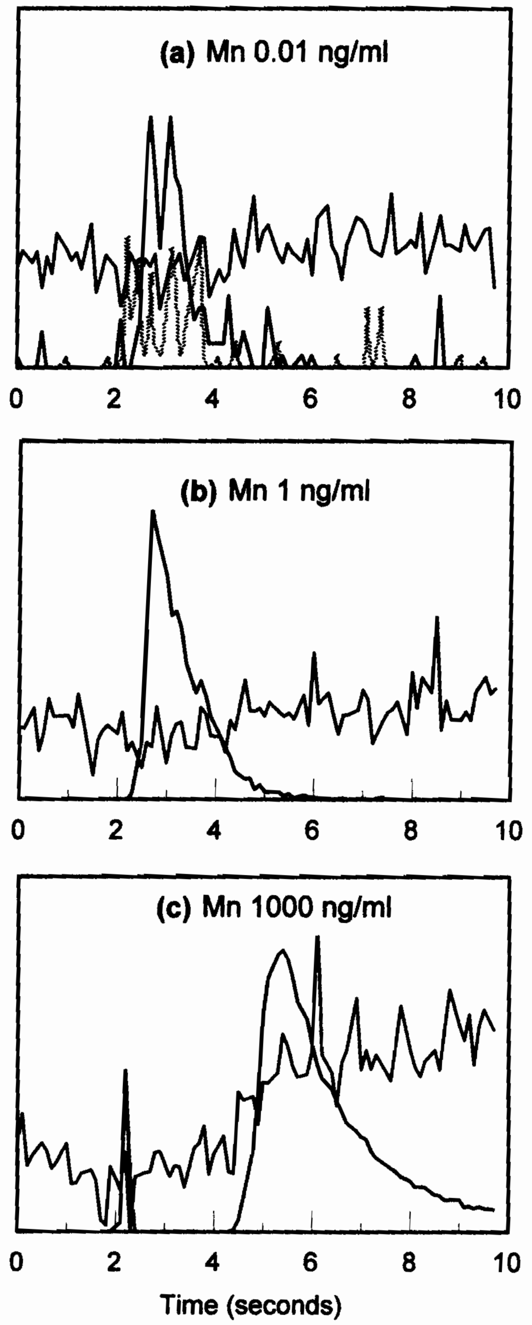

Figure 5-8. Transients obtained for manganese for the blank (dotted line, on graph (a) only) and 0.01 ng/ml standard (solid line) (a), for the 1 ng/ml standard (b) and for the 1000 ng/ml standard (c). The argon hydride (ArH^+) recorded simultaneously at m/z 37 is also illustrated (gray lines). All argon hydride traces can be directly compared as they are plotted to the same scale.

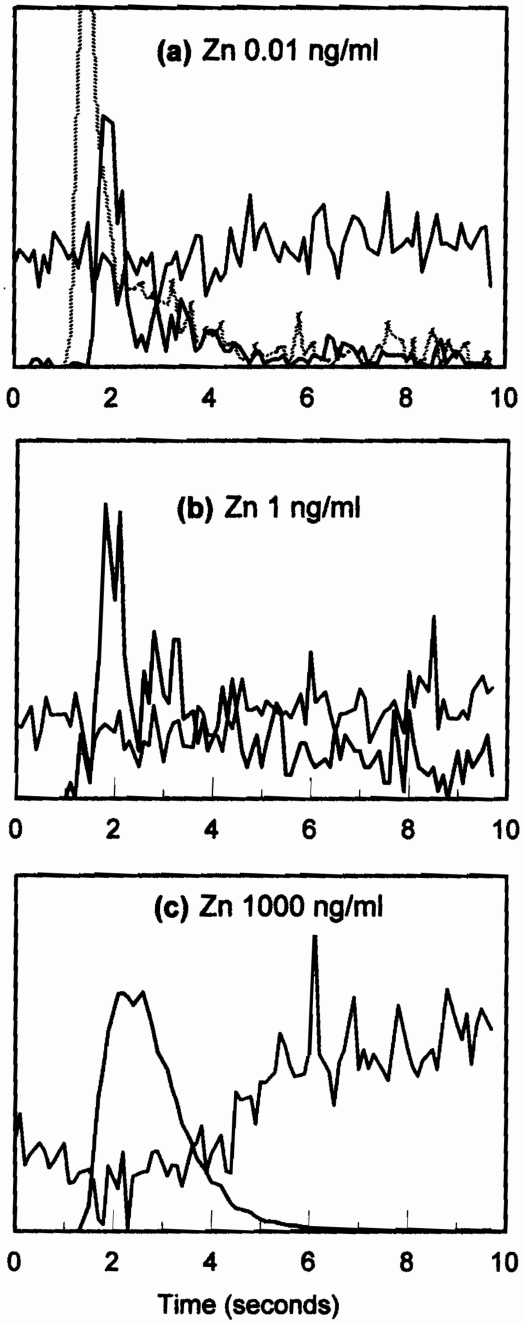

Figure 5-9. Transients obtained for zinc for the blank (dotted line, on graph (a) only) and 0.01 ng/ml standard (solid line) (a), for the 1 ng/ml standard (b) and for the 1000 ng/ml standard (c). The argon hydride (ArH^+) recorded simultaneously at m/z 37 is also illustrated (gray lines). All argon hydride traces can be directly compared as they are plotted to the same scale.

It is conjectured at this point that the blank for ubiquitous elements such as zinc and copper suffered the most from dust contamination. Arsenic and molybdenum exhibited important tailings suggesting an incomplete vaporization of sample. While for molybdenum the tailing can be explain by formation of molybdenum carbides. The explanation is less obvious for arsenic.

The suppression of signal observed over 100 ng/ml for all element except cadmium and zinc was probably not caused by space charge effects since lead at *m/z* 208, showed a signal suppression very similar to manganese at *m/z* 55. Transport losses are also ruled out as they would have primarily affected the elements with low boiling points [8,14] such as cadmium and zinc. A possible explanation might be related to the high amount of analyte deposited in the furnace. Up to 830 ng of each element was sprayed in the graphite tube for the 1000 ng/ml standard, which summed up to nearly 16 μg of analytes for the 19 elements. Such a load of sample is rarely used in ETV-ICP-MS and could explain the unusual behavior observed. The transients for intermediate and high concentration standards are illustrated in Figures 5-7, 5-8 and 5-9(b) and (c), for cadmium, manganese and zinc respectively. Although the transient shape remained relatively unaffected for cadmium and zinc when passing from a concentration of 1 ng/ml (graphs (b)) to 1000 ng/ml (graphs c), molybdenum appeared to suffer from an important signal suppression for the high standard. It should be mentioned that these experiments were conducted with the same multielement standards and using the same operational parameters and can be directly compared. The significant depression of the ArH^+ signal during the first seconds of the transient, *i.e.* at the peak of sample impulse, can be interpreted as being indicative of a matrix effect in the plasma. Similar conclusions were drawn from identical variations observed in Ar_2^+ studies for ETV-ICP-MS studies implying high matrix loading [15,16]. A temporary signal suppression was also observed for copper, arsenic, and lead and appeared to be the general cause for calibration curves leveling off at high concentration. There is no clear explanation on why zinc and cadmium escaped suppression except that they both exhibited an high first ionization potential (IP) of 9.4 eV and 9.0 eV respectively; Arsenic, however, has also a comparable first IP but still suffer from signal suppression.

These distortions leave a linear range covering from 3 to 4 orders of magnitude depending on the element, which is less than initially expected, however one should keep in mind that the solution is multielement thereby providing a high load. It seems that the sample preconcentration exacerbated the inherent limitations of the ETV-ICP-MS instrumental pairing. It would be expected from the results of Chapter 4 that using the argon hydride as ratioing species would at least correct partially for the enhancement in signal caused by the water vapor as well as nulling the signal suppression at high concentration. Calibration curves established using the ArH^+ ratioed transients are illustrated in Fig. 5-10 and they showed little improvement for most elements when compared with those of Fig. 5-6. Using this correction, the linearity of the cadmium curve was significantly ameliorated above 100 ng/ml and the slope of the molybdenum curve was now closer to unity.

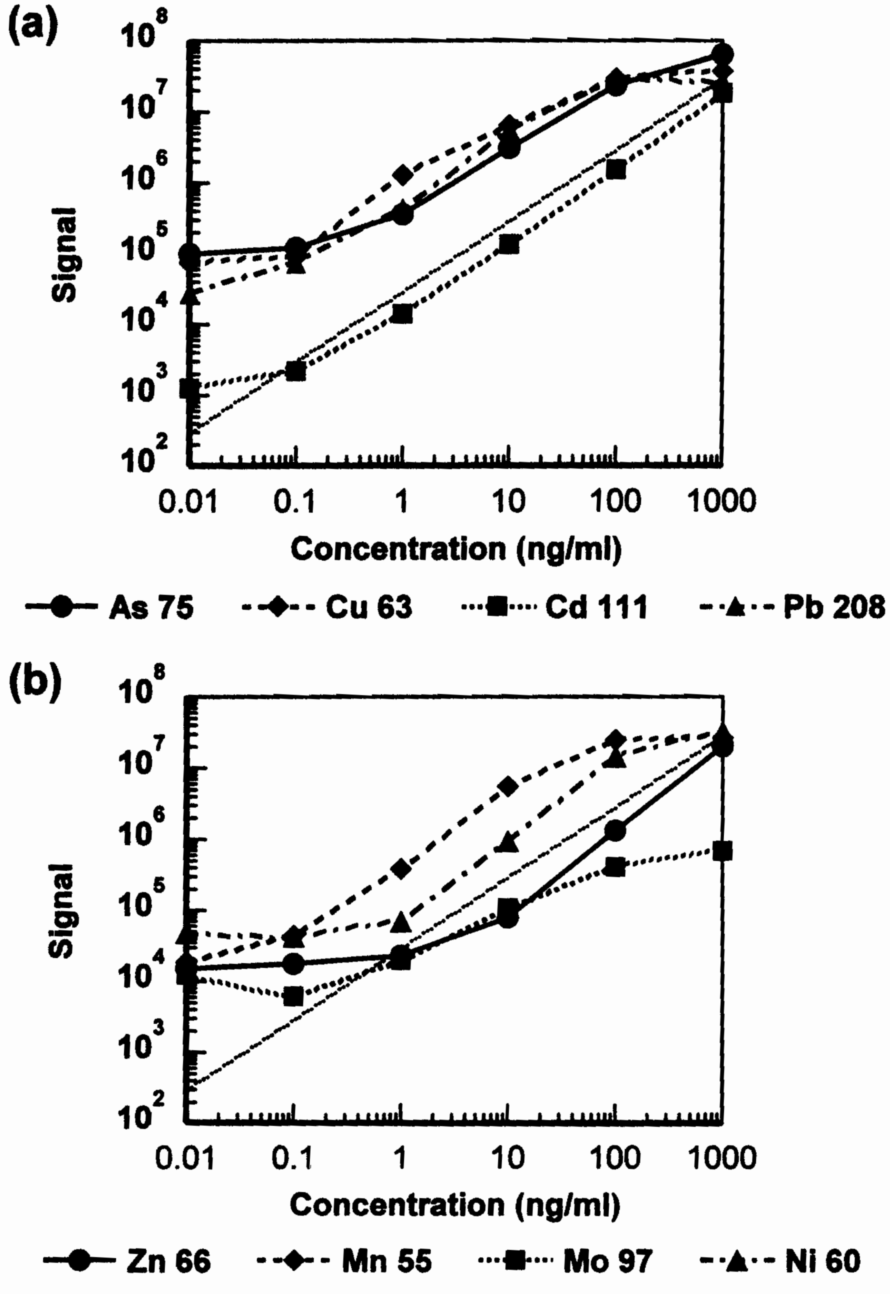

Figure 5-10. Calibration curves obtained from integrated signal for (a) arsenic, copper, cadmium, lead and (b) zinc, manganese, molybdenum and nickel as obtained with Spray ETV_ICP-MS, after ratioing with ArH^+. Standard multielement solutions in HNO_3 1% were sprayed for 250 seconds at 215 µl/min which resulted in a sample size of 0.9 ml. The thin dotted line illustrates an ideal calibration curve with unity slope.

Calibration curves obtained from ratioed transients were therefore used for determination of reference materials and in detection limit calculations. The deceiving amelioration obtained from ratioing with argon hydride might ironically be due to the improvements brought to the ETV temperature programming; improvements that greatly limited the surge of water at sample vaporization. Also, the argon hydride do not seem to be as sensitive to high matrix loading as the argon dimer.

5.3.2.2 Precision and Detection Limits

The detection limits (DL) for Spray ETV-ICP-MS were determined using the operational parameters found during the signal optimization studies. The spray deposition of the sample was done using a deposition rate of 215 µl/min for a total period of 250 seconds (resulting into a sample volume of 0.9 ml), the furnace temperature was 160°C and the gas pressure (N_2) applied to the nebulizer was of 28 psi. At sample vaporization, the plasma power was of 900 W (slightly above the optimized value to add some robustness to the plasma), the carrier/injector argon gas flow was of 1.2 dm^3/min and the TOLC distance was of 16 mm. The detection limits with conventional nebulization (Type A Meinhard concentric nebulizer with a Scott chamber) were obtained using operational parameters manually optimized and were acquired on the same instrument shortly before the Spray ETV-ICP-MS experiments. The resulting DLs are listed in Table 5-3 with the relative standard deviations (RSD) for conventional nebulization, Spray ETV and Spray ETV ratioed with ArH^+. In general, there was a significant gain observed in detection limits for most elements, gains that were marginally improved through ratioing with ArH^+. Manganese benefited the most from spray deposition but other elements showed only marginal improvement or even a decrease (for magnesium) in DL. The RSDs were also improved by ratioing although they generally remained above the values observed with conventional nebulization.

Table 5-3. Detection limits (ng/ml) for liquid standards as obtained with conventional nebulization, Spray ETV-ICP-MS and Spray ETV with ratioing with ArH^+, with improvement factors observed for Spray ETV relatively to nebulization.

Element and *m/z*	**Nebulization**	**RSD**	**Spray ETV**	**RSD**	**Spray ETV (ArH^+ ratioed)**	**RSD**	**Improvement Factor[a]**
As 75	0.6	2.4%	0.06	3.8%	0.03	3.9%	10
Be 9	0.07	5.4%	0.03	2.6%	0.03	3.9%	2.3
Ca 44	5	5.5%	0.4	3.5%	0.5	4.4%	10
Cd 111	0.1	1.7%	0.2	4.3%	0.1	16%	1
Cu 63	0.06	2.1%	0.03	8.1%	0.02	9.1%	3
Mg 24	0.02	1.6%	0.04	2.0%	0.04	3.7%	0.5
Mn 55	0.2	2.7%	0.008	15%	0.006	7.6%	33
Mo 97	0.2	1.7%	1.4	23%	1	27%	5
Ni 66	0.5	1.7%	0.08	7.6%	0.07	1.2%	7
Pb 208	0.06	3.4%	0.007	3.8%	0.005	9.6%	12
Sb 121	0.08	1.8%	0.03	1.1%	0.03	1.6%	3
Zn 66	3	11%	0.4	12%	0.3	17%	10

a) Calculated using transients ratioed with ArH^+.

5.3.2.3 Comparison between Spray and Drop Deposition

The improvement factors obtained with Spray DSI [11] were 900 for As, 608 for Zn and 89 for Cu when compared to nebulization. For the same metals, we have obtained improvement factors of 10, 10 and 3, respectively, with Spray ETV. Although significant, these unexpectedly average results raised the question as to whether these gains were in proportion with the added complexity of the spray deposition and in particular with the low sample throughput inherent to this technique. The best comparison would be with conventional ETV-ICP-MS instrumentation in which the sample is drop deposited.

In order to make a fair comparison between both sample deposition techniques, manganese and cadmium were selected as test elements for determining the detection limits with drop and spray deposition. Identical operational parameters were used for sample vaporization and for the ICP-MS instrument throughout this experimental work. The two metals were evaluated in separate experimental sequences. Consequently, the mass spectrometer was locked at a single *m/z* value for the time of the ETV transient. An optimum signal-to-noise ratio was therefore obtained for each metal since the spectrometer did not have to share a restricted time frame (10 seconds) among several *m/z* locations as for multielement determination (no argides were recorded). In Table 5-4, the mean detection limits calculated from 5 replicates are listed with the precision of the determination. An estimate of blank noise was determined using the noise extracted from the last portion of the transient as in Spray ETV-ICP-AES experiments (see section 3.4) and used in DL calculations.

Table 5-4. Detection limits(3σ) and relative standard deviations (RSD) for manganese and cadmium as obtained in ETV-ICP-MS with spray and drop deposition.

Deposition Technique	**Mn**				**Cd**			
	Signal[a]	DL pg/ml	DL pg	RSD	Signal	DL pg/ml	DL pg	RSD
Spray[b]	2.73×10^6	0.1	0.09	3.9%	6300	30	27	18%
Drop[c]	1.26×10^6	5	0.25	13%	16500	200	10	65%
Improvement[d]	2	50	3		0.4	7	3	

a) Normalized to the quantity of analyte.
b) For 0.9 ml of a 1 ng/ml multielement standard (0.9 ng).
c) For 50 µl of a 10 ng/ml (Mn, 0.5 ng) or 100 ng/ml (Cd, 5 ng) multielement standard manually deposited with a micropipette.
d) Ratio of spray over drop experiments. The calculation were done to one significant figure so that the best analytical performance appeared as the highest numerical value.

The improvement factor for detection limits expressed in unit of concentration showed that better Dls were related to the larger amount of sample deposited in the furnace. The sample volume ratio was 18 and the observed improvements factors for the two metals were in reasonable agreement with this figure if we consider that these factors also included variations in noise. The improvement factors calculated from the DL expressed in units of mass compared the differences introduced in sample deposition and vaporization, irrespective of the sample volume. It is readily apparent that the simple fact of spraying the sample was beneficial to DL when compared with drop experiments. Moreover, the precision of the sample deposition (from 5 replicates) appeared to be improved with spray deposition but it can be due to the inexperience of the experimenter in the art of reproducibly depositing a drop. The poor reproducibility for cadmium in drop experiments was caused by two severe outliers. Otherwise they exhibited DL very similar to the other replicates. No obvious reason was seen to cause such surges in Cd signal.

Figure 5-11 compares the shape of transients obtained with spray deposition with that obtained for drop deposition. It is apparent that for manganese, the spray transient was narrower with a steeper initial ramp and decayed more rapidly to baseline. The spray transient also exhibited a higher specific intensity (*i.e.* integrated count rate per nanogram of analyte) as shown in data of Table 5-4. The transients for cadmium showed the exact opposite characteristics; however, the time of first appearance was not changed for the two elements. Although it remains purely speculative at this point, it is believed that spraying the sample and especially evaporating water on a continuous basis, has prevented the liquid sample from soaking into microscopic openings and cracks at the surface of the pyrolytic graphite surface. This coating could have modified the high temperature volatilization process for metals with intermediate or high boiling points, or those exhibiting an affinity for active sites present within the structure of the graphite [17,18].

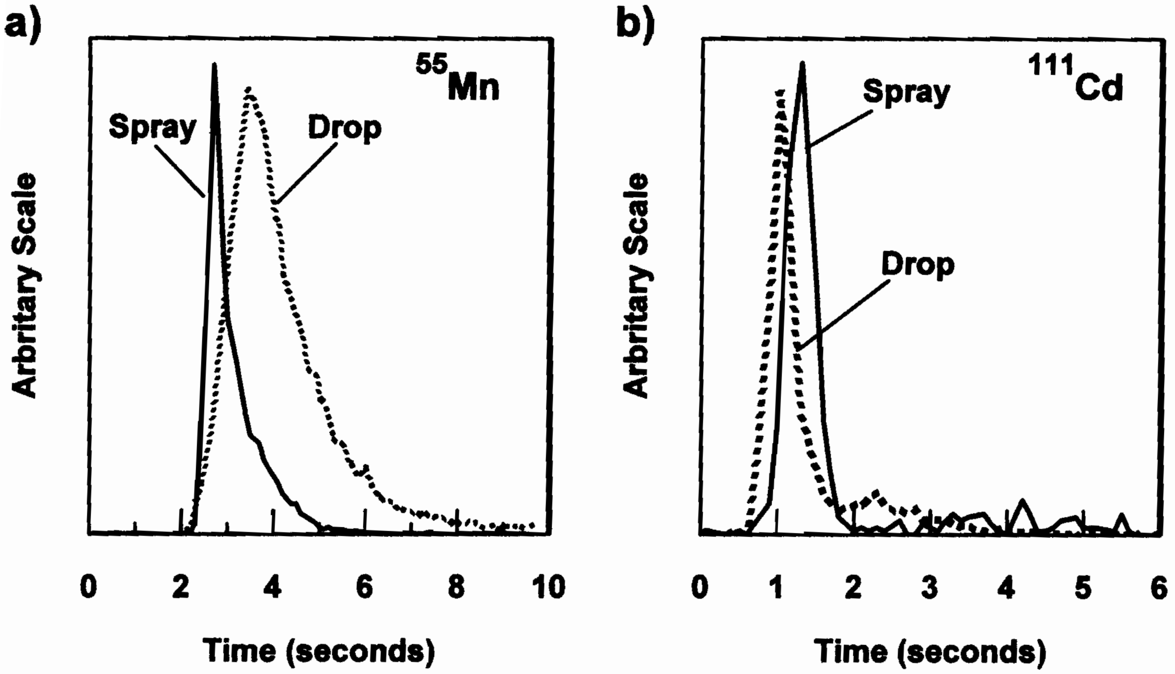

Figure 5-11. Transients for(a) manganese and (b) cadmium, as obtained from spray and drop deposition. Sample sizes and concentrations are described in footnote c of table 5-4. Drop and spray traces were plotted on different scales.

In spray deposition, the metals were deposited and immediately dried at the surface and, most probably, did not have to diffuse later toward the surface at vaporization [17]. Even when deposited as an aqueous drop and allowed to penetrate the graphite, cadmium has been observed to return to the surface at moderate temperature (400°C). It is therefore not surprising to observe that spray deposition had little positive effect on the subsequent vaporization of this metal; However, it seemed that manganese exhibited a behavior similar to that reported for copper, which showed a tendency to penetrate and to stay strongly adsorbed a few microns below the surface [17]. Signal tailings similar to the one observed in this work for manganese, were also noticed for copper samples intercalated into graphite in

GFAAS [17]. For these metals, the spray deposition can do more than just enhance the sample signal, it can also improve the quality of the sample deposition.

5.3.3 Interferences from Salt Matrices

A study of the interference caused by a concentrated matrix was done using NaCl as the interfering salt. Matrix effects related to dissolved salts have been reported in literature for ICP-MS with conventional nebulization [19-21]. These effects are expected to be exacerbated in Spray ETV-ICP-MS as there is no matrix separation other than with the solvent and non-volatile matrix salts are concentrated along with the sample. Calculation of the matrix loading expected from what would be otherwise easy matrices, such as the one presented in Table 5-1, illustrates well the potential for amplification of interference problems when spray deposition is used as a sample introduction technique. However, in moderated quantities, matrix salts such as NaCl act as signal enhancer [22]. The salt from the matrix, which is several orders of magnitude more abundant than any analyte, will nucleate easily and form self-sustained particles acting as physical carriers. This fact was exploited to enhance signal and metal transportation efficiency in both ETV and DSI-ICP [23-25], although the effect observed in DSI was attributed in part to the formation of chlorides.

For this study, a solution of 2 ng/ml of cadmium, bismuth and copper were prepared with a concentration of NaCl increasing from 0 to 100 μg/ml. For each sample, a volume of 0.93 ml was sprayed and submitted to the same analytical sequence used in previous Spray ETV experiments. ICP-MS parameters were also identical. The transients obtained for cadmium and bismuth (Figure 5-12) exhibit important changes in shape, position and intensity as the concentration of the salt matrix increased.

Both metals appeared earlier in the vaporization stage and with a higher intensity for matrices of intermediate concentrations. At high matrix loading, however, the onset of the signals returned close to their initial positions in time and both transients intensities were suppressed. The recording of the argon dimer as a diagnosis species revealed that important changes in plasma conditions occurred 1.6 seconds into the vaporization stage and lasted for 2 to 3 seconds, a time frame which corresponds with the arrival of massive amounts of matrix material in the plasma [15,16]. The effect was severe for matrix concentrations above 10 µg/ml, and can explain the attenuation of the tailing part of transients observed for both metals. This attenuation led eventually to the extinction of signal at high matrix loading.

The effects of the NaCl matrices were also observed for the signal of isotope 63 of copper. This *m/z* location exhibits an interference caused by the sodium argide ($^{40}Ar^{23}Na^+$) formed from the vaporized matrix [26]. Figure 5-13 illustrates the effect of NaCl on isotopes 63 and 65 of copper. The isotope 63 signal exhibited a complex behavior as it first expanded in the presence of low matrix concentration, then decreased with the intermediate ones and finally greatly increased with the high concentrations. This last increase is presumably caused by $^{40}Ar^{23}Na^+$. Transients for isotope 65, in contrast, increased steadily with low and intermediate matrices, but finally decreased in highly concentrated matrices.

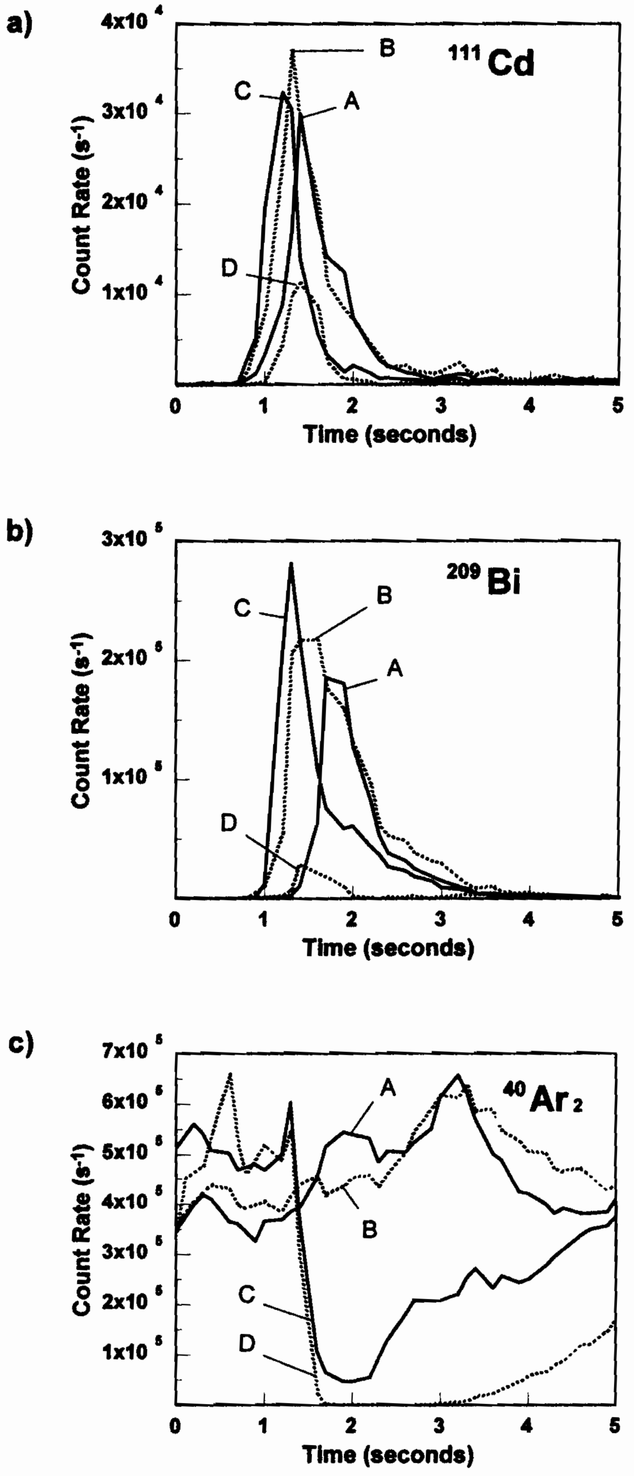

Figure 5-12. Transients for (a) ^{111}Cd, (b) ^{209}Bi and (c) ^{80}Ar$_2$. A 2 ng/ml solution of Cd, Bi and Cu was sprayed with a NaCl matrix of increasing concentration: A, 0; B, 1; C, 10; and D, 100 µg/ml Na as NaCl.

Since these data sets were obtained during the same sequence of measurements as in Fig. 5-12, the argon dimer transients of Fig. 5-12(c) can be used as diagnosis species for explaining in part the behavior of copper. As copper is a metal with intermediate volatility, it appeared simultaneously with the maximum suppression of the argon dimer signal. The copper transients were therefore evenly suppressed, a fact that prevented the distortion of the transient shape observed for Bi and Cd, but which significantly lowered the integrated signal. However, the enhanced transport efficiency counteracted the suppression of signal from matrices of low concentration. If we consider that matrix suppression and vaporization enhancement effects applied equally to the two isotopes, the isotopic ratio $^{65}Cu/^{63}Cu$ should be a direct measure of the sodium argide interference. The change of this ratio with matrix loading, shown in Fig. 5-13(c), indicated a significant departure from the natural ratio of 0.447 at a matrix concentration as low as 10 μg/ml in Na (i.e. with about 10 μg of Na in the furnace).

Other sodium salt matrices were also investigated in order to discriminate for the effect of chloride. The transients for cadmium, bismuth and the two isotopes of copper were measured in matrices of Na_2NO_3 and Na_2SO_4, all having concentration in sodium similar to the NaCl matrix previously used. The relative integrated signals are plotted against the matrix concentration in sodium in Fig. 5-14(b) and (c). The results obtained in a NaCl matrix are illustrated in Fig. 5-14(a) for comparison purpose.

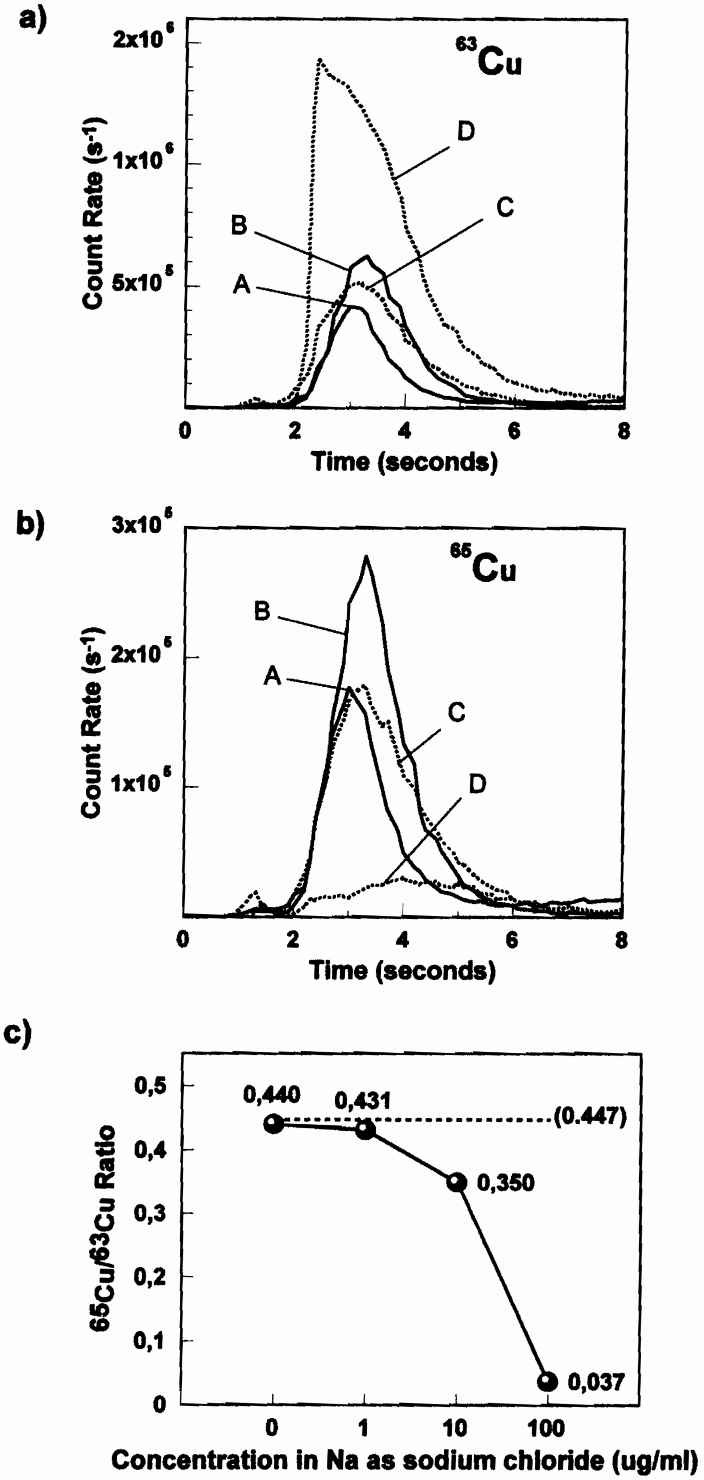

Figure 5-13. Transients for (a) ^{63}Cu and (b) ^{65}Cu, with the evolution of the ratio ^{65}Cu/^{63}Cu in (c). A 2 ng/ml solution of Cd, Bi and Cu was sprayed with a NaCl matrix of increasing concentration: A, 0; B, 1; C, 10; and D, 100 µg/ml Na as NaCl. Dotted line in (c) indicates the expected ^{65}Cu/^{63}Cu ratio.

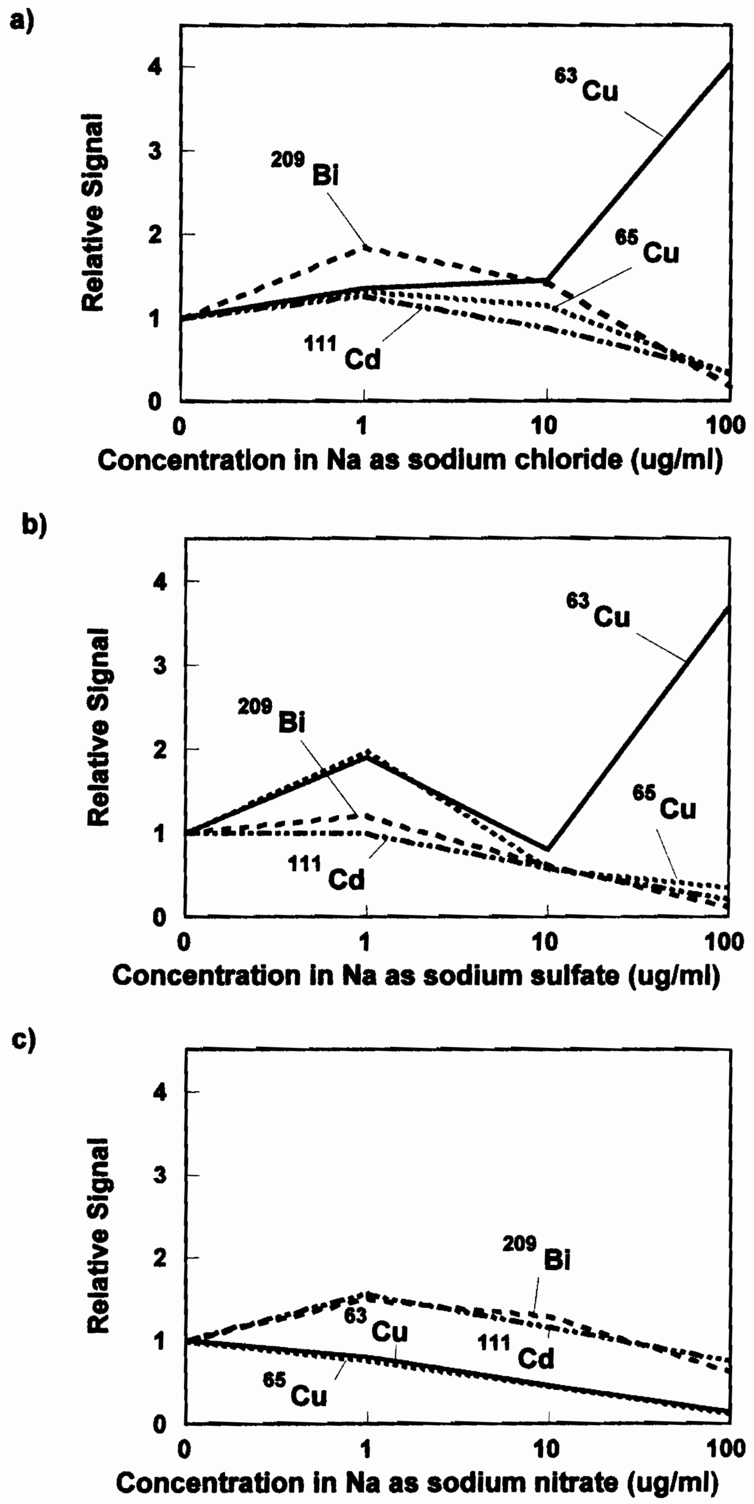

Figure 5-14. Integrated signals of transients recorded for ^{63}Cu, ^{65}Cu, ^{111}Cd and ^{209}Bi with increasing concentration of Na as (a) NaCl, (b) Na_2SO_4 and (c) $NaNO_3$.

NaCl sublimates at 1413°C and sodium sulfate melts at 884°C. They both survive the furnace ashing stage (400°C) and are in all probability vaporized with the rest of the sample. Sodium nitrate, in contrast, decomposes at 380°C, possibly into sodium monoxide (Na_2O) which later sublimates at 1275°C. A comparison between NaCl and Na_2SO_4 matrices will contrast the effect of the chloride with the sulfate anions (although sulfates are probably decomposed to smaller molecules at high furnace temperature) for a constant sodium load. The sodium nitrate matrix should exhibit effects generated by the sodium load, as the oxygen and nitrogen from the nitrate are atomic species already present in the plasma.

From examination of these curves, it can be concluded that Bi and Cd were enhanced in presence of 1 μg of Na and that the effect was independent of the chemical form of the sodium salt. This confirmed our initial statement that these salts act mainly as physical carriers [8,22]. Moreover, enhanced volatilization of metals in the form of volatile chlorides was unlikely given that similar behavior was also observed in the presence of Na_2SO_4, which is a chloride free sodium salt, for the three metals studied.

With a sodium sulfate matrix, however, the interference from sodium argide at *m/z* 63 appeared to be absent with high matrix loads as well as the enhancement in signal expected at low matrix load. The evolution of the ratio $^{65}Cu/^{63}Cu$ ratio illustrated in Fig. 5-15 for the matrices studied, revealed no interferences at *m/z* 63 in the presence of sodium sulfate matrices as opposed to the two other type of matrices. An important depression in Ar_2^+ was also observed for the higher concentrations in Na_2SO_4, exhibiting the same appearance time and duration as the ones illustrated in Fig. 5-12(c) for NaCl, and also for $NaNO_3$ (not shown). This fact signaled that the matrix pulse reached the plasma in the same way for the three salts.

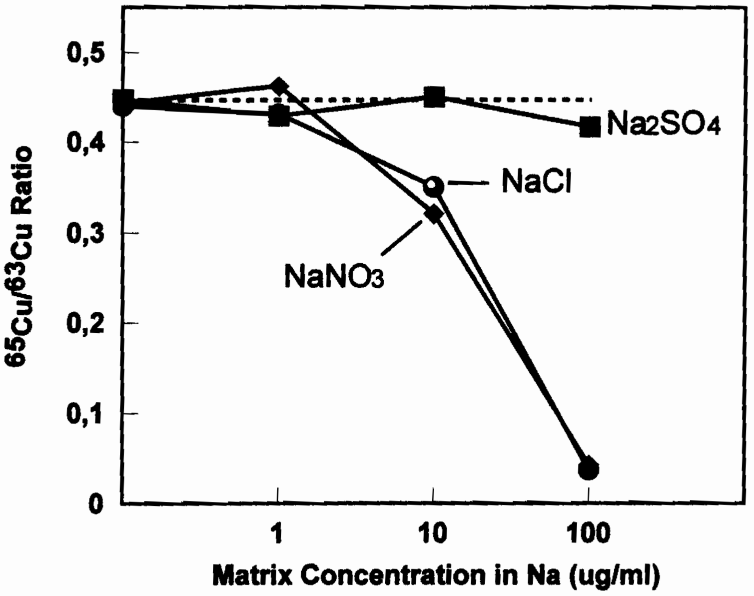

Figure 5-15. Evolution of the isotopic ratio $^{65}Cu/^{63}Cu$ as measured from integrated transients, with increasing concentration of Na as NaCl, Na_2SO_4 and $NaNO_3$. The broken line is the natural ratio for copper (0.447).

At this point, no explanation can be furnished to explain the stability of the isotopic ratio of copper even at high matrix loading of sulfate. It might be speculated that the plasma state changes briefly during the matrix pulse in such manner that the formation of the $ArNa^+$ species normally interfering at *m/z* 63 was inhibited. Such inhibition of interfering argides has been deliberately used for determining the isotopes of K, Ca and Fe without substantial interferences from Ar+, ArH+ and ArO+ [12,13]. The suppression of argides occurred in "cold" plasmas *i.e.* set at very low power and at high injector gas flow with conventional nebulization of aqueous HNO_3 as explained previously. In these conditions, the plasma ion population becomes dominated by molecular species such as NO^+ and H_3O^+ instead of Ar^+, and the level of species derived from the argon ion are therefore greatly reduced [12,13]. It is possible that the same conditions occurred briefly during the sulfate matrix pulse. Since the copper transient appeared at the same time and with approximately the same duration as the matrix, the argide suppression was effective over the length of the copper transient. As a consequence, the isotopic ratio of copper was preserved even with concentrated matrices, as illustrated in Fig. 5-15. The cooling effect on plasma from Na_2SO_4 matrices can be more severe than with NaCl matrices at equal weight, because the thermal decomposition of sulfates releases gaseous molecular species (SO_2) that must be later dissociated in the plasma at a high cost in energy. A study of background species abundances at various steps of the vaporization should help making this point clearer.

Even if preserved from the sodium argide interference, copper with sodium sulfate still suffered from matrix induced suppression with the same magnitude as Cd and Bi, as illustrated in Fig. 5-14(c). Also, there is no explanation at this moment as to why no transportation enhancement whatsoever was observed for copper with this matrix.

5.4 Conclusion

Throughout this study, it appears that spray deposition for ETV-ICP-MS provided significant enhancement in detection limits for an extended set of elements. The study is still at a preliminary stage and several aspects of the technique need to be improved or understood more thoroughly. Some encountered problems are of purely technical nature and can eventually be solved with appropriate modification to the instrumentation or to the laboratory environment. Notably, the high blanks are expected to be reduced if greater care is brought to the control of the immediate environment of the ETV unit and to the use of very clean deionized water.

Some other aspects revealed in this study are related to more fundamental phenomena. The ratioing with argon hydride was seen to produce some improvement to detection limits as well as to the accuracy of the determination. It is not yet clear, however, which criteria should be used for applying the ratioing to certain elements and not to others. Ratioing with the argon dimer (Ar_2^+) surely warrants extensive studies in the future. Also, one has to pay great attention to matrices which, although innocuous with other sample introduction techniques, can briefly induce fundamental changes in the plasma state during sample vaporization. A complete assessment of all parameters in play should be made before selecting an appropriate calibration strategy, and the isotope ratioing, plasma diagnosis using argides, Simplex optimization and experimental design are just some of the various tools that the analyst can use to decipher complex parametric interactions and thereby generate robust data.

At this point, it appears also that future research in this topic should focus on the improvement in the quality of the spray deposition (when opposed to drop deposition). Some metals appeared to interact differently with the graphite surface when they are spray deposited and improved transients were obtained, probably through modified adsorption properties of the metals. The negative effects associated with a higher mass of analyte are, however, exacerbated in Spray ETV-ICP-MS because of the susceptibility of the instrument to matrix effects. While maximal sample concentration is desirable in Spray ETV-ICP-AES and translates there directly into improved detection limits, it is less an advantage in mass spectrometry as revealed by the lower improvement factors obtained; however, if the total amount of material is kept within the capacity of the ICP-MS, it is likely that this technique, once fully developed, will eventually compete with the most sensitive ones. It looks promising especially for samples with matrices of low concentration.

5.5 References

[1] N. Jakubowski, I. Feldmann and D. Stuewer, *J. Anal. At. Spectrom.* **8,** 969 (1993).

[2] N. Jakubowski, I. Feldmann and D. Stuewer, *Spectrochim. Acta* **47B,** 107 (1992).

[3] H. Niu and R. S. Houk, *Spectrochim. Acta* **51B,** 779 (1996).

[4] J. P. Matousek and J.-M. Mermet, *Spectrochim. Acta* **48B,** 835 (1993).

[5] M. Murillo and J.-M. Mermet, *Spectrochim. Acta* **44B,** 359 (1989).

[6] Y. Q. Tang and C. Trassy, *Spectrochim. Acta* **41B,** 143 (1986).

[7] D. J. Douglas, *Spectrochim. Acta* **41B,** 197 (1986).

[8] T. Kántor, *Spectrochim. Acta* **43B,** 1299 (1988).

[9] A. G. T. Gustavsson, *Anal. Chem.* **55,** 94 (1983).

[10] (a) S. Nukiyama and Y. Tanasawa, *Experiments on the Atomization of Liquids in an Air Stream*, E. Hope transl., Defense Research Board, Department of National Defense, Ottawa, Canada (1950).

(b) S. Nukiyama and Y. Tanasawa, *Y. Trans. Soc. Mech. Eng., Tokyo* **4-6,** Reports 1-6 (1938-40).

[11] R. Rattray and E. D. Salin, *J. Anal. At. Spectrom.* **10,** (1995).

[12] S. D. Tanner, *J. Anal. At. Spectrom.* **10,** 905 (1995).

[13] S.-J. Jiang, R. S. Houk and M. A. Stevens, *Anal. Chem.* **60,** 1217 (1988).

[14] J. R. Dean and R. D. Snook, *J. Anal. At. Spectrom.* **1,** 461 (1986).

[15] D. C. Grégoire, N. J. Miller-Ihli and R. E. Sturgeon, *J. Anal. At. Spectrom.* **9,** 605 (1994).

[16] F. Vanhaecke, L. Galbács, S. Boonen, L. Moens and R. Dams, *J. Anal. At. Spectrom.* **10,** 1047 (1995).

[17] J. G. Jackson, R. W. Fonseca and J. A. Holcombe, *Spectrochim. Acta* **50B,** 1837 (1995).

[18] R. W. Fonseca, J. McNally and J. A. Holcombe, *Spectrochim. Acta* **48B,** 79 (1993).

[19] G. M. Hieftje and G. H. Vickers, *Anal. Chim. Acta* **42B,** 467 (1989).

[20] D. Beauchemin, J. W. McLaren and S. S. Berman, *Spectrochim. Acta* **42B,** 467 (1987).

[21] S. H. Tan and G. Horlick, *J. Anal. At. Spectrom.* **2,** 745 (1987).

[22] R. D. Ediger and S. A. Beres, *Spectrochim. Acta* **47B,** 907 (1992).

[23] V. Karanassios, V. Abdullah and G. Horlick, *Spectrochim. Acta* **45B,** 119 (1990).

[24] J. P. Matousek, R. T. Satumba and R. A. Bootes, *Spectrochim. Acta* **44B,** 1009 (1989).

[25] J. P. Matousek and H. K. J. Powell, *Spectrochim. Acta* **43B,** 1167 (1988).

[26] Y. Shao and G. Horlick, *Appl. Spectrosc.* **45,** 143 (1991).

Chapter 6

CONCLUSIONS AND RECOMMENDATIONS

It was demonstrated in Chapter 3 and in Chapter 5 that the spray deposition of great quantities of a liquid sample can be efficiently achieved in a commercial graphite furnace unit. Most analytes are retained in the graphite tube and the separation from the solvent matrix is easily achieved with the proper gas flow path and temperature setting during spraying. In Spray ETV-ICP-AES, the sample preconcentration reduced the detection limits for several elements by two orders of magnitude on average. In atomic emission, analyte signals appeared to be rather insensitive to the water vapor surge originating from the furnace during the high temperature stage. In mass spectrometry, it is believed that small variations in water vapor load shift the physical position of the ion maximum concentration over significant distances in a plasma operating in almost dry conditions. This behavior confirmed other findings already reported in literature. The sudden and random releasing of the water vapor previously condensed during sample spraying has therefore a negative impact on the precision and accuracy of the analysis. Selected argides species and solvent derived molecular species, presented in chapter 3, have demonstrated some potential to be used as internal standard for the correction of rapid fluctuations in plasma conditions, that in turn influence the excitation efficiency of analytes. The use of more elaborated mathematical strategies - such a principal component analysis - may lead to sophisticated computing models allowing instant diagnosis of the plasma state in routine work. Potential applications include analytical plasmas coupled with sample introduction systems which generate a low but varying solvent load combined with intense sample pulse. Laser ablation and ultrasonic nebulization with desolvation stage are prime candidates along with ETV and spray ETV.

Future research should focus on designing a furnace assembly more adapted to spray deposition. The design would allow the deposition of several milliliters of sample volume with minimal deposition of water within the furnace by physically separating the spray deposition area from the sample vaporization area. This can be achieved by translating the sprayed surface toward a high temperature enclosure having the proper connection to the plasma torch. A carrousel type revolving support, as illustrated in Fig. 6.1, would provide the desirable level of automation while insuring a separation between the sample spraying and the vaporization sections. Moreover, since the sample deposition exhibited low dependencies on spraying conditions, sample spraying could be done concurrently on two or more surfaces. The low sample throughput inherent to the spray preconcentration technique would be improved by a factor equivalent to the number of simultaneously sprayed surfaces. Alternatively, the sample vaporization can be performed in a separate ETV unit.

The ability of spray deposition to form uniform coatings over the graphite surface without penetration of the solvent may be of interest for applying solutions other than the sample itself. The formation of successive sample, modifier, surface modifier or stabilizer layers sprayed using an elaborated deposition strategy may well provide a “universal” ETV strategy for routine sample introduction into ICP instruments. Moreover, all the instrumentation used for spray deposition can be easily automated and the availability of concentric nebulizers with low internal volume allows quick rinsing time and a rapid solution change-over. A direct interfacing with FIA manifolds should be straightforward with the use of these concentric nebulizers. An almost integral recovery of the analyte can be obtained by spraying the FIA outflow synchronically with the sample pulse. Maximum sensitivity is therefore achieved and an appropriate chemical modifier can even be included in the formulation of the FIA carrier solution. The use of an FIA manifold may also remove one inherent drawback of spray preconcentration which consists in preconcentrating the dissolved matrix as well. In that respect, the availability of a wide range of polar and non-polar resins allows the selective removal of unwanted ionic species. Undoubtedly, spray deposition with organic solvents also warrants more investigation.

It appears for spray ETV-ICP-AES that the sample preconcentration provides immediate improvement in detection limits given the relative robustness of the technique toward high matrix loads. In contrast, spray ETV-ICP-MS may benefit more from the improved quality in sample deposition. The limits of detection exhibited in mass spectrometry are already very low and this technique is more sensitive to high sample loads, thus limiting the advantages provided by the preconcentration of the sample.

The use of halogenating gas mixture has exhibited a definitive action in releasing refractory elements from graphite surfaces and stable mineral matrices. Still, a commercial unit had to be modified to resist highly corrosive atmospheres and these changes have to be included in a novel ETV designed for sample introduction into ICP instruments. The transport efficiency is greatly improved for a wide range of elements and the analytical performance is less dependent on the matrix stability or on chemical interaction with the vaporizing surface. It is probably another step toward a more general use of ETV by the ICP users.

Appendix A

FORTH program of the CTF 188 Thermo Jarrell Ash ETV unit.

This appendix contains a listing of the modifications made to the original FORTH program controlling the CTF 188 Thermo-Jarrell Ash ETV unit. The temperature programming of the furnace and other physical events occurring during analytical sequences - such as gas flow switching and sample tip positioning - are under control of the inboard computer through action of actuators, input-output (I/O) binary port and digital-to-analog (D/A) interfaces. FORTH is a programming language in which functions are defined from other functions in a pyramidal hierarchy, starting from a small set of primary functions. The main program is executed by invoking a function located at the top of the pyramid, although any other functions can be individually called by the user. Modifications were introduced either as new functions or as new declaration for already existing functions (*i.e.* redefining an old function). Usually, new functions are specific to spray deposition, such as the function performing the initial warm-up of the furnace assembly. The reader is encouraged to consult an introductory book on FORTH programming for more details.

In the following program listings, commands such as “PROC MAIN”, “TRANSMIT” and “WAITFOR” are part of the macro language used by the serial communication software (PCPLUS). PCPLUS is run on the PC computer attached to the ETV unit and acting as terminal. The FORTH program lines are transmitted as lines of text. For each line of program transmitted using the macro command “TRANSMIT”, a reply from the furnace’s computer is expected (“ok”) and the transmission is paused for 200 msec before sending the next line of text. The sequence WAITFOR "ok^M^J"/MSPAUSE 200 originally followed all TRANSMIT macro command instances, but have been stripped out here for clarity.

All FORTH command lines starting with colons are new function definitions issued to the FORTH compiler. In the example below:

“: 1MAN 0 KEEPING ! FLOW -DOOR RAMPS 0 TIMES C@ ?DUP ; `r”

1MAN is the name of the new function; 0 KEEPING is a function previously defined with the value 0 transmitted before execution; FLOW, -DOOR and RAMPS are other functions that will execute in the sequence specified in the 1MAN declaration line. The semi-colons signals the end of the function definition and tells the system to compile the newly defined function into memory. This function can then be called directly by the user for immediate execution or alternatively, other functions can include this function in their definition. The “`r” character sequence instructs the communication program to send a carriage return character to the ETV computer, as if the user has hit the return key. FORTH functions sent without colons or semi-colons are just executed in sequence.

ETV.ASP

```
PROC MAIN

    COMMENT

    Modification done on March 22nd, 94:
    (To try the drying vent, opposite to the exit to the plasma)
        -External-inert always on
        -Door closed at the beginning of the second stage
```

Modification of March 24th, 94:
(To heat up the electrode before the sample deposition, water flow off)
-Close door, 450C for 30 sec then open the door and deposit.

Modification of April 28th, 94:
(To cool the door to near room temperature after each run)
-Extend the cooling stage to 120 seconds, with door closed and making contact with the graphite cylinder.
-Internal argon flow reduced to LOW during cooling stage.

Modification of May 3rd, 94:
(To assure a better warm up)
-Extend the warming up stage to 45 sec. at 550C.

Modification of March 14th, 95:
(To control the solenoid box)
-Uses the INTERNAL-AIR channel to control cooling water flow and carrier gas flow at ashing and vaporizing stages.
-Warm-up temp. reduced to 400C (still 45 sec).

Modification of May 4th, 95:
- Spread "A"s' at various points in the temperature program to report furnace temperature on screen.
  ("A" is a short command that print the actual furnace temp. as seen by the detector)

Mod. of July 19th, 95:
- Include a 30 seconds delay after spray deposition to plug the dosing hole.

Mod. of August 18th, 95:
- Deposition time is expressed in 10th of second to allow a fine adjustment of the sample deposition.

Mod. of Oct 25, 95:
- Delay to plug the dosing hole shortened to 10 seconds.

Mod. of Dec 30, 95:
- Warm-up stage at 550C for 15 seconds, then 400 for 15 sec.
- Programmed "1DRY" and "2DRY" in 4GO, to heat the furnace at 2000C for 10 sec under controlled condition (Takes about 1 minute and replace the warmup stage).

Mod. of march 3, 96:

```
            - Allow the water to flow for one second every 15 seconds
              at spray deposition, to prevent tripping ( since the water line
              pressure was lowered to 60 psi from 100 psi).
              Initial drying set at 1800C for 10 seconds.

     ENDCOMMENT

TRANSMIT "`r"
WAITFOR "ok^M^J"
MSPAUSE 200


TRANSMIT ": WHODAT .`" FAPES, modified by J.F.Alary, March 3rd, 1996 `" ;`r"
WAITFOR "ok^M^J"
MSPAUSE 200

TRANSMIT "VACUUM-PINCH CONSTANT VACUUM-ARM`r"
TRANSMIT ": WATER INTERNAL-AIR ;`r"
TRANSMIT ": 1MAN 0 KEEPING ! FLOW -DOOR RAMPS 0 TIMES C@ ?DUP ;`r"
TRANSMIT ": 2MAN 0 TEMPS @ 50 - 50 ROT 0 ;`r"
TRANSMIT ": 3MAN DO OVER I I' */ OVER + T2S D/A 1 SECS LOOP 2DROP ;`r"
TRANSMIT ": 4MAN 0 TEMPS @ HEAT ;`r"
TRANSMIT ": 5MAN 0 TEMPS @ T2S D/A HOLDS 0 TIMES C@ SECS ;`r"
WAITFOR "ok^M^J"
TRANSMIT ": MANUAL 1MAN IF 2MAN 3MAN ELSE 4MAN THEN 5MAN ;`r"
TRANSMIT ": 1AU 1 KEEPING ! 0 TEMPS @  HEAT RAMPS 0 TIMES C@ ;`r"
TRANSMIT ": 2AU ?DUP IF 0 TEMPS @ SWAP KEEPS THEN ;`r"
TRANSMIT ": 3AU FLOW 0 TEMPS @ 1 KEEPS DRAIN-PINCH OFF ;`r"
TRANSMIT ": 4AU VACUUM-ARM ON 0 TEMPS @ 1 KEEPS NEBULIZER ON 0
DELAY @ ?DUP ;`r"
TRANSMIT ": 5AU IF 10 /MOD 0 TEMPS @ SWAP KEEPS 0 TEMPS @ SWAP
KEEPSS THEN DOOR ON ;`r"
TRANSMIT ": 6AU NEBULIZER OFF 0 TEMPS @ 1 KEEPS VACUUM-ARM OFF 0
TEMPS @ 1 KEEPS ;`r"
TRANSMIT ": 7AU A 0 DEPOSIT @ DUP ;`r"
TRANSMIT ": 8AU IF BOOST +ARM 0 TEMPS @ 1 KEEPS NEBULIZER ON THEN
150 /MOD ?DUP ;`r"
TRANSMIT ": 9AU IF 0 DO 0 TEMPS @ DUP 14 KEEPS WATER ON 1 KEEPS WATER
OFF A LOOP THEN ;`r"
TRANSMIT ": 10AU 0 TEMPS @ SWAP KEEPSS CR ;`r"
WAITFOR "ok^M^J"
TRANSMIT ": 11AU NEBULIZER OFF 0 TEMPS @ 1 KEEPS -ARM 0 TEMPS @ 10
KEEPS ;`r"
TRANSMIT ": 12AU -DOOR 0 TEMPS @ 1 KEEPS R> ;`r"
WAITFOR "ok^M^J"
```

```
TRANSMIT ": AUTOMATIC 1AU 2AU 3AU 4AU 5AU 6AU 7AU 8AU 9AU 10AU
11AU 12AU ;`r"
TRANSMIT ": 1SAMP 50 T2S D/A 1 STAGE RAMPS BOOSTER 2@ 6 5 BOOSTER 2!
;`r"
TRANSMIT ": 2SAMP 0 DELAY @ 0 DEPOSIT @ OR IF AUTOMATIC ELSE
MANUAL THEN ;`r"
TRANSMIT ": 3SAMP TEMP DROP BOOSTER 2! ;`r"
TRANSMIT ": SAMPLE 1SAMP 2SAMP 3SAMP ;`r"
TRANSMIT ": 1COOL-DOWN 0 D/A 0 KEEPING ! ;`r"
TRANSMIT ": 2COOL-DOWN INTERNAL-INERT OFF INTERNAL-INERT-LOW DUP
ON ;`r"
TRANSMIT ": 3COOL-DOWN 30 SECS OFF 0 DELAY @ 0 DEPOSIT @ OR ;`r"
TRANSMIT ": 4COOL-DOWN IF -DOOR ELSE +DOOR THEN ;`r"
TRANSMIT ": COOL-DOWN 1COOL-DOWN 2COOL-DOWN 3COOL-DOWN 4COOL-
DOWN ;`r"
TRANSMIT ": 1GO ACTIVE-METHOD 0METHODS ! >run< >on< ;`r"
TRANSMIT ": 2GO EVERY OFF -DOOR SENSOR-COOLANT ON DRAIN-PINCH ON
EXTERNAL-INERT ON ;`r"
TRANSMIT ": 3GO TEMP DROP BG INIT PROBE ;`r"
TRANSMIT ": 1DRY INTERNAL-INERT ON A 300 25 KEEPS A INTERNAL-AIR ON
1800 10 ;`r"
TRANSMIT ": 2DRY KEEPS A 200 8 KEEPS A INTERNAL-AIR OFF 150 15 KEEPS A
CR ;`r"
TRANSMIT ": 4GO 1DRY 2DRY ;`r"
TRANSMIT ": 5GO SAMPLE  1 KEEPING ! FLAT ;`r"
TRANSMIT ": 6GO INTERNAL-INERT-MEDIUM ON A 2 RAMP A FLAT ;`r"
TRANSMIT ": 7GO INTERNAL-AIR ON INT A 3 RAMP A FLAT ;`r"
TRANSMIT ": 8GO INT A 4 RAMP A FLAT ;`r"
TRANSMIT ": 10GO A CLEAN A COOL-DOWN A -ARM 1000 MS EVERY OFF
>every< >off< ;`r"
TRANSMIT ": 11GO DRAIN-PINCH ON +DOOR INTERNAL-INERT-MEDIUM ON A
CR ;`r"
TRANSMIT ": GO 1GO 2GO 3GO 4GO 5GO 6GO 7GO 8GO 10GO 11GO ;`r"
TRANSMIT "EVERY OFF`r"
TRANSMIT "DRAIN-PINCH ON`r"
TRANSMIT ": +RINSE -ARM DRAIN-PINCH OFF 1 SECS VACUUM-ARM ON 1 SECS
NEBULIZER ON ;`r"
TRANSMIT ": -RINSE NEBULIZER OFF 1 SECS DRAIN-PINCH ON VACUUM-ARM
OFF ;`r"

ENDPROC
```

SPRAY.ASP

```
PROC MAIN
TRANSMIT "`r"
WAITFOR "ok^M^J",2
MSPAUSE 200

TRANSMIT "DELAYS 5 SECONDS DEPOSITS 260 SECONDS 4 ST-INT`r"
WAITFOR "ok^M^J"
MSPAUSE 200

TRANSMIT "4 STAGE 2200 DEGREES RAMPS 2 SECONDS HOLDS 8 SECONDS 2 LPM`r"
TRANSMIT "5 STAGE 2600 DEGREES HOLDS 3 SECONDS 2 LPM`r"
TRANSMIT "1 STAGE 160 DEGREES RAMPS 2 SECONDS HOLDS 10 SECONDS 2 LPM`r"
TRANSMIT "2 STAGE 200 DEGREES RAMPS 10 SECONDS HOLDS 20 SECONDS 2 LPM`r"
TRANSMIT "3 STAGE 400 DEGREES RAMPS 10 SECONDS HOLDS 20 SECONDS 2 LPM`r"
TRANSMIT "ITIME 5 SECONDS IDELAY 5 SECONDS`r"

ENDPROC
```

DROP.ASP

```
PROC MAIN
TRANSMIT "`r"
WAITFOR "ok^M^J",2
MSPAUSE 200

TRANSMIT "DELAYS 5 SECONDS DEPOSITS 0 SECONDS 4 ST-INT`r"
WAITFOR "ok^M^J"
MSPAUSE 200

TRANSMIT "4 STAGE 2200 DEGREES RAMPS 2 SECONDS HOLDS 8 SECONDS 2 LPM`r"
TRANSMIT "5 STAGE 2600 DEGREES HOLDS 3 SECONDS 2 LPM`r"
TRANSMIT "1 STAGE 20 DEGREES RAMPS 2 SECONDS HOLDS 10 SECONDS 2 LPM`r"
TRANSMIT "2 STAGE 200 DEGREES RAMPS 30 SECONDS HOLDS 0 SECONDS 2 LPM`r"
TRANSMIT "3 STAGE 400 DEGREES RAMPS 20 SECONDS HOLDS 10 SECONDS 2 LPM`r"
TRANSMIT "ITIME 5 SECONDS IDELAY 5 SECONDS`r"
```

```
ENDPROC
```

DRY.ASP

```
PROC MAIN

TRANSMIT ": DRY1 -ARM 100 1 KEEPS -DOOR INTERNAL-AIR ON EXTERNAL-INERT ON ;`r"
WAITFOR "ok^M^J"
MSPAUSE 200

TRANSMIT ": DRY2 SENSOR-COOLANT ON INTERNAL-INERT-HIGH ON ;`r"
TRANSMIT ": DRY3 2400 10 KEEPS 20 10 KEEPS EVERY OFF +DOOR ;`r"
TRANSMIT ": DRY DRY1 DRY2 DRY3 ;`r"

ENDPROC
```

GO.ASP

```
PROC MAIN

TRANSMIT "GO`r"
QUIT

ENDPROC
```

METHOD.ASP

```
PROC MAIN
TRANSMIT "`r"
WAITFOR "ok^M^J",2
MSPAUSE 200

TRANSMIT "DELAYS 5 SECONDS DEPOSITS 240 SECONDS 4 ST-INT`r"
TRANSMIT "4 STAGE 2200 DEGREES RAMPS 2 SECONDS HOLDS 8 SECONDS 2 LPM`r"
TRANSMIT "5 STAGE 2600 DEGREES HOLDS 3 SECONDS 2 LPM`r"
TRANSMIT "1 STAGE 160 DEGREES RAMPS 2 SECONDS HOLDS 10 SECONDS 2 LPM`r"
TRANSMIT "2 STAGE 200 DEGREES RAMPS 10 SECONDS HOLDS 20 SECONDS 2 LPM`r"
TRANSMIT "3 STAGE 400 DEGREES RAMPS 10 SECONDS HOLDS 20 SECONDS 2 LPM`r"
TRANSMIT "ITIME 5 SECONDS IDELAY 5 SECONDS`r"
ENDPROC
```

Appendix B

Schematic of the Spray ETV instrumentation

ETV with Accessories:

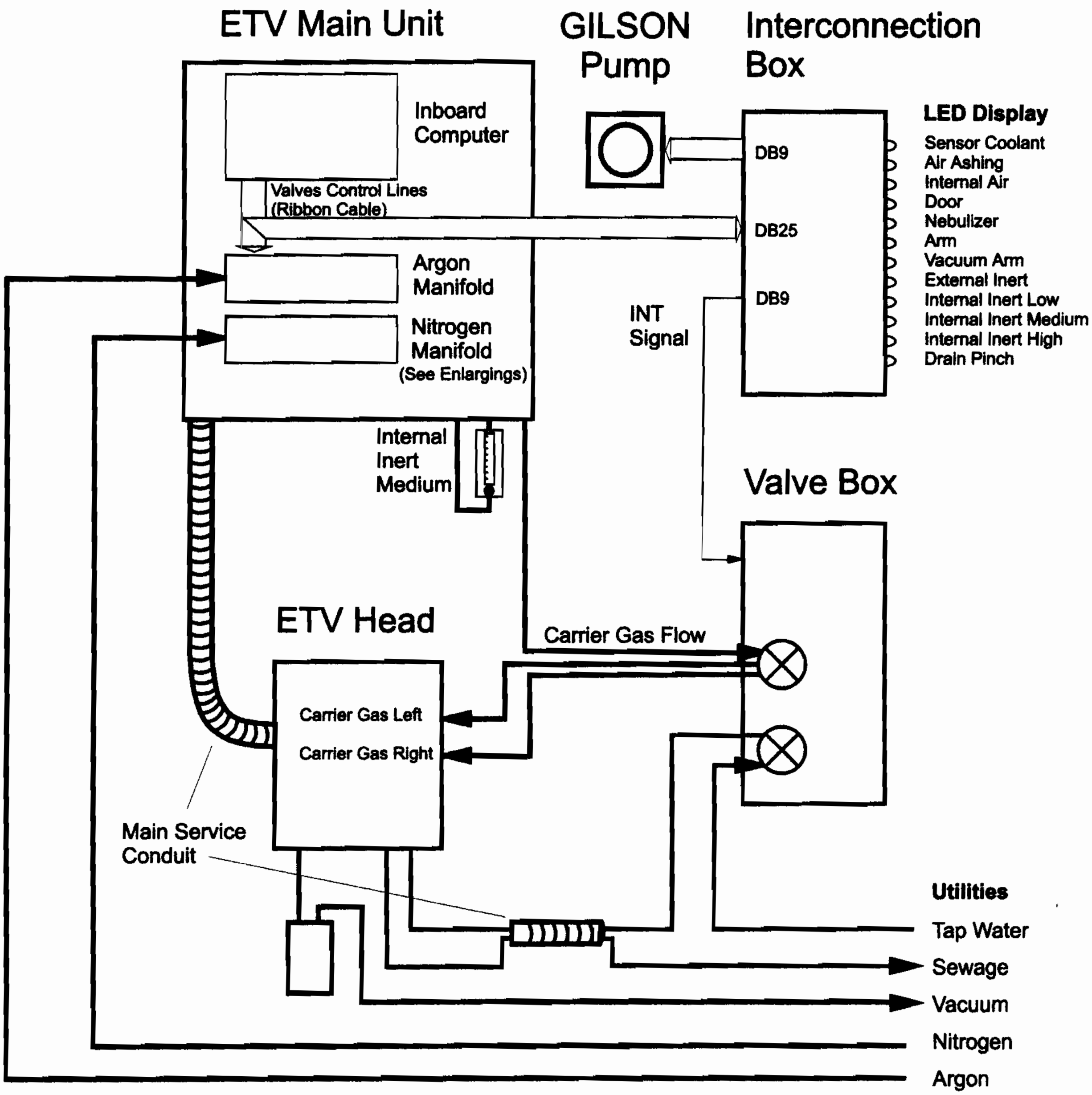

Gas Distribution Manifolds in the ETV Main Unit:

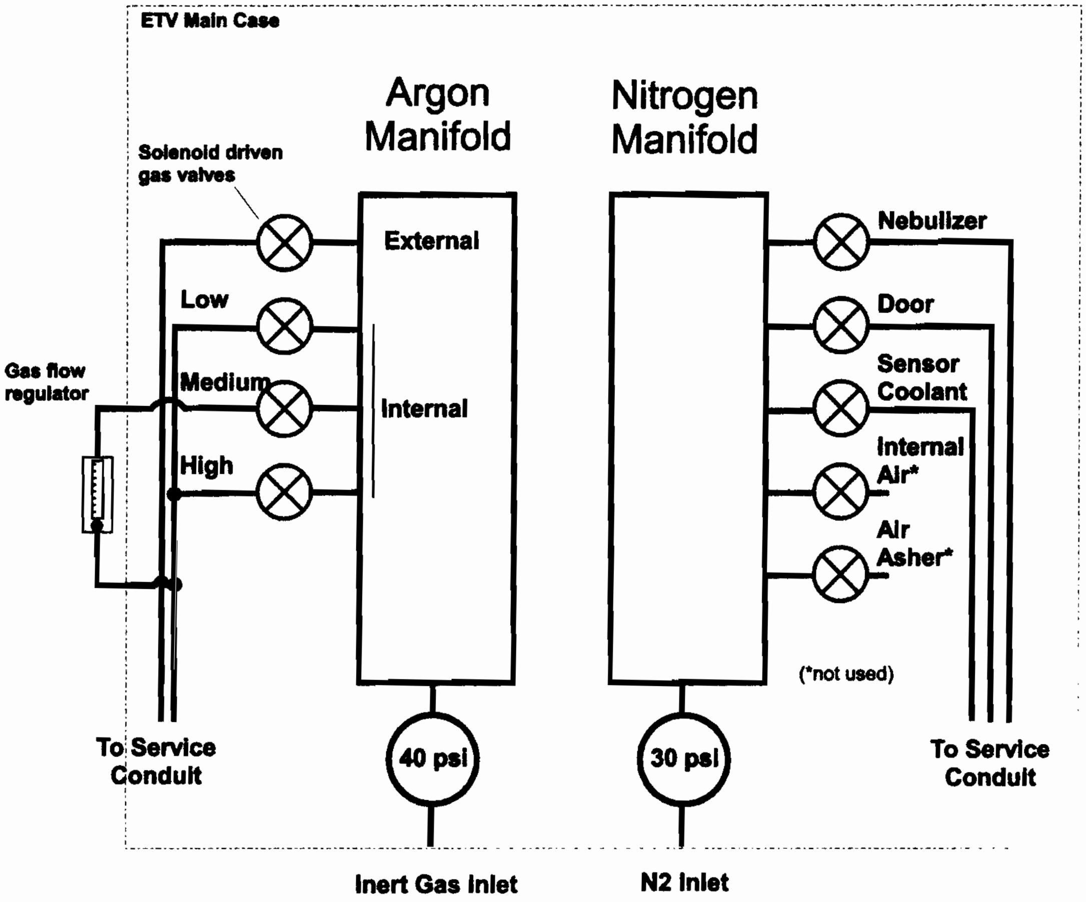

Interconnection Box Schematic:

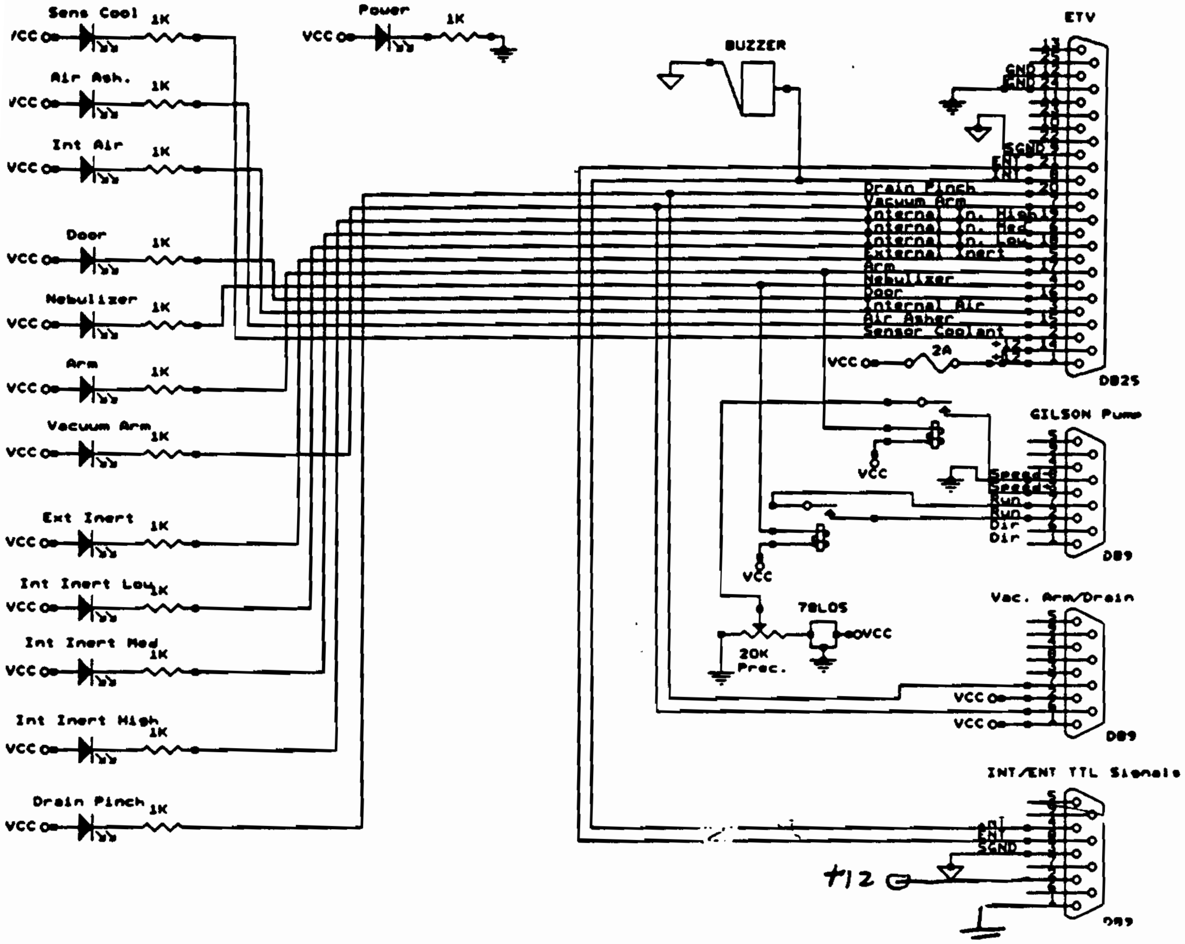

Appendix C

Actual Dimensions of the ETV Insert and Tube Parts

Assembled Furnace Used For Spray Deposition (to exact scale):

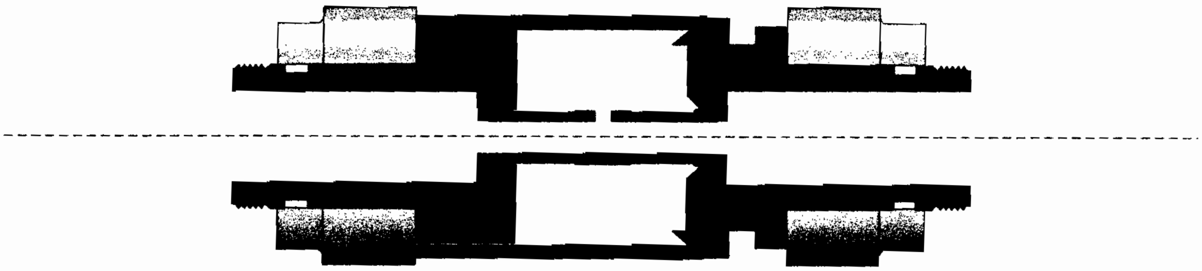

ALLIED Analytical System
Furnace Atomizer 188
(Thermo Jarrell Ash)

Furnace Parts (to exact scale):

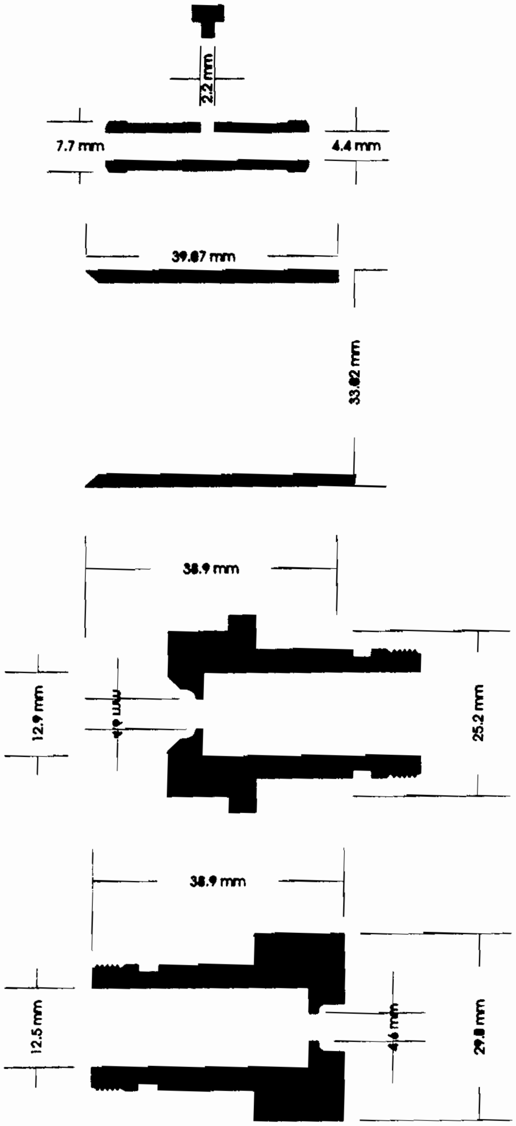

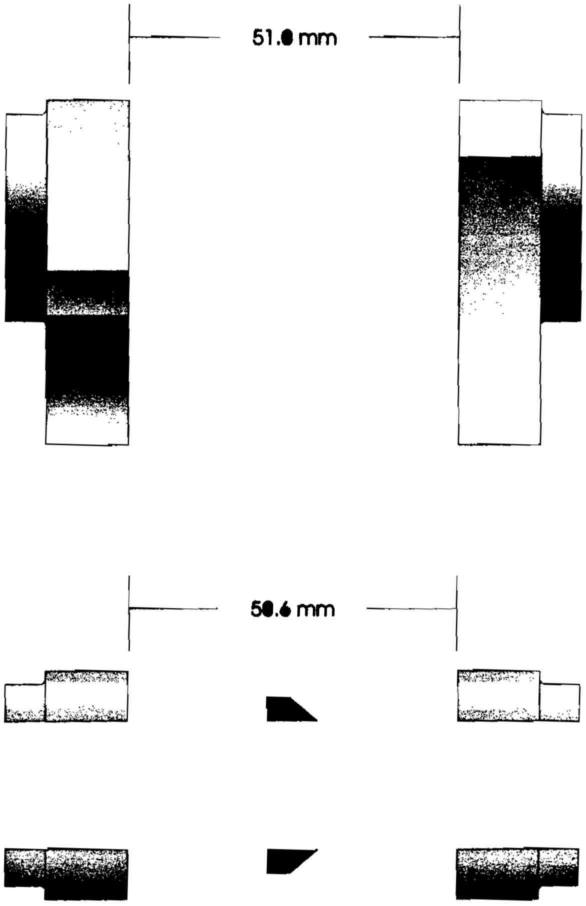

ALLIED Analytical Systems
Furnace Atomizer 188
(Thermo Jarrell Ash)